Sediment dispersal and accumulation in an insular sea: deltas of Puget Sound

Kristen L. Webster

A dissertation
submitted in partial fulfillment of the
requirements for the degree of
Doctor of Philosophy

University of Washington

2013

Reading Committee:
Andrea S. Ogston, Co-Chair
Charles A. Nittrouer, Co-Chair
Mark Holmes

Program Authorized to Offer Degree:
Oceanography

University of Washington

Abstract

Sediment dispersal and accumulation in an insular sea: deltas of Puget Sound

Kristen L. Webster

Co-Chairs of the Supervisory Committee:

Associate Professor Andrea Ogston

Professor Charles Nittrouer

Oceanography

Small rivers carry several million tons of sediment annually into Puget Sound and the Strait of Juan de Fuca. Once delivered to the marine environment, processes in the water column and on the seabed dictate dispersal, deposition and accumulation of these particles. To investigate these mechanisms, water-column measurements, including long-term bottom-boundary-layer time-series, water-column profiles and shipboard velocity, and seabed sampling, such as sediment cores, multibeam bathymetry and seismic reflection profiling, were collected from 2007-2009 on the Elwha and Skagit River deltas.

Tidal currents at both study sites were strong and capable of dispersing muds to more distal portions of the delta. At the Skagit delta the intertidal topset had strong ebb

tidal currents that exported most of the Skagit River mud rapidly beyond the topset. The mud found on the flat was limited spatially, near channels and at the outer flat edge and temporally, following high discharge. Physical processes drive shear stresses that act on the seabed to mobilize sands and muds and rework the seabed at various frequencies and depths: on a semi-diurnal tidal timescale, both channel and flat seabeds are reworked to 1-2 cm; and over a decadal timescale, lateral channel migration acts to rework the seabed to 1-2 m, making the limited mud deposits available for export.

The Skagit muds were rapidly transported > 10 km into two distinct distal basins; southward within the deep quiescent basin of Saratoga Passage mud accumulates up to 10 mm y^{-1} for a total of ~0.5 MT annually, and northward within the high-energy unconstrained basin of Rosario Strait some mud accumulates in small local deposits, but much is likely broadly dispersed. Throughout Puget Sound deltas typically form bay head (muddy progradation) or sidewall (broad mud dispersal), and the Skagit River dispersal system has both characteristics.

The Elwha River delta is a coarse-grained sidewall delta and tidal currents act to broadly disperse muds. Over the past 10,000 years the dominant sediment sinks have shifted from foreset beds to alongshore spits. This was likely related to variations in sea level as a result of deglaciation and sediment supply. As sea-level rise slowed slightly, wave-driven longshore transport began to actively shape delta morphology

and created paleospits, which formed successively one at a time, stepwise as sea-level rose. These sediment sinks were formed under similar processes as the modern spit, Ediz Hook.

It is shown that deltas in insular seas can form complex deposits, and this has implications for interpreting the geologic record in areas of constrained basins. In the modern environment, basin morphology and tidal currents determine accumulation patterns. Over longer timescales, the effects of previous glaciations have a major role in delta evolution.

Table of Contents

List of Figures

List of Tables

Acknowledgements

My deepest gratitude goes to my advisors Andrea Ogston and Chuck Nittrouer, whose guidance and support were essential to my development as a scientist. More than just academic advisors, their friendship and mentorship saw me through the ups and downs of my journey at UW. I would also like to thank my committee members, Mark Holmes, Parker MacCready, and Si Simenstad, for their patience and insight. Additionally, I would like to thank Dick Sternberg taking me under his wing and for his willingness to read and edit my raw, first attempts at scientific writing.

I greatly appreciate the support of my lab mates over the years, including Tina Drexler, Emile Flemer, Rip Hale, Katie Boldt, Dan Nowacki, Aaron Fricke and Emily Eidam. A tremendous amount of field work and logistics went into this project and I would like to thank the crews of R/V Barnes and R/V Centennial, the School of Oceanography engineering staff, and the multitude of graduate and undergraduate students who assisted me.

Lastly, I'd like to thank my friends and family for their continued love, support, and encouragement.

1 Chapter: Introduction

1.1 Broader context

Rivers are the major source of sediment to the global ocean, and small mountainous rivers play a disproportionately large role in this supply (Milliman and Syvitski, 1992; Milliman et al., 1999). Rivers deposit sediment upon entry into the marine environment creating deltas, which consist of three main strata, the topset, foreset and bottomset (Fig. 1.1). Sediment delivery to deltas is controlled by the rate of river discharge (Syvitski et al., 2000), sediment availability within the drainage basin that may vary temporally with deglaciation, tectonic activity and human engineering (Milliman and Meade, 1983; Milliman and Syvitski, 1992; Syvitski et al., 2005; Vörösmarty et al., 2003). Over a 100-yr timescale, event-driven sedimentation is a major component of strata formation (Palinkas and Nittrouer, 2007; Wheatcroft and Drake, 2003) with high-river discharge periods providing most of the annual load (Syvitski et al., 2000).

Once discharged from the river, sediment dispersal is controlled by oceanic effects (Wright and Nittrouer, 1995) and related depositional patterns have been defined for fluvial dispersal systems, e.g.: Eel River, with a bulls-eye pattern offshore (wave-dominated)(Wheatcroft et al., 1997), Fly River, with a prograding clinoform foreset (tide-dominated)(Harris et al., 1993; Walsh et al., 2004), and the Rhone and Po River systems, where currents direct sediment along shelf (Palinkas and Nittrouer, 2007).

In contrast to these regions, fjords are commonly associated with strong tidal currents with macro to meso tidal ranges, limited wave action, relatively large sediment supply and complicated receiving basins. And while fjords behave as sediment sinks (Jaeger et al., 1998), the sediment dispersal and accumulation within these basins is not well studied.

This study investigates the mechanisms that dictate fluvial mud dispersal into constrained receiving basins, through observations of both water column processes and seabed deposits. Fine-grained particles (muds, <63 μm) are the dominant grain size discharged by rivers, which pollutants readily adsorb to, making an understanding of the fate of these particles key to tracking ecological hazards in the marine environment. These properties are also ideal for use in geochronological studies, and muds can be documented both in the water column transported in suspension (i.e., not complicated by complexities of bedload transport) and within the seabed.

The tectonically-active Olympic and Cascade mountain ranges provide an abundance of small mountainous rivers that discharge into the Salish Sea (Puget Sound and the Strait of Juan de Fuca and Strait of Georgia; Fig. 1.2). This receiving basin is composed of a series of glacially carved valleys, which were drowned by Holocene sea-level rise. Here, tides combined with complex morphology drive strong currents (~100 cm s^{-1}) and these interactions can act as a control on delta progradation

(Barnhardt and Sherrod, 2006; Bornhold and Prior, 1990). Previous glaciation has also driven large fluctuations in sea levels from +180 m to -60 m due to isostatic glacial loading and rebound (Dethier et al., 1995; Hutchinson et al., 2004; Mosher and Hewitt, 2004), which can affect shoreline evolution over longer timescales (Barnhardt et al., 1997; Galster and Schwartz, 1990; Hewitt and Mosher, 2001; Kelley et al., 2005; Shipp et al., 1991). Thus this region represents an ideal setting to compare the modern processes and evolution of small mountainous river deltas that build into insular seas.

1.2 Organization of Text

The overall objective of this work is to compare and contrast river deltas within the Salish Sea in order to determine, over various time scales, the fate of sediment particles. Specifically, to evaluate sediment dispersal, deposition and accumulation on the Skagit and Elwha River deltas (Fig. 1.2) where fine-grained sediment particles are traced on a delta topset (Chapter 2) and beyond, through the entire delta system (Chapters 3 and 4). The observed processes and delta formation are then evaluated with respect to basin morphology (Chapter 3) and regional sea level (Chapter 4). The findings in this thesis are based on a) water-column measurements including long-term bottom-boundary-layer time-series measurements and water-column profiles of salinity, temperature, suspended sediment and velocity, b) seabed sediments samples including grabs and cores (ranging from 30 to 400 cm long) and c) geophysical tools

(multibeam bathymetry and seismic reflection profiling) used to observe sediment transport, deposition and accumulation over various timescales.

In Chapters 2 and 3, the temporal (tidal impacts, river discharge) and spatial (basin geometry) variations in sediment dispersal and accumulation on the Skagit River delta were examined. The research included in Chapters 2 and 3 was completed in conjunction with a larger research effort focused on mesotidal flats (Nittrouer et al., 2013). Chapter 2 examines mud deposition, seabed reworking and sediment bypass on a sandy tidal flat (delta topset). The premise behind this chapter is that physical processes operating on an intertidal delta topset dictate retention of fine-grained sediment, or its export to deeper water. Chapter 3 evaluates the role of basin geometry on the Skagit River system through the documentation of sediment dispersal and accumulation of two distinct receiving basins (delta bottomset). It then compares the depositional patterns of the Skagit system to those of other deltas. It is proposed that basin geometry has a significant impact on physical processes, and together these dictate the depositional patterns of river deltas within insular seas.

In Chapter 4 oceanic measurements are paired with traditional geophysical tools to contrast coastal sediment processes occurring today with ancient deposits formed by similar processes throughout the Holocene. This chapter considers a longer range of timescales (tidal to 1000-yr), evaluating modern sediment dispersal (tidal impacts, river discharge) and interpreting the depositional history of the Elwha delta (~9,000

yrs). A premise is that modern observations of oceanic condition can be used to aid in the interpretation of delta evolution over longer timescales.

The three chapters were originally written as separate articles that have been published or are in preparation for submittal to peer-reviewed journals. This leads to some repetition between chapters, especially in the Background and Methods sections. Chapter 2 was published in Continental Shelf Research (Webster et al., 2013) and Chapters 3 and 4 are in preparation. Chapter 2 was written with coauthors Chuck Nittrouer and Andrea Ogston. Chapter 4 was written with coauthors Andrea Ogston, Chuck Nittrouer and Mark Holmes. The concluding chapter, (Chapter 5) summarizes the primary contributions of the dissertation.

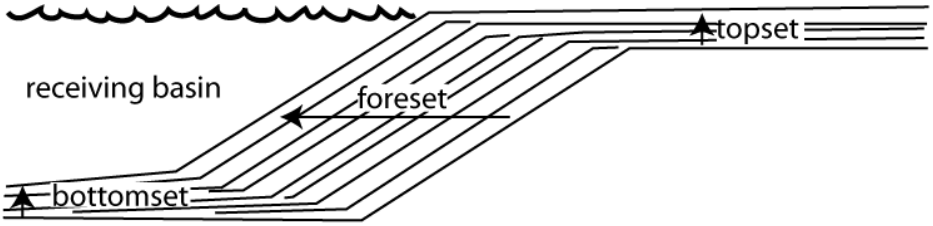

Figure 1.1. Schematic of a Gilbert-type delta, with topset, foreset and bottomset bed locations (modified from Nemec, 1990).

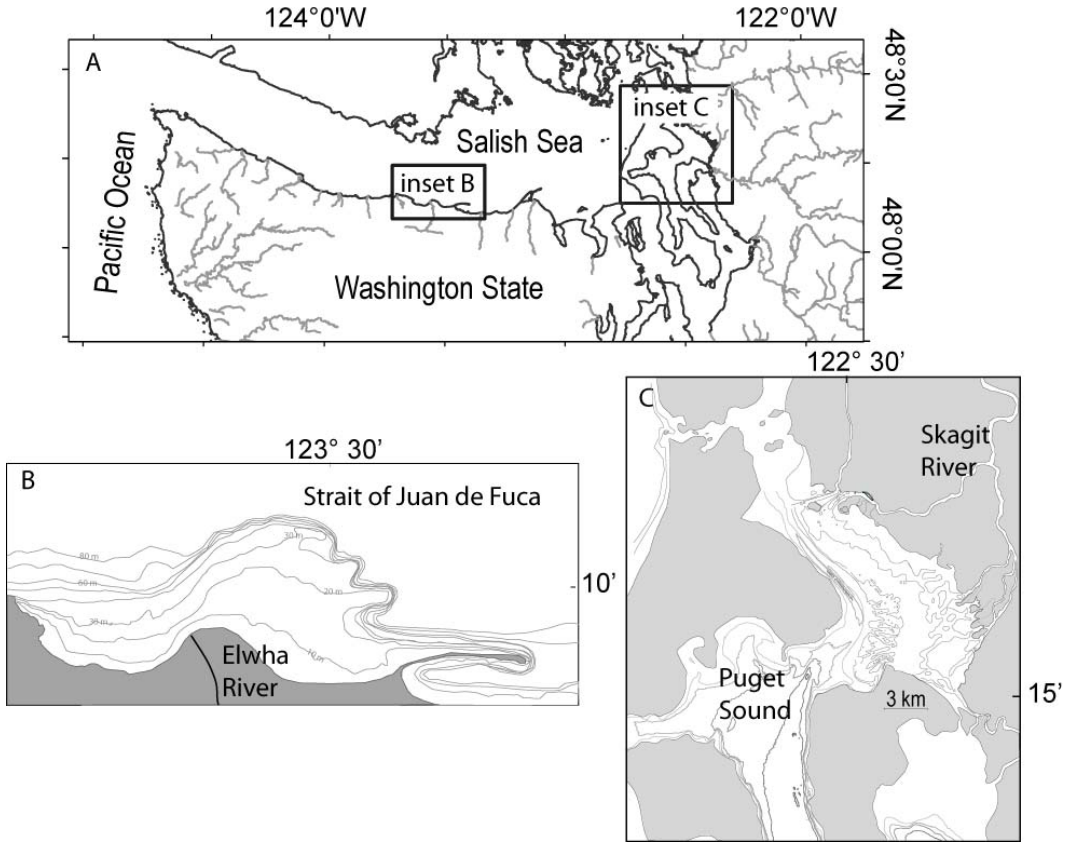

Figure 1.2. A) Map of northwestern Washington State, black box outlines locations of study area. B) Map of Elwha River receiving basin, located within the Strait of Juan de Fuca. C) Map of Skagit River receiving basin, located within Puget Sound.

2 Chapter: Delivery, reworking and export of fine-grained sediment across the sandy Skagit River tidal flats

2.1 Introduction

Sandy intertidal flats can be found in deltaic settings (Hale and McCann, 1982; Houser and Hill, 2010) and represent a gateway for particles between terrestrial and marine environments. Fluvial sediment must pass through complexes of intertidal channels and banks on the way seaward, creating a shallow (few meters) and broad (kilometers) estuarine environment. River discharge can vary seasonally and can be episodic, causing variation in the sediment and water reaching the flat (Wright and Schoellhamer, 2004). The morphology of the sandy flats commonly consists of shallow braided channels, which are subject to flow reversal on daily tidal cycles.

It is thought that tidal channels tend to be the preferred conduits for sediment and water crossing flats (Wells et al., 1990), due to a longer duration of inundation. However, sediment motion is driven by physical forcing in a different manner than water, especially in reversing flows, and net sediment transport can occur differently than net water transport (Ridderinkhof et al., 2000). The seabed of sandy tidal flats is also active, migrating bedforms rework the seabed and remobilize deposited particles (Dolphin et al., 1995), and distributary channels migrate laterally, cutting through the flat (Coleman, 1969). Previous studies of tidal flats have focused on the sediment and hydrodynamics within the water column (Christiansen et al., 2006; Christie and Dyer,

1998; Grabemann et al., 1997; Lee et al., 2004; Ridderinkhof et al., 2000; Talke and Stacey, 2008; Uncles and Stephens, 2000) or separately on the seabed surface and sedimentary structure (Dolphin et al., 1995; Hale and McCann, 1982; Reineck and Singh, 1967; Yang et al., 2008). However, particle transport is often stepwise, through multiple occurrences of deposition and resuspension (Christiansen et al., 2002; Grabemann and Krause, 1989; van Leussen, 1991). To understand the fate of particles, it is important to study the coupling of the dynamic seabed to the water column.

On sandy tidal flats, the physical mechanisms for moving fine-grained material (mud) off the flats are not well understood. Currently, concepts such as settling and scour lags can explain the trapping of fine-grained material on flats (Pejrup, 1988; Postma, 1961). Much material delivered to deltaic sand flats is fine-grained, so there must be effective mechanisms that remove the mud. The timescales of physical variability hypothesized to dominate the tidal flats encompass fortnightly and semi-diurnal tidal cycles, as well as episodic storm activity and river discharge. To understand the seabed structure and the mechanisms by which the fine-grained sediment is removed from the flat, we paired seasonal and rapid-response seabed observations with deployments of small instrumented tripods and spatial studies of water-column observations. We are able to examine the temporal and spatial variations of fine-grained sediment deposition on the seabed concurrently with observations in the

water column, and document delivery, reworking and export of fine-grained material across and off the flat.

The premise behind this study is that processes operating on tidal flats dictate retention of fine-grained sediment, or its export to deeper water. Specifically, the objectives are to: 1) evaluate where, if ever, mud is deposited and under what discharge conditions; 2) investigate the mechanisms of transport of fine-grained sediment within tidal channel networks; and 3) examine the mechanisms that remobilize deposited sediment.

2.2 Study Area

The Skagit River discharges into the Salish Sea, the inland water body located on an active continental margin in Washington State and British Columbia (Fig. 2.1). Mesotidal conditions combine with complex morphology to drive strong tidal currents in the region. Within the Salish Sea, wave energy varies due to shoreline orientation of the small basins, which affects fetch relative to the predominant wind direction from the south. The temperate maritime climate receives 100 cm y^{-1} of precipitation in the Puget lowlands and 230 cm y^{-1} in the mountains.

The Skagit River originates in the Cascade Range and is 240 km in length, with a drainage basin of 8,500 km^2. It flows into Whidbey Basin of Puget Sound, and its delta has nearly filled the receiving basin, which has created a high-energy channel

between the Skagit tidal flats (delta topset) and Whidbey Island, referred to as "Whidbey Channel" (Fig. 2.1). The river hydrograph is bimodal, with one peak during the late spring and early summer freshet (May-July) and another during late autumn and winter as a result of storms (Oct-Feb) (Fig. 2.1D). Measurements of the annual suspended-sediment discharge at Mount Vernon, located 25 km from the mouth, ranged from 0.9 to 4.4 Mt y^{-1} between 1980 and 1991 (Collins, 1998). The upper limit occurred during the largest event (1990) over the 1946-2011 record. Downstream of Mount Vernon, at the apex of delta, the river splits into North Fork and South Fork distributaries, which carry 55-70% and 30-45% of the water, respectively (Hood, 2007; Yang and Khangaonkar, 2009).

The Skagit delta is a productive agricultural region, and protection of the fertile floodplain has caused >90% of the 327 km^2 delta topset to be isolated from riverine and tidal influence (Collins et al., 2003). The remaining marsh occurs along distributary channels in the South Fork region and to a lesser extent in the North Fork region (Hood, 2006). The distributaries then enter a tidal flat mostly composed of sands (McBride et al., 2006), which has two braided channel networks (south and north) and an unchannelized segment between them (see aerial photo in Fig. 2.1 of Chen et al., 2010 and Nittrouer et al., 2013). The South Fork network consists of many shallow (<2 m) braided channels oriented across the flat. The North Fork is more confined on the marsh and flat by a jetty and by islands (Ika and Goat islands) and has fewer but deeper channels. Because of this, the North Fork is a distributary

channel, which enters the flat at one location and bifurcates into a channelized network that is constrained to the north (Fig. 2.1). Channels through the marsh can be purely tidal channels (known as "blind" channels), or Skagit River distributary channels. The blind channels are old distributaries no longer connected to the river (Hood, 2006). The active distributary channels through the marsh show evidence of avulsion, but recently only in response to extreme storms (e.g., 30-y storm) (Hood, 2010). In comparison, channels on the sand flat can move >100 m within a decade (Hood, 2006), or disappear in as few as 4 y (Hood, 2007).

2.3 Methods

2.3.1 Field methods

Data collection (2008-2009) consisted of: water-column profiles collected by combinations of CTD systems (Conductivity, Temperature and Depth) with OBS (Optical Backscatter Sensor for suspended-sediment concentrations) and boat-mounted ADCP (Acoustic Doppler Current Profiler for water velocity); and long-term bottom-boundary-layer measurements using time-series bottom tripods. Seabed sediments were collected using grab samples, push cores (~30 cm long), box cores (~50 cm long), and vibracores (~4 m long).

Three conditions are defined for this study based on river discharge: quiescent periods with low river discharge (Mar-Apr and Aug-Sep); summer freshet with high river discharge, which coincides with the summer solstice when diurnal tidal ranges are

greatest (May-Jul); and autumn-winter periods with episodic river discharge (Oct-Feb) (Fig. 2.1). The Skagit River daily water discharge data for these periods were obtained from the gauging station located in Mount Vernon, WA (USGS gage 12200500, http://waterdata.usgs.gov/nwis/).

2.3.1.1 Water-column processes

In Jun-Jul 09, CTD/ADCP transects were completed in the South Fork portion of the flat (Fig. 2.1). Spring tides were the focus, as they were hypothesized to display a strong signal of sediment export. The transects across the flat in channel Q (Fig. 2.1) were from the middle flat (~2.5 m) to outer flat (~4.5 m), each transect included 5 to 8 stations, and was completed within 30 min. On station, the CTD and OBS were lowered through the water column by hand, and simultaneously a water sample was collected ~0.25 m below the water surface. The water sample (~1 L) was passed through a nitrocellulose 0.47-µm filter to measure suspended-sediment concentrations (SSC) and to calibrate the OBS. When the initial bulk OBS calibration using bottle samples (34 bottle samples; R^2 value of 0.51) failed to plot linearly, two separate OBS calibrations were completed by separating flood tide (16 bottle samples; R^2 value of 0.70) and ebb tide (11 bottle samples; R^2 value of 0.75), and two linear transformations were applied. This difference in calibration suggests smaller particles during flood and larger particles during ebb tides. The 1200-kHz ADCP collected velocity data in 0.25-m bins while transiting between stations, and provided currents and backscatter throughout the water column.

2.3.1.2 Bottom-boundary-layer time-series data

Time series instruments were deployed on the flats within both the North and South Fork channelized regions in Aug 08, Nov 08, and Jun 09 to capture fortnightly tidal cycles. Deployments were composed of a small tripod system containing an ADV (Acoustic Doppler Velocimeter) with sensing volume at ~15 cm above the seabed (cmab), CTD (60 cmab), and OBS (15 cmab); except for Nov 08 and Jun 09 at the North Fork site, when an upward-looking Aquadopp current profiler was deployed. In Jun 09, additional tripods were deployed at the South Fork: one within channel Q at -1.78 m MLLW; and the other on the adjacent flat at -1.35 m MLLW.

The tripod legs were equipped with a 0.3-m-diameter foot to prevent settling into the seabed, and each leg was anchored 0.3 m into the seabed to prevent dislodgement. Tripod settling was tested by applying 65 kg of body weight and no change in bed elevation was observed. In addition, time series pressure data was inspected for evidence of settling, both in episodic events and trending over the deployment. No settling was evident.

Measurements were obtained at 2 Hz every 30 min for 6-min burst length. The Aquadopp collected velocity data in 10-cm bins. Data retrieved from each instrument (Table 2.1) were evaluated and were disqualified for periods when sensor correlation value was low, for example at low tides when sensors were out of water. Data were averaged over the sample interval (6 min) to obtain mean half-hourly currents, and

were rotated into north and east coordinates. Progressive vector diagrams were completed by summing the current velocities. Bottom shear velocities were calculated using the Karmen-Prandtl equation, and a friction factor of 0.008 was assumed (Nikuradse, 1950).

Suspended-sediment measurements included surface bottle samples at the tripods and nearby locations. In addition, at instrumented sites, uncalibrated ADV backscatter measurements were obtained and are used as a proxy for relative SSC within a deployment. Each technique measures slightly different suspended-sediment characteristics, and therefore some inconsistency is expected. Optical backscatter observations at the tripod were unreliable due to biological fouling through much of the time-series deployments, and mass balances are not possible with these data sets.

2.3.1.3 Seabed coring

On the flat, sediment samples were collected seasonally (Jun 08, Aug 08, Nov 08-Jan 09, Jun 09) using a mini Van Veen grab sampler during high tide, and by hand using push cores at low tide. The push cores were collected with Plexiglas trays (2.2 cm thick x 11 cm wide x 30 cm long). Longer cores were collected using a portable vibracore system with aluminum barrels (7.5 cm diameter, ~400 cm long). The vibracores were cut into 30-cm sections and split; a 1-cm-thick center slab was examined by x-radiography and the remainder of the core was subsampled for textural and radioisotopic analyses. On the prodelta, box cores (20 x 30 cm cross

section, 50 cm long) were collected from ship in Feb 09, along with surficial Shipek and Van Veen grab samples. Box cores and grab samples were subsampled for textural and radioisotopic analyses.

2.3.2 Lab methods

Sediment slabs collected with push cores (tidal flat), box cores (prodelta) and vibracores (tidal flat) were examined for sedimentary structures using a digital x-ray imaging system. Results are presented as x-radiograph negatives, where opaque areas (light color) have greater bulk density and coarser sediment relative to transparent areas (darker color) with low bulk density and finer sediment. X-radiograph images were enhanced to heighten contrast within each image, and bulk density is not necessarily comparable between images.

2.3.2.1 Grain-size analysis

Sediment samples (~12 g) were homogenized, mixed with the dispersant sodium hexametaphosphate, and placed in a sonic bath for 15 minutes. Then samples were wet-sieved at 63 μm to separate the fine and coarse fractions. The size distributions were measured for the silt and clay fractions using a Micromeritics® Sedigraph at ¼-phi intervals, and for the sand fraction using a 2-m automated settling column. If a sample had <10% of either fine or coarse fractions by mass, size distributions were completed for only the fraction >90%.

2.3.2.2 Radioisotope analysis

Sediment samples were analyzed for the radioisotopes ^{7}Be and ^{137}Cs by gamma (γ) detection (Mullenbach and Nittrouer, 2000; Sommerfield and Nittrouer, 1999), and their activity was determined from the 477.7 and 661 KeV γ spectra photo peaks, respectively. The short-lived isotope ^{7}Be was measured in surficial grab samples and box cores (upper 10 cm in 1-cm intervals) shortly after collection. ^{137}Cs and ^{210}Pb activities were measured in muddy sediment layers subsampled from vibracores. Activities were measured by alpha spectroscopy for ^{209}Po and ^{210}Po, and ^{210}Pb activities were calculated from the ^{210}Po content (Nittrouer et al., 1979). Supported ^{210}Pb activities (due to the decay of its effective parent, ^{226}Ra, in the seabed) were determined from Saratoga Passage samples deep in the cores.

2.4 Results

2.4.1 River discharge and tides in Skagit Bay

Over the year of sampling (Oct 08-Sep 09), the mean Skagit River discharge was ~480 m^3 s^{-1} (Fig. 2.1D), nearly equivalent to the long-term average flow over the gauging records (470 m^3 s^{-1} between 1941 and 2009). The distinguishing events over the year were three floods in response to storms on 8 Nov 08, 13 Nov 08, and 8 Jan 09 reaching hourly discharges of 1830 m^3 s^{-1}, 1890 m^3 s^{-1}, and 2260 m^3 s^{-1}, respectively. The snowmelt freshet peaked in early Jun 09, reaching 930 m^3 s^{-1}. Over the Aug 08 instrument deployment, the river was in low flow, while discharge was

variable and high in the Nov 08 deployment and consistently high in the Jun 09 spring freshet deployment (Table 2.1).

The Nov 08 and Jun 09 tripod deployments were over full fortnightly tidal cycles, with maximum tidal ranges of ~4.3 m and ~4.5 m, respectively (Fig. 2.2; Fig. 2.3). The Aug 08 instrument was deployed for 7 days, and recorded a maximum tidal range of ~3.3 m.

2.4.2 Time-series data

2.4.2.1 Currents

Currents at elevations of ~15 cmab on the Skagit tidal flat ranged from 0 to 70 cm s^{-1}, and varied with the tidal cycle, in which maximum currents occurred at late ebb. At the North Fork site, currents were similar in both Aug 08 and Nov 08. Maximum currents reached 35 cm s^{-1}, and cumulative velocities were directed offshore and northward, obliquely flowing off the flat (Fig. 2.4B; Table 2.1).

At the South Fork site, in Nov 08 (Fig. 2.3), maximum currents reached 40 cm s^{-1} at the start of the deployment and weakened through the deployment; however, our ability to interpret these magnitude changes was limited by seabed elevation changes relative to the sensing volume. Bed shear velocities peaked at the start of flood tides, and reached a maximum value of 1.7 cm s^{-1} during spring tides (Fig. 2.3).

The Jun 09 deployment (Fig. 2.2), allowed for a comparison of dynamics within the South Fork channel network. Greatest velocities were found within the channel, where maximum velocities reached 70 cm s^{-1} at the end of the ebb during the spring tides of the fortnightly tidal cycle. A typical tidal period had peak ebb velocities that were >40 cm s^{-1} and peak flood velocities that were 20-30 cm s^{-1}. On the nearby nonchannelized seabed, or nearby "flat surface", maximum velocities were less than those in the channel and reached ~50 cm s^{-1} at the end of ebb tide during the spring tidal cycle. Other tidal flows on the flat surface were similar to those in the nearby channel as seen in the detailed time series (Fig. 2.5). Wave-orbital velocities in the channel and on the flat surface were greatest at lowest recorded water elevations, reaching ~10 cm s^{-1}. The sensor located on the higher elevation flat surface was exposed and unable to record data for a longer portion of low tide. Progressive vector diagrams of velocity both in the channel and on the flat surface indicate that net currents were down channel (seaward) (Fig. 2.4A). Shear velocities within the channel had greatest values at the end of ebb tides and start of flood tides, ranging from 1.0 to 3.5 cm s^{-1} over 9 days, with maximum values occurring during spring tidal cycles (Fig. 2.2). On the flat, maximum shear velocities were less, but followed a similar pattern, with greatest shear velocities surrounding low tide and a maximum value of 2.7 cm s^{-1} at the end of ebb tide during the spring tidal cycle.

2.4.2.2 Suspended Sediment

Of all surface water samples, the greatest concentration was 232 mg L^{-1} collected on 13 Nov 08, where the North Fork distributary channel reaches the tidal flat. At the time-series locations, surface water had SSCs of 4-106 mg L^{-1} (Table 2.2). During the Aug 08 deployment, surface SSCs were <6 mg L^{-1}. The Nov 08 deployment had surface concentrations that were 45-106 mg L^{-1} during the high discharge event (13 Nov 08) and were 4-6 mg L^{-1} during typical winter discharge (Dec 08 in Table 2.2). Following a Nov 08 storm, divers observed mud, wood and leaf litter in channels, highlighting the ability to transport much material at high discharge. During the Jun 09 deployment, surface-water samples at the tripod locations were 10-70 mg L^{-1}. Samples collected during rising tides fell within the lower end of the SSC range for all tidal cycles.

Within the time-series data, the greatest acoustic backscatter values were closely aligned with maximum ebb and flood currents (Fig. 2.5), a time of little water over the flat. During this period, collection of bottle SSC was not possible, and therefore the range is likely biased towards the low end. The smallest SSC values from the acoustic backscatter were observed at high tide and the largest values occurred just before and after low tide.

2.4.2.3 Seabed-elevation change

Seabed elevation as recorded with the ADV altimeter showed changes on the order of 1 to 5 cm. The Nov 08 deployment had rapid bed aggradation during low tides on 17-19 Nov 08. The waning winter flood of Nov 08 (Fig. 2.1) aggraded the bed of the channel at this site at least 5 cm (Fig. 2.3), an elevation maintained throughout the following 10 days of the deployment.

During the Jun 09 deployment, the bed fluctuated by 1-2 cm on tidal time scales (Fig. 2.2). On the flat surface, the seabed rose ~1 cm over a low-tide period, and subsequently remained stable (Fig. 2.5). In the channel, the seabed rose 2 cm over the first low tide cycle and then elevation remained steady (Fig. 2.5). The bed eroded ~1 cm during the following low-tide cycle (Fig. 2.5). Reliable observations within the channel over six semi-diurnal cycles of spring tides showed that the bed elevation changed by +/- 0.74 cm. On the nearby flat surface, over eight semi-diurnal cycles, bed elevation changed by +/- 0.43 cm (Fig. 2.2).

2.4.3 Hydrography during the late spring-summer freshet

Over a spring tidal cycle with a 4 m range, the flood-tide water column had a strong horizontal gradient in salinity and temperature (Fig. 2.6A) across the 2.25-km Q transect. Salinity varied from 0 psu at mid flat to 25 psu at the seaward flat edge and temperature varied from 15° to 9°C. Vertically, a thin surface plume of less than 50 cm was identified by lower salinity and higher temperatures (Fig. 2.6A). The greatest

values of SSC were found on the mid-flat (100's of mg L^{-1}) and lowest values (10 mg L^{-1}) were on the outer edge of the flat. Velocities were in the shoreward (east) direction and typical magnitudes ranged from 40 to 70 cm s^{-1}.

In contrast, on the greater ebb tide (associated with higher-high to lower-low tides), the water column was vertically well mixed and uniform in salinity and temperature (Fig. 2.6B). There was a weak horizontal gradient in salinity (12-15 psu) and no gradient in temperature (12°C) over the outer flat. All SSC values across flat were >50 mg L^{-1} with concentrations >100 mg L^{-1} within 10 cm of the bed (Fig. 2.6B). Velocities were in the offshore direction (west) and magnitudes ranged from 50 to 100 cm s^{-1}. The most seaward profile was beyond the flat edge and within Whidbey Channel, where the upper 2 m of salinity and temperature was consistent with the water-column structure over the flat, and currents were directed off-flat at slightly lower magnitudes (50-65 cm s^{-1}). Current measurements deeper than 2.5 m within Whidbey Channel, were southward at ~40 cm s^{-1}.

Over a neap tidal range of 1.4 m, water-column properties of channel Q were vertically stratified over the outer-flat transect (Fig. 2.6C). On the lesser ebb (associated with lower-high to higher-low tides), salinity and temperature were relatively uniform horizontally. Vertically, there was a strong gradient in both temperature and salinity. The surface salinity was 0 psu and nearbed it was 28 psu; the temperature was 16°C at the surface and 12°C near the bed. SCC values were

lower (<10 mg L^{-1}) than during the spring tidal cycles (Fig. 2.6C). Velocities were in the seaward (west) direction and magnitudes ranged from 15 to 60 cm s^{-1}, with most measurements <35 cm s^{-1}.

2.4.4 Seabed grain-size characteristics

The grain-size distribution across the flat (Fig. 2.7) is characterized by well-sorted fine sand, with 1-3% mud content (i.e., sediment with grain size <63 μm). Over the vast majority of the tidal flat, these distributions remained constant. Locations with greater mud percentages (up to 60% mud fraction) had a high level of seasonal and spatial variability, and were found in and near (<75 m) channels. In general, the greatest mud percentages were found within channels at the seaward edge of the flat (Fig. 2.7), where channels deepen. At a few locations, mud percentages reached 20-60% (Fig. 2.7).

After high-discharge events of the river, some fine-grained sediment was observed mixed with sand in and near channels on the mid and inner flat. For example, following a flood on 8 Jan 09, high-porosity muddy sand was found within and adjacent to a channel in a small splay deposit (overbank sediment deposit formed at flood stage) with spatial extent of ~75 m x ~250 m. The deposit consisted of 23% sand and 77% mud (silt and clay), and was not present in the previous (Aug 08) sampling period. The earlier surface sample from this site was 98% sand, 2% mud.

The splay deposit may have formed from the high-discharge event 8 Jan 09 or may have preserved the cumulative effects of the winter storm season.

2.4.5 Fine sediment deposits and radioisotopes

2.4.5.1 Recent mud deposits

In Aug 08, no ^{7}Be was detected in surface seabed samples, indicating the absence of recently deposited fluvial sediment. During winter sampling, ^{7}Be was found at the seaward edge of the tidal flat and in a channel splay deposit adjacent to a North Fork channel (Fig. 2.8). Jun 09 surface sampling showed ^{7}Be associated with the flat edge and channels; on the middle flat, the presence of ^{7}Be was found in one sample (in a channel within the South Fork network). The middle flat of the North Fork channelized region was not sampled in Jun 09.

X-radiographs from the upper 30 cm of the bed exhibited sandy cross bedding and climbing ripples (Fig. 2.9A). At the seaward flat edge, the sedimentary structures commonly had buried mud layers 1-2 cm thick with evidence of bioturbation. In the recent mud layers and splay deposits, x-radiographs revealed a mixture of physical sedimentary structures. A core collected within a channel following the 8 Jan 09 flood contained parallel laminations (8-cm thickness) between layers of cross-bedded sand (Fig. 9B). Adjacent to the same channel, a splay deposit had a 1-3 cm muddy layer draped over a sandy ripple, (2-5 cm depth) interpreted as flaser bedding, which consists of alternating sand and mud layers (Fig. 2.9C). The recent splay deposit

accounted for the upper 10 cm of the bed (Fig. 2.9C). X-radiography paired with grain size also showed some mud layers below the sandy flat surface, typically in the flanks of channels (Fig. 2.7D; Fig. 2.9D). In Feb 09, following the winter storm season, ^{7}Be was present in surface samples beyond the tidal flat (i.e., in water depths >4.5 m), within northern Saratoga Passage and seaward of the North Fork (Fig. 2.8).

2.4.5.2 Long-term fine-grained sediment retention on flat

Two vibracores were examined from the vicinity of the North Fork channel network (Fig. 2.1C), and the cores contained preserved physical sedimentary structures composed of sand with some mud layers 0.5-2 cm thick (Fig. 2.10). The bulk sand percentages within the cores were 85-90%, and ranged from fine to medium sand. The x-radiographs revealed parallel layers, small ripple cross bedding, and interbedded mud and sand (Fig. 2.10). Individual mud layers were typically composed of thin parallel laminations in packets 20-50 cm thick (Fig. 2.10). With the mud were isolated wood fragments and layers 5-30 cm thick that were composed of wood chips. Radioisotopic analyses of the muddy layers in the inner-flat core, B3, found ^{137}Cs down to 189 cm below the surface (not deeper) and excess ^{210}Pb throughout the 210-cm long core. The maximum depth of ^{137}Cs in the outer-flat core, B1, was more difficult to constrain. ^{137}Cs was found 30 cm beneath the seabed, and was absent in the next mud layer at 147 cm. Excess ^{210}Pb was identified in the B1 outer-flat core at ~163 cm (interval 160-165 cm) below the surface, but not at the next interval (165-170 cm) or below.

2.5 Discussion

Tidal flats composed mostly of sand are found around the world, and are commonly associated with a great sediment supply and energetic wave conditions (Hale and McCann, 1982; Yang et al., 2005). The seabed on the Skagit tidal flats is dominantly sandy with mud found only isolated in time (after floods) and space (near channels; on outer flat). An estimated 1-4 Mt y^{-1} of suspended sediment is delivered by the Skagit River (Collins, 1998), and yet little of this mud is preserved on the flats. In other tidal settings, mud is thought to accumulate due to net landward transport (e.g., Carling, 1982), overtopping the tidally influenced river distributary channels and trapping by vegetation. Between the limited salt-marsh and outer-flat muds, only a small amount of the Skagit River fine-grained sediment can be recognized within the tidal-flat complex. It can, therefore, be hypothesized that physical transport processes on the flats are efficient at transporting mud to more distal parts of the dispersal system.

2.5.1 Evidence of mud deposition on the Skagit tidal flats

Episodic sediment delivery to the marine environment associated with high river discharge, has been documented in previous studies of small mountainous river systems (Kniskern et al., 2010; Ogston et al., 2000; Sommerfield and Nittrouer, 1999; Warrick and Milliman, 2003). Locally, discharge gauging records at Mt. Vernon (1981-1991) document that sediment is delivered from the Skagit River to the flats,

with the greatest discharge during winter floods (Collins, 1998). Therefore, not surprisingly, the amount of sediment observed in the water column over the flats also varies temporally (Table 2.1).

Although most of the intertidal area of the Skagit delta is covered with well-sorted sand (Fig. 2.7), some fine-grained sediment (mud) deposition was observed after high river discharge, and provides evidence of temporary mud deposition. Fine-grained material was found near channels on the middle flat both during the spring freshet and the winter storm season, and this sediment had ^{7}Be, which indicated deposition from a terrigenous (fluvial) source a short time before sampling (Fig. 2.8). Layering observed from near and within channels also provides evidence of deposition of fine-grained material (Fig. 2.9B, 2.9C). The flaser bedding typical of tidal flats (Reineck and Singh, 1986), was only observed under conditions of excess fine-grained sediment and rapid deposition (as evidenced by climbing ripples and mud drape; Fig. 2.9C).

Time-series measurements from the Nov 08 flood illustrate that sediment can be rapidly transported to and through channels, and the circumstances under which it is deposited. During the Nov 08 storm, surface suspended-sediment concentrations reached the greatest values observed on the flat (Table. 2.1), and resulted in at least 5 cm of deposition under the South Fork channel tripod (Fig. 2.3). This deposition occurred following the transition from ebbing to flooding tidal currents, a time when

our summer profiling studies showed highest concentrations of suspended sediment on the middle flat (Fig. 2.6A) and flow was dominantly constrained to the channels. Much of this bed elevation gain remained over the deployment, thus documenting that depositional events can occur during floods.

The observed sedimentary signals in the water column and on the seabed coincide with the seasonal delivery of terrigenous fine-grained sediment. Mud is most abundant on the flat in association with autumn-winter floods and the spring-summer freshet, and is deposited in and adjacent to channels. These associations suggest that the fine-grained sediment is supplied directly from the river. Previous studies of sandy and mixed grain-size tidal flats (Aubry et al., 2009; Lee et al., 2004; Yang et al., 2005) have shown seasonal mud deposition on the flat during mild wave energy with surficial grain size fining landward. In contrast, the Skagit River provides its flats with episodic sediment and freshwater input and surficial grain-size patterns are imparted by proximity to channels, similar to muddy tidal flats (e.g., Willapa Bay; Law et al., 2013).

2.5.2 Mechanisms of fine sediment export from the flat

Seabed evidence shows that Skagit River sediment is rapidly dispersed across the flat and beyond. Following both the winter storm season and the spring freshet, recent mud deposits occur on the outer edge of the tidal flat, where channels coalesce and deepen (Fig. 2.8), and velocities are reduced (Fig. 2.6). Recent mud deposits are also

observed beyond the tidal flat (e.g., Saratoga Passage; Fig. 2.8) following the winter storm season, having transited a distance of at least 10 km in several months or less. These observations suggest effective mechanisms for immediate sediment bypass of the flat.

The time-series data in the North and South Fork channelized regions show very different patterns of transport, which could be functions of instrument locations. The southern tripods were centrally located within the channel network (Fig. 2.1C), and net flow was west-southwestward (i.e., across-flat), parallel to channel orientation (Fig. 2.4A). The northern tripod was located on the southern edge of a channelized region, and net flow was west-northwestward (Fig. 2.4B), oblique to channel orientation. Here, greater ebb currents follow the local channel orientation; however, the greater flood currents were northward, likely driven by the flow in Whidbey Channel. On the northern inner flat, Pavel et al. (2013) observed velocities with net offshore components and slightly different along-flat components. Differences in net flow between study sites are attributed to placement within the channel network. Small-scale spatial differences on other flats have been attributed to tidal-flat geometry (Grabemann and Krause, 1989; Ridderinkhof et al., 2000; Uncles and Stephens, 2000). During the spring freshet on the Skagit tidal flats, our results show that the flow dynamics vary based on location within the channelized regions.

Physical modeling suggests ebb dominance of net flow in the summer due to frictional drainage, reinforced by river input at low tides, may cause sediment export (Nidzieko and Ralston, 2012). Yet the timing of suspended-sediment transport also is linked to the interaction between the tidal flows and water-column structure. This interaction controls the transport of sediment across the flats, retaining or releasing sediment, and dictating when sediment is exported from the flat. Greater flood tides constrained high concentrations of suspended sediment to the middle flat and the water column was stratified (Fig. 2.6A). During the greater ebb, suspended sediments were released and high SSC was observed across the middle to outer flat, within a well-mixed water column (Fig. 2.6B). Due to the sharp bathymetric gradient between the flats and Whidbey Channel, sediment transported during ebb tide is unlikely to return to the flats on flood tide, as indicated by the relatively low SSC observed on the outer flat edge during flooding spring tides (Fig. 2.6A; Table 2.2). A vertically mixed water column on the outer flat was observed during greater tides at a separate channel within the southern channel network (Ralston et al., 2013), suggesting the release of sediment on greater ebb tides is probable across the southern channels.

In addition, the greater flood and ebb tides produce currents that are able to resuspend and transport sediment throughout the middle to outer tidal flat. Bed resuspension on flood tide is suggested by enhanced nearbed SSC (Fig. 2.6A), and at the channel tripod (1.2 km landward of the observed zone of resuspension; Fig. 2.1C) by coincident shear velocities that reached 1.4 cm s^{-1} (Fig. 2.2). Based on Miller et al.

(1977), this is above the threshold of motion for the fine-sand seabed. Ebb currents reached larger magnitudes than those on the flood (Fig. 2.2A; Fig. 2.6B) and at the mid-flat site, bed shear stresses are great enough during ebb to put sand-sized sediment into suspension (Fig. 2.2) throughout falling and low tidal levels. Seaward sediment fluxes also were observed within channels at low tidal levels and modeled in Ralston et al. (Ralston et al., 2013) and Chen et al. (2010), respectively.

The observations show a lesser falling tide has a water-column structure that is vertically stratified with low velocities incapable of carrying sediment from the inner flat (Fig. 2.6C). Net currents flowed in the off-flat direction, but shear velocities at the tripod site reached only ~0.7 cm s^{-1} (Fig. 2.2), which is not sufficient to remobilize fine sand (Miller et al., 1977). The measurements of bed stress paired with the hydrography suggest settling and temporary deposition within channels may occur, especially at neap tides. Model results discussed by Ralston et al. (Ralston et al., 2013) and Chen et al. (2010) support deposition on the inner flat with decreased tidal range and increased stratification. However, we find limited evidence of fine-grained sediment on the middle to inner flat (Fig. 2.7), despite extensive surficial seabed sampling. The absence of fine-grained sediment deposition on the tidal flat suggests that any material deposited in the inner and middle flat during neap tides is subsequently removed with stronger tidal currents.

During the spring freshet, we observed rapid transfer of fine-grained sediment across the flat during greater tides and the potential for deposition on lesser tides. However, there is little evidence of fine-grained sediment on the seabed. Traditionally, tidal flats are considered importers of fine-grained sediment (Nowacki and Ogston, 2013; Pejrup, 1988), and tidal channels have been shown to trap sediments (Boldt et al., 2013; Wells et al., 1990). On the sandy Skagit tidal flat, the channels act as both tidal conduits and deltaic distributaries and are observed to rapidly export fine-grained sediment.

2.5.3 Dynamic seabed reworking and releasing mud

Sediment cores from across the tidal flat, including in distributary channels, contain physical structures that indicate seabed mobilization. Bedform migration is a mechanism that may release mud from the seabed. Seabed and hydrodynamic observations allow us to determine if and when the seabed is active and to what depth the seabed is reworked.

Crossbedding preserved within the seabed (Fig. 2.9A) and bed-elevation changes on the flat surface (Fig. 5) support that much of the expansive flat surface is mobilized on a daily cycle through bedform migration. Symmetric ripples observed on the sandy flat surface indicate formation by short-period waves with orbital velocities >10-15 cm s^{-1} (Allen, 1985). At times, measured wave-orbital velocities exceeded 10 cm s^{-1} (Fig. 2.2B), and may have been greater, as our instruments were unable to

record when water depths were <30 cm. Local winds are the driving force for wave generation and were strongest in the afternoon (Raubenheimer et al., 2013), generally coinciding with summer lower-low tidal levels, and creating conditions of enhanced near-bed wave-orbital velocities. Bedform migration was recorded in net bed-elevation changes of +/- 0.43 cm (Fig. 2.2B), suggesting active reworking on the order of a cm into the bed. Previous studies on tidal flats in Manukau Harbour, NZ, observed similar magnitude seabed mixing by wave ripples (Dolphin et al., 1995).

Tidal current measurements suggest the seabed is also mobilized in slightly deeper water depths. The peak bed stresses occurred in the channel as the water level approached the flat elevation, and flow was mainly channelized (Fig. 2.2A). Similar patterns have been shown in a separate channel of the South Fork network (Ralston et al., 2013) and on the muddy Willapa flats (Nowacki and Ogston, 2013). During observed spring tides, bed shear velocities (Fig. 2.2A) significantly exceeded the threshold of motion for sand-sized sediment (~1.2 cm s^{-1}, 2.5 Φ; Miller et al., 1977). On the nearby flat surface (Fig. 2.2B), bed stresses also exceeded the threshold for sand resuspension during a short period of time on the ebb tide, as the water level approached the flat elevation.

Measured tidal bed stresses and preserved crossbedding (Fig. 2.9B) suggest a second mechanism of reworking due to asymmetric bedform migration. The fine-sand seabed and peak currents of 70 cm s^{-1} are conducive to bedload transport and

formation of unidirectional-flow ripples to megaripples (Reineck and Singh, 1986). Changes in bed elevation of +/- 0.74 cm were recorded in channels associated with the strong nearbed stresses (Fig. 2.2A), and were likely a function of bedform migration. This illustrates that channel-bed sediment on the order of centimeters deep is mobile and any fine-grained sediment in the seabed can be winnowed and placed into suspension. Thus, fine-grained flood deposits can be erased from the record, and the signature of flood deposits within channels can be lost.

A cored seabed deposit recorded another mode of bed mobilization within channels. Within a few days of the Jan 09 flood, a core was collected from within the North Fork channel network that had sandy fine-scale parallel laminations (Fig. 2.9B), which are interpreted as planar bedding deposited in a shallow channel under very high velocities. A 1-cm-thick layer of crossbedding overlies the laminae, and likely was deposited as flood conditions waned to subcritical. This crossbedded surface may have been reworked by reversing tidal currents after initial deposition. The parallel fine-scale laminations give evidence that velocities in channels are strong enough to reach critical flow. This observation further supports that hydrodynamics within channels range from lower to upper flow regime and can facilitate a range of bed mobilization (e.g., small ripples, megaripples, planar bed) (Simons et al., 1965). Therefore, the depth of reworking within channels could be larger than the 1-2 cm that were observed at instrumented sites (Fig. 2.5).

A third method of seabed reworking has a vertical scale of meters, and results from lateral channel migration across the flat over decades. The mud layers found in long cores (Fig. 2.10) are similar to the short-term surficial splay deposits found following the Jan 09 flood (Fig. 2.9C), and likely are flood deposits. Based on the presence of ^{137}Cs, an inner-flat core (B3) showed 189 cm of deposition within <50 y (Fig. 2.10). This is the result of lateral movements of the channel, in which fine sediment appears to have been deposited on a former channel bed and preserved by subsequent burial. As channels migrate across the flat, channel splay deposits fill the abandoned channel remnants and these deposits can retain fine-grained flood signatures. Based on excess ^{210}Pb, the outer-flat core (B1) showed deposition of 163 cm within <100 yrs, which also is likely due to lateral channel migration, although here the interpretation could be complicated by delta growth on the outer flat. The time scale determined by radioisotopic measurements indicates that the deeper channels near the North Fork were filled with both sand and fine-grained flood deposits within the last 50-100 y. This is the same time scale as documented channel migration (Hood, 2006), where large channels moved laterally 100 m within a decade. This active channel migration further illustrates the dynamic nature of the sandy flat seabed.

As the channels move laterally back over these sites, the deposits will be remobilized, releasing the fine-grained sediment. In a braided system with rapidly migrating channels, buried mud deposits are ephemeral features that can be easily erased from the sedimentary record. Meandering channels rework sediment on a decadal

timescale through a cycle of avulsion and channel fill extending to a vertical depth of 1-2 m. In contrast, muddy flat environments are more likely to have stable channels with little channel migration (e.g., Willapa Bay, Boldt et al., 2013).

2.6 Conclusions

Although other studies have found that >1 Mt of fine-grained sediment is delivered to the Skagit flats in most years (Collins, 1998), our observations show little of that sediment is deposited on the tidal-flat surfaces. What does get deposited is reworked and released on multiple timescales. Fine-grained sediment deposition was found only during the spring freshet and winter floods. The minor occurrence of fine-grained material on the seabed year round implies efficient mechanisms for transport across and removal from the flats.

^{7}Be observed on the outer-flat edge and prodelta region (>10 km from the mouth) provides evidence that Skagit River mud is rapidly transported across the tidal flats. Tidal flows are guided by the channel networks and net flows depend on the location within the channel network. For the channelized areas, greater flood tides temporarily confine freshwater and sediment on the inner to middle flat and greater ebb tidal currents act to draw them across the flat. Sediment reaching the deeper Whidbey Channel either settles at the outer-flat edge (where stresses are slightly reduced) or disperses beyond. Spring-tide observations record high-magnitude ebb-channel currents, coincident with a well-mixed water column, conditions capable of

maintaining resuspended particles throughout the water column and transporting them in the seaward direction.

Sediment deposited on the tidal flat during river flood periods is subject to bed stresses that can mobilize sands, creating bedforms that rework the seabed to several centimeters deep. Three types of reworking mechanisms are observed. 1) Wave-orbital ripples rework the seabed up to 1 cm deep. These likely are most active when shallow-water depths exist over the flat. 2) Unidirectional ripples are observed in channels and rework the seabed to at least 1-2 cm depths. These are most active when the strongest near-bed stresses occur, at tidal elevations where the water is shallow or non-existent over the flats (ebb and low tides) and flow dynamics are channelized. 3) Channel migration reworks the seabed on the order of 1-2 m deep and over decadal timescales. As channels migrate laterally, previous fill of abandoned channels is reworked and muddy deposits are released. All of these bed reworking processes likely act to winnow mud from the seabed.

Distributary channels on the Skagit flat deliver river-derived sediment to the flats, and tidal and riverine forcing moves fine-grained sediment efficiently off the flat. Therefore, the channels are recognized as being essential to the development of the sandy flat, and to the export of fine-grained material supplied from the Skagit River.

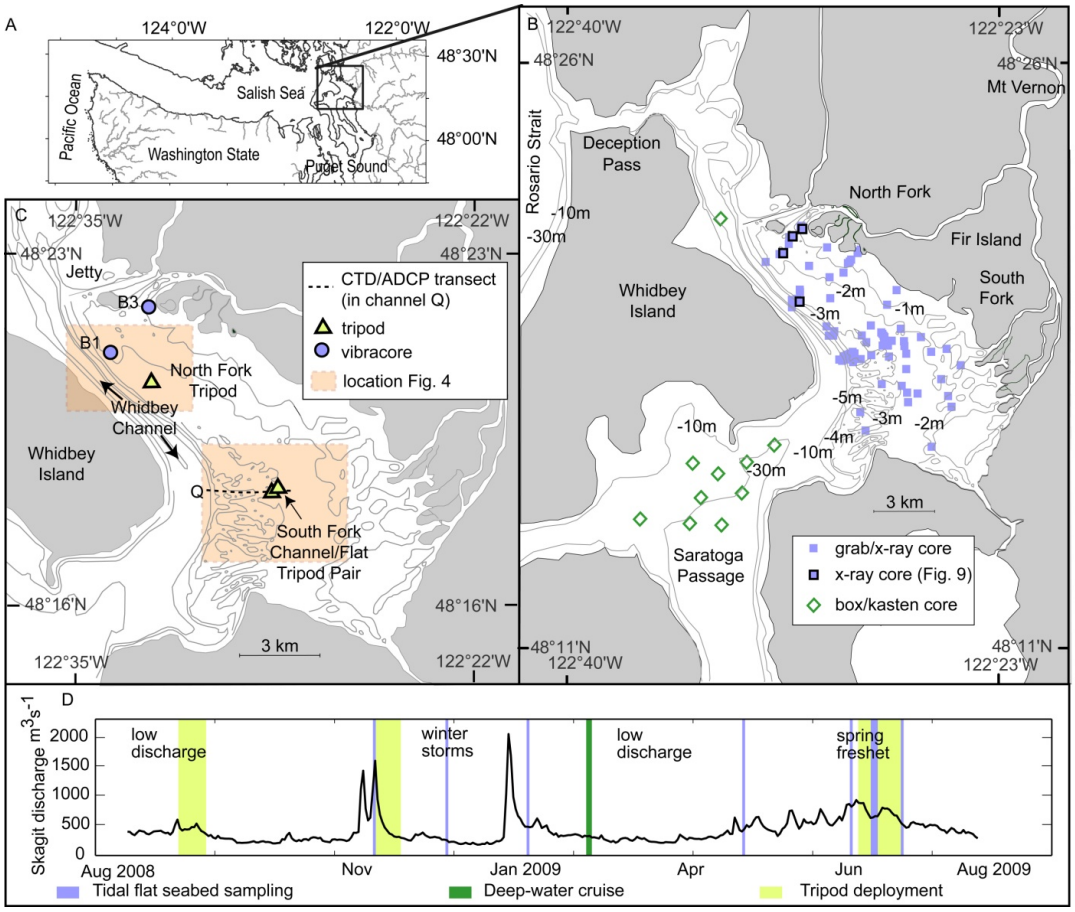

Figure 2.1. A) Map of northwestern Washington State, black box outlines location of study area. B) Map of Skagit River receiving basin. Sediment samples collected on tidal flat and collected in deeper basins (Saratoga Passage) are shown. The North and the South Forks of the Skagit River enter from the northeast and southeast sides of the tidal flats, respectively. C) North and South Fork tripod locations (triangles), tidal channel Q CTD transects (black dashed line), vibracore locations (circle) and location of Fig. 2.4 (orange box). To the west, the outer edge of the flat is bounded by a deep channel, referred to as "Whidbey Channel". D) Skagit River discharge during the sampling period. Seasonal sampling scheme during periods of freshet, winter storms and low discharge are indicated by vertical lines. Bathymetry from Yang and Khangaonkar (2009).

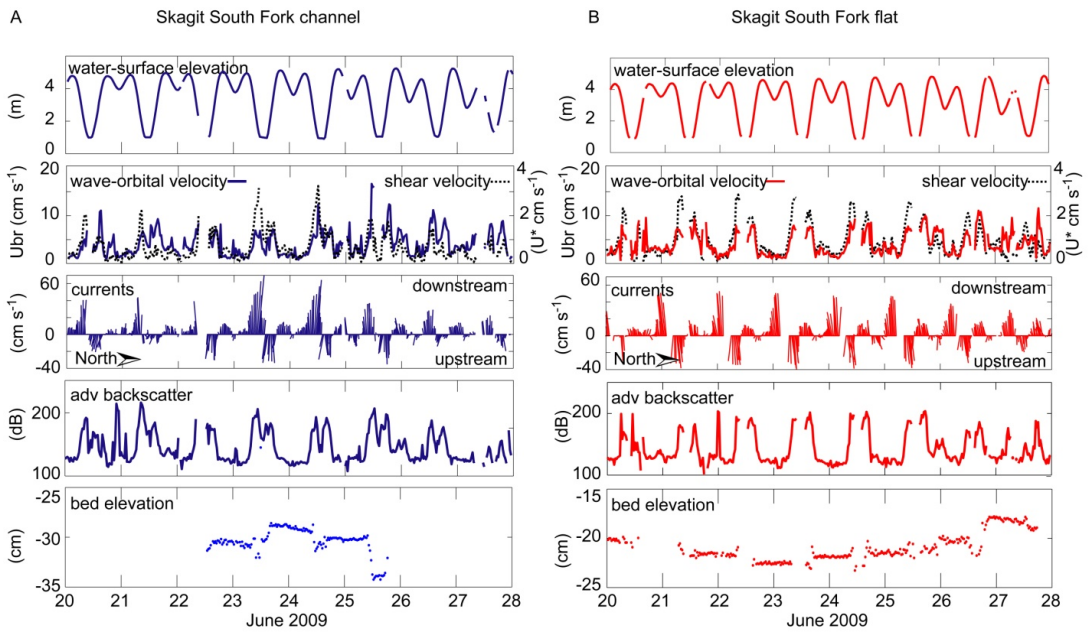

Figure 2.2. Time-series data from a channel (A) and a flat (B) tripod deployed on the southern flat in June 2009 for a 9-d period. Water-surface elevation, wave-orbital velocity, shear velocity, currents, ADV backscatter as a proxy for suspended-sediment concentration and bed elevation are shown. The values of bed elevation near low tide are unreliable because of the proximity of the water surface to the sensor.

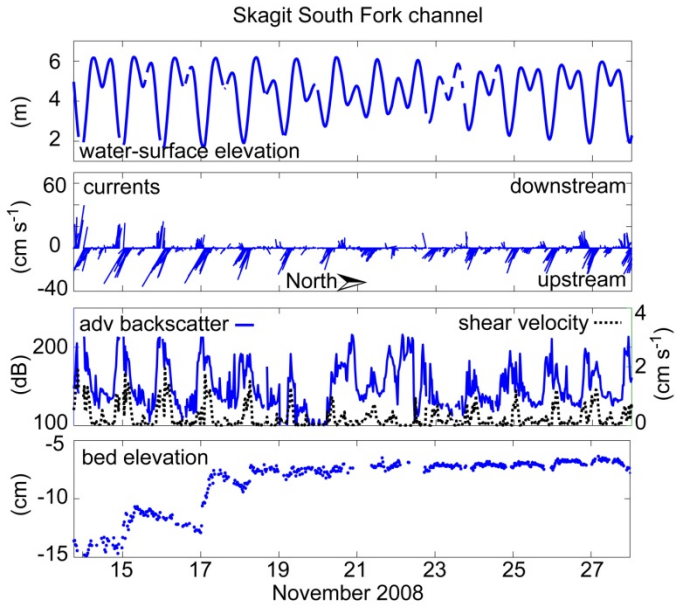

Figure 2.3. Time-series data from a channel tripod on the southern flat during November 2008, showing a 14-d period of water-surface elevation, currents, ADV backscatter as a proxy for suspended-sediment concentration, shear velocity and bed elevation. Following a large river discharge event (1700 m^{-3} s^{-1}, Fig. 2.1D), bed elevation indicates deposition of ~5 cm of sediment.

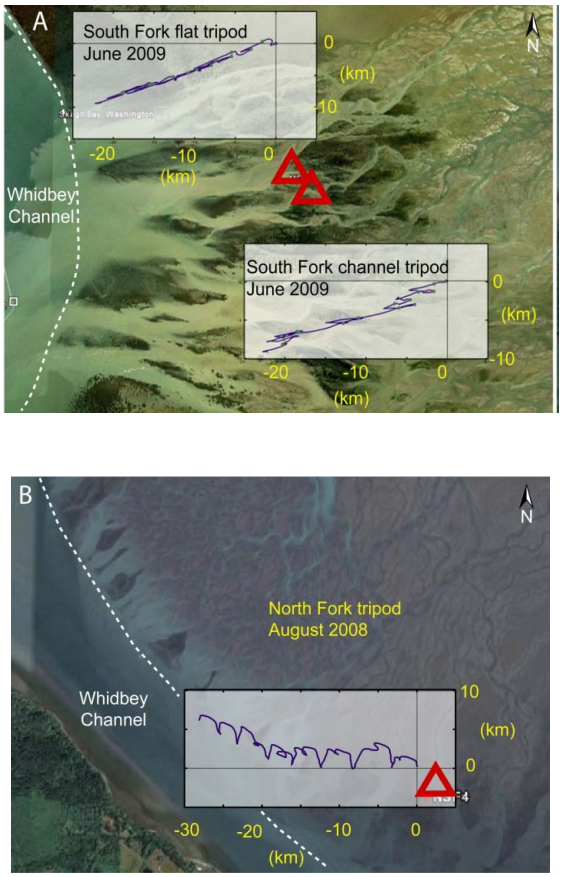

Figure 2.4. A) Progressive vector diagram of currents near the South Fork. B) Progressive vector diagram of currents near the North Fork. The dashed lines indicate the outer edge of the flat (>~4.5 m water depth).

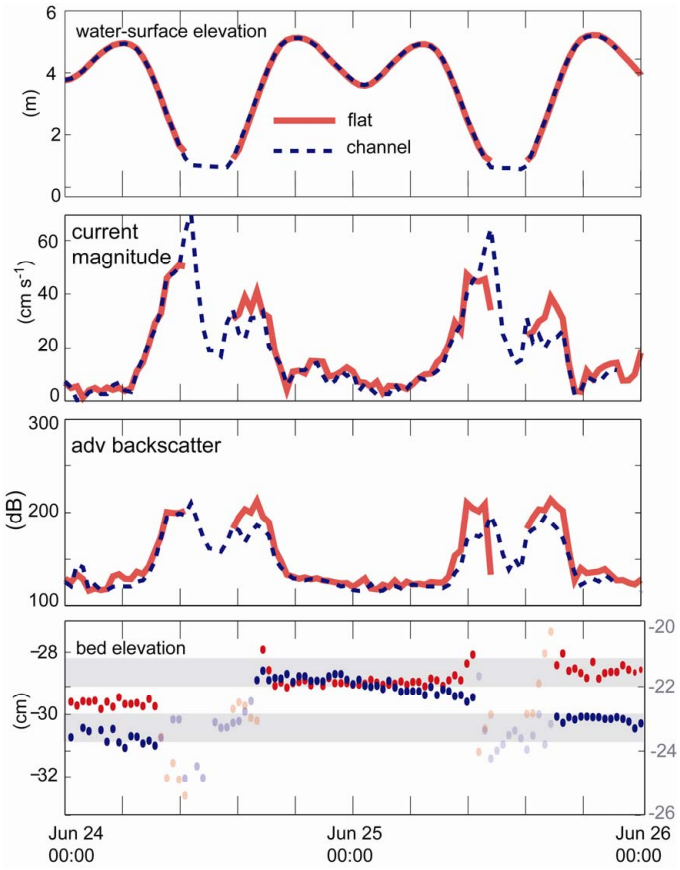

Figure 2.5. Detailed elevation of channel and flat time-series data during spring tides in June 2009 (for full records see Fig. 2.2), including two days of water-surface elevation, currents, ADV backscatter as a proxy for suspended-sediment concentration and bed elevation. On the flat (red), the seabed rose ~1 cm over a low-tide period, and remained stable through the next tidal cycle, where as in the channel (blue), the seabed rose 2 cm over the first low tide cycle and elevation remained steady and then eroded ~1 cm during the following lower-low tide. The cyclic bed elevation changes are interpreted as bedform migration.

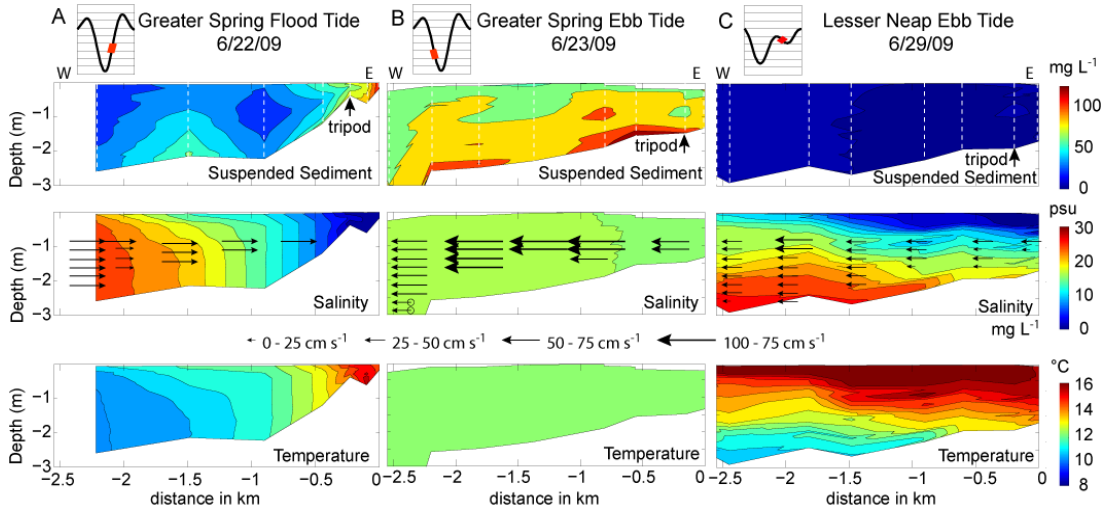

Figure 2.6. Hydrography along the Q channel transect, from middle to outer flat, of suspended sediment, salinity and temperature. Within transects, dashed white lines indicate locations of CTD casts and vertical arrows point to tripod location. Magnitudes of averaged velocities are denoted by horizontal arrow length, measurement located at each arrowhead, circle at arrow tail indicates southward flow direction (out of page). A) On the greater spring flood tide, sediment is trapped on the middle flat, and currents are shoreward. B) On the greater spring ebb tide, sediment is released to the outer flat and moderate SSC is found across the flat, while currents flow seaward. C) During lesser neap ebb tides, there is limited ability to bring sediment to flat edge, and most SSC values are low across the outer flat. Note that the transects originate (distance = 0 km) on the middle flat and the seabed depicted does not provide information on the channel morphology or the overall dip of the flat surface.

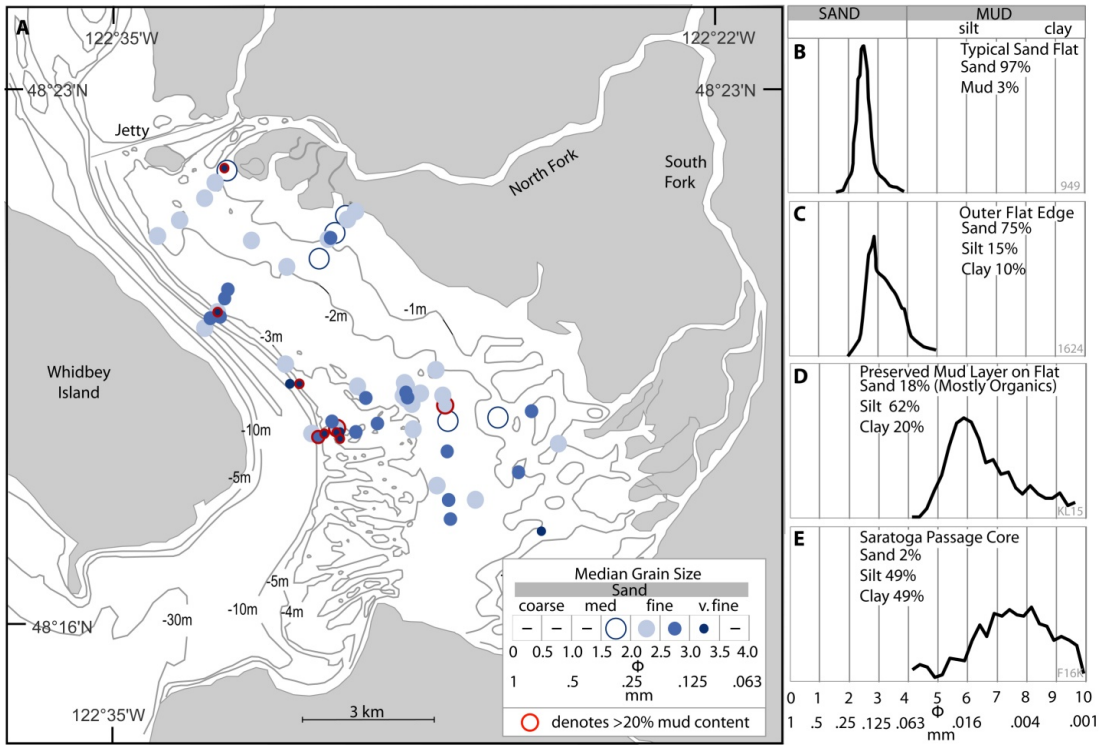

Figure 2.7. A) Map showing variation in median grain size on the Skagit flats. Surface samples with >20% mud content denoted with red outline. Also shown are examples of grain-size distributions from various points in the system: B) typical intertidal flats, C) outer edge of flat, D) preserved mud layer (Fig. 2.9D), and E) northern Saratoga Passage.

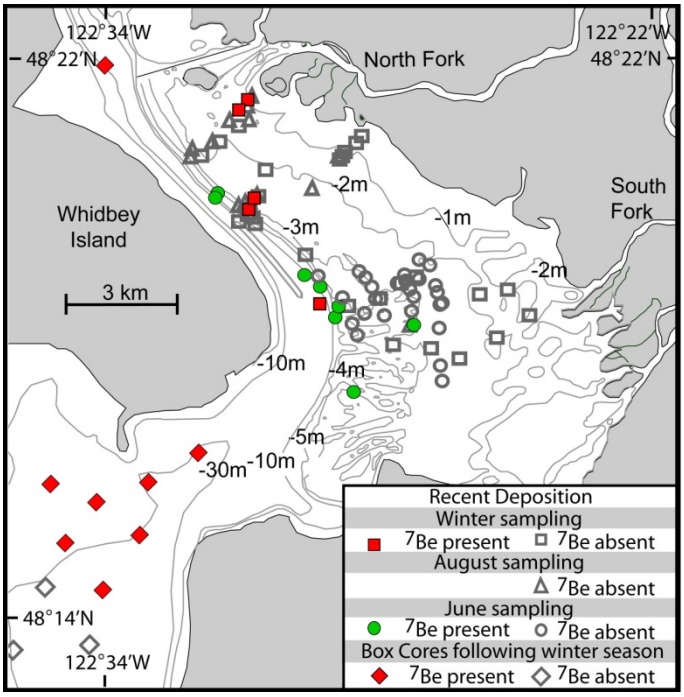

Figure 2.8. Map indicating the presence or absence of ^{7}Be from sediment samples collected seasonally. Recent fine-grained sediment was observed on the outer flat and within channels during winter 2008 (red) and spring 2009 (green). No recent fine-grained sediment was observed in August. Following the winter storm season (red), ^{7}Be was found in northern Saratoga Passage. This indicates that fine-grained sediment was rapidly distributed up to 10 km within several months.

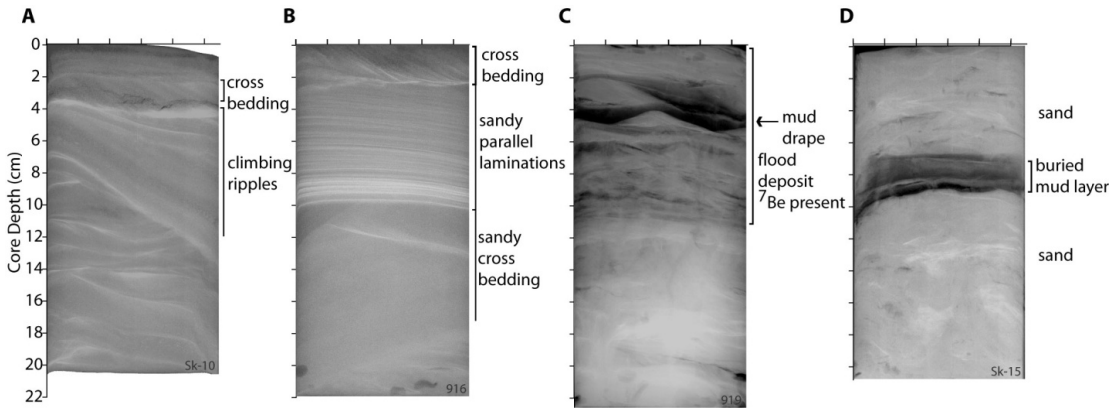

Figure 2.9. X-radiographs (negatives) of cores from the Skagit tidal flat (locations indicated in Fig. 2.2) showing a variety of sedimentary structures. A) Core collected in summer (Aug 08) reveals sandy cross bedding of several scales, which is the most common sedimentary structure found on the flat. B) Core collected in winter 2009 (after Jan 09 storm) has ~8 cm of graded sand (2-10 cm depth in core). C) Core from Jan 09 contains a mud layer 1-3 cm thick overlying a sandy ripple (2-5 cm depth in core). D) Core collected summer (Aug 08) shows a mud layer at 7-10 cm depth in core (see Fig. 2.7D).

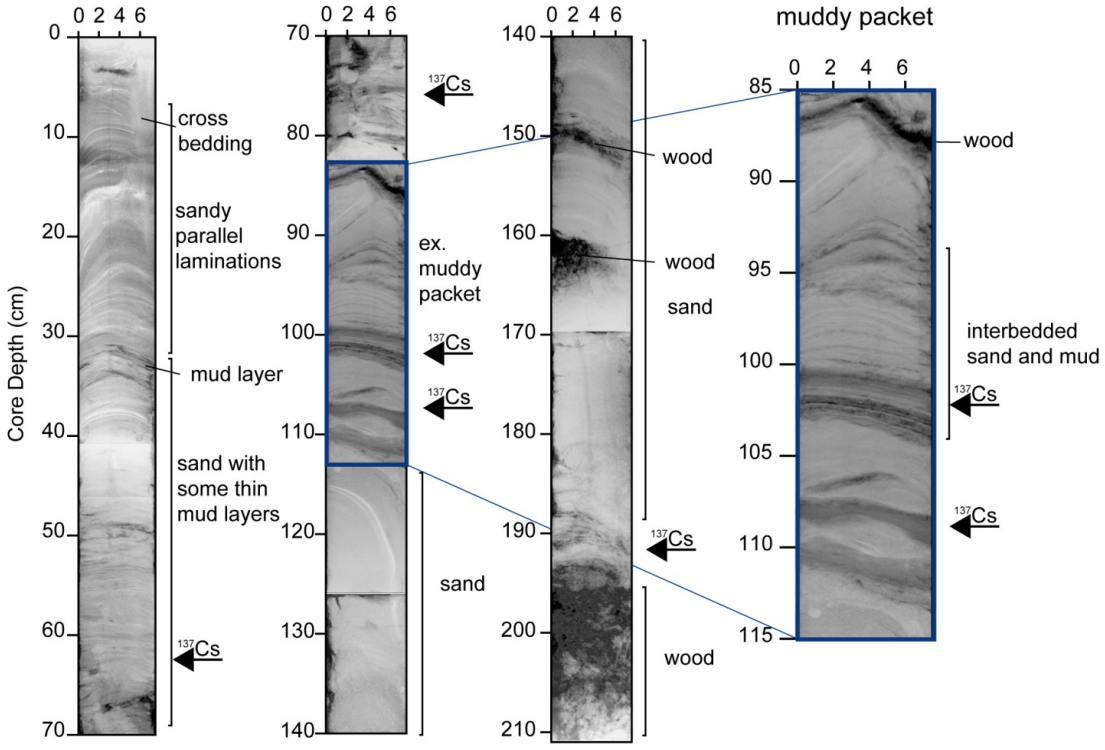

Figure 2.10. X-radiographs (negatives) of vibracore B3 from a near major North Fork tidal channel, showing mud layers (dark gray). ^{137}Cs was present (arrow) to depths of 189 cm, and excess ^{210}Pb was present throughout the core, indicating accretion at a rate of 3.4 cm y^{-1}. This is attributed to migration of braided tidal channels.

Table 2.1 Maximum currents and net flow direction during time-series deployments. Note that the river discharge is averaged over the deployment period.

			North Fork			South Fork		
Deployment	days of usable data	Average River Discharge (range) (m^3 s^{-1})	Site Description	Max Current (cm s^{-1})	Net Direction	Site Description	Max Current (cm s^{-1})	Net Direction
Aug 08	7	440 (396-515)	On flat surface near channel	35	W-NW	---	---	---
Nov 08	14	460 (225-1590)	On flat surface near channel	35	W-NW	Channel	40	---*
Jun 09	9	524 (515-651)	---	---	---	Channel	70	W-SW
Jun 09	14	510 (444-651)	---	---	---	On flat surface near channel	50	W-SW

*Net direction not determined due to a problem with sensor height relative to local seabed.

Table 2.2 Suspended-sediment concentrations collected in surface water bottles. River discharge is averaged over days of sampling.

	Aug 08	**Nov 08**	**Dec 08**	**Jun 09-Jul 09**
River discharge (daily discharge)	425 $m^3 s^{-1}$	1590 $m^3 s^{-1}$	325 $m^3 s^{-1}$	560 $m^3 s^{-1}$
SSC: at tripods on rising tide	4-6 mg L^{-1}	45-106 mg L^{-1}	4-6 mg L^{-1}	10-70 mg L^{-1}
SSC: total range over all tidal cycles (number of locations)	<15 mg L^{-1} (n=4)	45-232 mg L^{-1} (n=5)	4-81 mg L^{-1} (n=18)	4-150 mg L^{-1} (n=67)

3 Chapter: Fluvial sediment dispersal through an insular sea: Modern sedimentation associated with the Skagit River delta, Washington State

3.1 Introduction

The accumulation of sediment supplied to an insular sea from rivers with small mountainous drainage basins depends on the interaction between several factors, including flood events that deliver sediment, oceanic effects that enhance transport, and especially receiving basin geomorphology. Delta deposits forming in insular seas (including epicontinental shelves and fjords) are prevalent in the modern and the ancient rock record. Studies suggest insular seas act as effective sediment sinks, trapping much of the terrestrial input (Cowan et al., 2010; Jaeger et al., 1998). To understand formation of these strata, it is helpful to understand the particle pathways and sediment accumulation within the complicated receiving basins. Not only is mud the dominant grain size discharged by rivers, it is transported in suspension (i.e., not complicated by complexities of bedload transport) and is ideal for use in geochronological studies. Based on these properties fine-grained sediment (<63 μm) can be documented both in the water column and within the seabed.

Previous studies have related delta morphology and stratigraphy to receiving-basin geometry. Modern examples from Puget Sound (e.g., Nisqually delta) and British Columbia fjords demonstrate that receiving-basin constraint can increase tidal currents and impact delta morphology by limiting progradation (Barnhardt and

Sherrod, 2006; Bornhold and Prior, 1990). Similar ancient delta morphology is recognized in the rock record within constrained linear basins (Zelilidis and Kontopoulos, 1996). From a process standpoint, it is vital to put these small delta systems in perspective relative to the modern settings and to the stratigraphic record.

The tectonically active Olympic and Cascade mountain ranges provide an abundance of small mountainous rivers that discharge into the Salish Sea (Puget Sound and the Strait of Juan de Fuca). This represents an ideal setting to examine the roles of receiving basin shape and sediment accumulation. The Skagit River (Fig. 3.1), the largest river in the region, carries much mud. However, only a small fraction is accumulating on the topset of its delta (Webster et al., 2013), suggesting the mud is dispersed within and through its constrained receiving basin.

The hypothesis of this study is that basin geometry has a significant impact on physical processes, and together these dictate the depositional patterns of river deltas within insular seas. Specifically, the objectives of this study on the Skagit River delta are to: 1) measure temporal (tidal impacts, river discharge) and spatial (basin geometry) variations in sediment dispersal pathways; 2) evaluate the role of basin geometry in controlling accumulation patterns by developing a fine-grained sediment budget for Skagit River sediment, and 3) compare depositional patterns of the Skagit system to those on other deltas.

3.2 Background

3.2.1 Sediment dispersal and deposition of small mountainous rivers

Rivers are the major source of sediments to the global ocean, and small mountainous rivers play a disproportionately large role in this supply (Milliman and Syvitski, 1992; Milliman et al., 1999). Over a 100-yr timescale, event-driven sedimentation is a major component of strata formation (Palinkas and Nittrouer, 2007; Wheatcroft and Drake, 2003) with high-river discharge periods providing most of the annual load (Syvitski et al., 2000). The largest discharge events occur within the time duration of the causative storm events and thus the dispersal of sediment in the ocean is largely dictated by the energetic oceanic conditions during floods (Nittrouer et al., 2007). Spring snowmelt from mountainous headwaters can produce high river discharge when ocean conditions are relatively calm, and then sediment dispersal operates differently. River sediment enters the marine environment through freshwater plumes and settling to the bottom boundary layer (BBL)(Geyer et al., 2000; Liu et al., 1999; Ogston et al., 2000; Warrick and Milliman, 2003).

The depositional patterns of small deltas have been classified in relation to the physical processes acting within the marine environment, (specifically e.g.: wind waves, tidal currents, and wind-driven currents) and have shown varied results. In the high-energy open-ocean environment of the Eel River continental margin (northern California), flood deposits are displaced seaward due to large swells and create a mid-

shelf mud deposit. For the low-energy and microtidal conditions near the Po and Rhone Rivers in the Adriatic Sea and Gulf of Lions, respectively, flood deposits are found close to the distributaries and are reworked alongshelf by oceanic processes (Drexler and Nittrouer, 2008; Palinkas and Nittrouer, 2006). In addition to these natural processes, humans play a large role in the export of sediment to insular seas, both decreasing (e.g., dams) and increasing (e.g., land use) sediment supply (Milliman and Syvitski, 1992).

For small mountainous delta systems, the end-member systems have been the focus, such as: the west coast of Taiwan, with extreme sediment yields (Hale et al., 2012); the Eel River, whose open-ocean waves inhibit delta growth (Wheatcroft et al., 1997); and fjords, with extreme basin constraint (Prior and Bornhold, 1990). The small mountainous rivers of the Salish Sea give us the opportunity to examine delta sedimentation and better understand small delta systems where multiple mechanisms drive the delta morphology, including the degree of basin constraint.

3.2.2 Regional Setting

The Skagit River discharges into the Salish Sea, a receiving basin with a series of glacially carved valleys, which were drowned by Holocene sea-level rise. Tides are mesotidal (3-4 m during spring tides) and combined with complex morphology, drive strong currents (~100 cm s^{-1}) in the region. The wave climate is fetch-limited due to

the small size of the basins, and wave energy varies with shoreline orientation and fetch length relative to the predominant wind direction from the south.

The Skagit River originates in the Cascade Mountains and flows 240 km west to the Whidbey Basin of Puget Sound (Fig. 1). The temperate maritime climate receives 100 cm y^{-1} of precipitation in the lowlands and 230 cm y^{-1} in the mountains. The river has a drainage basin of 8,500 km^2, where anthropogenic changes include logging and agriculture in the lower basin and dams built in the upper reaches. Although the largest tributary, the Sauk River (23%), is not dammed, sediment and water from about half of the Skagit basin is intercepted by dams.

The Skagit River hydrograph has bimodal peaks, with floods during a freshet in the late spring and early summer (May-Jul) and storms in late autumn and winter (Oct-Feb) (Fig. 3.1). It has a mean discharge of 470 m^3 s^{-1} and delivers about 35-50% of the river water reaching Puget Sound (Babson et al., 2006). Near Mount Vernon, located 25 km from the mouth, the river splits into North Fork and South Fork distributaries. The North Fork carries 55-70% of the water and the South Fork carries the remaining 30-45% (Hood, 2007; Yang and Khangaonkar, 2009). From Whidbey Basin, annually 38% of the Skagit River water exits to the north through Deception Pass and into Rosario Strait and the remaining 62% exits to the south into Saratoga Passage. These amounts vary seasonally with larger amounts of fresh water exiting to the north in winter (Sutherland et al., 2011). Measurements of the annual suspended-

sediment load at Mount Vernon ranged from 0.9 to 4.4 x10^6 tons y^{-1} between 1980 and 1991 (Collins, 1998), a period reflecting anthropogenic alteration to the basin. The upper limit of annual discharge occurred during 1991, and represents the largest event within the 1946-2010 period.

The Skagit delta is a productive agricultural region, and protection of the fertile floodplain has caused significant anthropogenic changes to the delta. After 1890, construction of levees and dikes prevented river flooding and tidal inundation on most of the delta topset. Today, over 90% of the 327 km^2 delta topset/marsh has been isolated from riverine and tidal influence (Collins et al., 2002). The remaining marsh occurs along channels in the South Fork region, and to a lesser extent in the North Fork region (Hood, 2004). Marshes associated with the South and North Forks are prograding, and the marsh between them is eroding (Hood, 2007).

Roughly 5,500 years BP a volcanic eruption of Glacier Peak caused the Skagit River to avulse to its present course, entering Whidbey Basin (Dragovich et al., 2000). Since then, the Skagit delta filled its receiving basin with fluvial sediment, and a high-energy channel (referred to as "Whidbey Channel" in this document; Fig. 3.1) developed between the Skagit tidal flats (delta topset) and Whidbey Island. Surface sediments on the Skagit tidal flats are mostly composed of sands (McBride et al., 2006), and the absence of fine-grained sediment suggests that muds are exported from the delta (Webster et al., 2013).

Two other rivers flow into Whidbey Basin, the Stillaguamish and the Snohomish Rivers. Except during river floods, the Stillaguamish flows southward into Port Susan (Fig. 3.1). Occasionally, the Stillaguamish River enters southern Skagit Bay (Fig. 3.1). This outlet has been observed to carry some Stillaguamish sediment to Skagit Bay at high discharge, however the amount is small relative to the Skagit River (i.e., the entire Stillaguamish River sediment load is ~1.6 x 10^4 tons y^{-1}). The Snohomish River is the second largest in Puget Sound with a yearly sediment load of 0.5 x 10^6 tons y^{-1} (Fig. 3.1), and enters outside, but near the south end of Saratoga Passage.

3.3 Methods

3.3.1 Field methods

Water-column profiling and time-series measurements were paired with seabed observations during 2008-2012, and were used to examine the intertidal and subtidal portions of the Skagit River delta. Data collection consisted of: water-column profiles measured by combinations of CTD systems (Conductivity, Temperature and Depth) with OBS (Optical Backscatter Sensor for suspended-sediment concentrations), and of boat-mounted ADCP systems (Acoustic Doppler Current Profiler for water velocity). Seabed sediments were collected in grab samples, push cores (~30 cm long), box cores (~50 cm long), kasten cores (~2 m long) and vibracores (~4 m long).

Three seasons are defined for this study based on river discharge: quiescent periods with low river discharge and weak wave energy (Mar-Apr and Aug-Sep); spring-summer freshet with high river discharge and weak waves, and coincides with the summer solstice when diurnal tidal ranges are greatest (May-Jul); and autumn-winter periods with episodic river discharge and energetic waves (Oct-Feb) (Fig. 3.1). The Skagit River daily water-discharge data for these periods were obtained from the gauging station located in Mount Vernon, WA (USGS gage 12200500 http://waterdata.usgs.gov/nwis/nwisman/?site_no=12200500).

3.3.1.1 Water-column processes

Three water-column profilers were used depending on water depth and vessel capabilities. The first is a small, compact CTD system with an OS200 CT and OBS lowered by hand. The second is the BLISP system, which is a small profiling tripod, composed of a similar OS200 CTD and OBS and adds the ability to collect water and suspended-sediment samples within 10 cm of the seafloor (Martin et al., 2008). The third was the shipboard CTD system, Sea-Bird 911 with a 25-cm path-length transmissometer and bottle sampler. The OBS on each system was calibrated with surface-water samples that were filtered to evaluate suspended-sediment concentrations.

The ship-mounted ADCP continuously collected data, while moving through the study area and while stopped at CTD stations. Two ADCPs were used: a 150-kHz

unit with 200-cm bins and a 600-kHz unit with 50-cm bins, and these recorded discrete measurements at each station for at least 2 minutes.

3.3.1.2 Seabed coring

In the marsh, push cores were obtained with Plexiglas trays (2.0 cm thick x 7.5 cm wide x 30 cm long). On the prodelta, surface samples were collected seasonally from ships with Shipek and VanVeen grab samplers. Box corers (20 x 30 cm cross section, 50 cm long) and kasten corers (12.7 x 12.7 cm cross section, 300 cm length) were used during four ship cruises (Sept08, Feb09, Aug09, and Apr10) that reoccupied the same sites. Push, box and kasten cores were subsampled for textural and radioisotopic analyses, and Plexiglas trays were inserted for x-radiography.

3.3.2 Lab methods

The Plexiglas trays were examined for sedimentary structures using a digital x-ray imaging system. Results are presented as x-radiograph negatives, where opaque areas (light color) have greater bulk density and coarser sediment relative to transparent areas (darker color) with low bulk density and finer sediment. X-radiograph images were individually enhanced to heighten contrast, using image-processing software.

3.3.2.1 Grain-size analysis

Sediment samples (~12 g) were homogenized and mixed with the dispersant sodium hexametaphosphate, and were placed in a sonic bath for 15 minutes. Then samples were wet-sieved at 63 μm to separate the fine and coarse fractions. The size

distributions were measured for the silt and clay fractions using a Sedigraph at ¼ phi intervals, and the sand fraction was measured using a 2-m automated settling column. If a sample had <10% of either fine or coarse fractions by mass, size distributions were completed for only the fraction >90%.

3.3.2.2 Radioisotope analysis

Seabed sediment on the topset (see Webster et al., 2013), Whidbey Channel and prodelta (Saratoga Passage and outside Deception Pass) were sampled during variable discharge and storm conditions: Aug08 (high discharge), Feb09 (storms), Sept 09 (low discharge) and Mar09 (low discharge). Sediment samples were analyzed using the radioisotopes ^{7}Be and ^{137}Cs by gamma (γ) detection (Sommerfield et al., 1999; Mullenbach and Nittrouer, 2000) and their activities were determined from the 477.7 and 661.0 KeV γ spectra photo peak, respectively. The short-lived isotope ^{7}Be was measured in push cores, grab samples and box cores (upper 10 cm in 1-cm intervals) shortly after collection. ^{210}Pb was measured in box and kasten cores by alpha spectroscopy, and ^{210}Pb activities were calculated from the ^{210}Po content (Nittrouer et al., 1979). Supported ^{210}Pb activities (due to the decay of its effective parent, ^{226}Ra, in the seabed) were determined from samples deep in the cores.

3.4 Results

3.4.1 Sediment grain sizes

3.4.1.1 Marsh and tidal flat

The intertidal portion of the Skagit River delta topset (Fig. 3.1) consists of an expansive sandy tidal flat (<10% mud) and fringing marsh (17-55% mud). The flat is characterized by well sorted fine sand, 1-3% surficial mud content and a median grain size of 2.5 phi (for more details see Webster et al., 2013). The quantities of mud increase seasonally (high-flow periods) and spatially (in/near channels and on the outer-flat edge). Mud percentages reach 60% in isolated pockets, and thin (1-5 cm) deposits can be buried. Long vibracores show the bulk composition of the channelized flat consists of ~12% mud and ~88% sand, and the fine-grained component includes silt-rich laminations.

3.4.1.2 Whidbey Channel

Seaward of the tidal flat is Whidbey Channel, which has its narrowest width (~350 m wide) near the northern flat (Fig. 3.1), and widens farther northward (800 m wide) and southward (1000 m wide). Three thalweg stations were cored in Sep08, Feb09 and Aug09 and they revealed seabed variability, ranging from consolidated mud (without ^{7}Be or excess ^{210}Pb) to sand, and even some gravel near Saratoga passage (Fig. 3.2). The northern end of Whidbey Channel widens and deepens, forming a basin immediately north of the North Fork that contains modern mud (^{7}Be present)

(Webster et al., 2013). Overall, however, the channel substrate is coarse grained or erosional.

3.4.1.3 Saratoga Passage

Southward into Saratoga Passage, grain-size distributions become progressively finer (Fig. 3.2). The northern station (A1), 2 km from the tidal-flat edge, is composed of 50% silt and 23% clay (the remainder is sand), and this fines to 37% silt and 62% clay ~ 30 km southward in Saratoga Passage. Replicate cores at a station on the same cruise (e.g., replicates were analyzed at A1, B3, and D10) show little variation in grain size within a site. Seasonal cores from the same stations on different cruises (e.g., A1, E12, E13, H21, F16; Fig. 3.1) show no seasonal variation in grain-size distributions on the seabed surface or down core.

3.4.1.4 Deception Pass

North of Whidbey Channel, a series of small basins connect Skagit Bay to Deception Pass. Coarser grain sizes (sand, shell hash) are found in narrow constrictions and bathymetric shallows, and finer sediment (mud) in bathymetric lows. Within this northern reach, referred to as Northern Basin, the flow of water is constricted by rocky outcrops and islands. West of Deception Pass, grab samples revealed a heterogeneous distribution of shell hash, coarse sand, gravel, mud, and muddy sand (Fig. 3.2).

3.4.2 X-radiographs

On the topset, typical x-radiographs revealed crossbedding, although there are some homogenous cores with no physical structures, as well as packets of interbedded sand and mud layers (Webster et al., 2013). The mud layers are generally located adjacent to the channel, and commonly contain leaf litter and wood fragments.

Throughout the bottomset regions of Saratoga Passage and in the Northern Basin, x-radiographs revealed homogenous or mottled structure, with no discernible physical laminations. This is attributed to intense bioturbation; many cores within Saratoga Passage contained sea cucumbers (*Molpadia intermedia*), and other large burrowing benthos. Although similar organisms were found in cores from outside Deception Pass, these cores had some sand and mud layers within their generally mottled appearance.

3.4.3 Water and sediment dynamics

Water-column profiles of velocity and water-column structure of salinity, temp and SSC through Whidbey Channel revealed two different transport pathways. On falling tide and low discharge (190 m^3 s^{-1}), the pathway from Whidbey Channel to Saratoga Passage is vertically stratified with a salinity of 20-28 psu and a temperature of ~11 °C (Fig. 3.3). Velocities are 30-100 cm s^{-1} throughout most of the water column and along the channel, with greatest velocities measured at the narrowest constriction (AA04). Upon entering Saratoga Passage, all velocities are in the southward

direction and are distinctly slower (10-30 cm s^{-1}). Bottle samples of suspended-sediment concentration are consistent with the low river discharge, <6 mg L^{-1} at the surface and 4-18 mg L^{-1} near the seabed. ADCP backscatter is in agreement, recording intense scattering at the surface within Whidbey Channel and near the seabed within Saratoga Passage.

On rising tide and low discharge (212 m^3 s^{-1}), the pathway from Whidbey Channel to Deception Pass water column is well mixed vertically with a salinity of ~28 psu and temperature of ~11 °C (Fig. 3.3). Peak velocities along the channel are 40-50 cm s^{-1} throughout the water column. Bottle samples contain <10 mg L^{-1} of sediment at the surface and 10-30 mg L^{-1} near the seabed in Whidbey Channel. Salinity ranges from 27 psu at the surface in Whidbey channel to 30 psu west of Deception Pass. Current velocities reach 50 cm s^{-1}, but are highly variable depending on geometries and depths in channels. Immediately west of Deception Pass, current velocities are >40 cm s^{-1} throughout the water column, and less (10-30 cm s^{-1}) in sheltered waters.

3.4.4 Radiochemistry

3.4.4.1 Sediment deposition

On the intertidal topset, ^{7}Be was located at the seaward flat edge and adjacent to distributary channels following high river discharge (Webster et al., 2013). In Whidbey Channel, ^{7}Be was absent from the seabed for all sampled seasons. Northward within the first basin (AA06), ^{7}Be was always present to seabed depths of

several centimeters (Fig. 3.2). In more distal portions of the dispersal system, ^{7}Be was found in northern Saratoga Passage (Webster et al., 2013) and westward outside Deception Pass. ^{7}Be was also found at M30 in southern Saratoga Passage, in close proximity to Snohomish River (Mar10). ^{7}Be was found west of Deception Pass following both the spring freshet and winter storm seasons (Sept08, Feb08).

3.4.4.2 Decadal sediment accumulation

^{210}Pb profiles revealed the three common vertical segments that are typical of marine sediments (Nittrouer et al., 1979): uniform high activities (>1 dpm g^{-1}) near the surface of seabed (i.e., surface mixed layer; SML), logarithmic decrease downward, and low activities (<1 dpm g^{-1}) at the bottom of cores. The SML is ~10 cm thick, and is attributed to intense biologic reworking. Supported ^{210}Pb values of 0.45 dpm g^{-1} are found in the lower most segments of cores, and are used to calculate excess ^{210}Pb from the middle segments. The ^{210}Pb decreases in the middle segments of profiles indicating accumulation rates of 1.6-10.4 mm y^{-1} (0.01 to 0.91 g cm^2 y^{-1}; Table 3.1). Depths of ^{137}Cs penetration are in agreement with predicted depths from ^{210}Pb accumulation rates, and confirm steady-state processes of accumulation. Overall, R^2 values for accumulation-rate measurements within Saratoga Passage cores were greater than 0.80, with n values of 4-15 samples per core.

In marsh areas, accumulation rates were 1.6-2.8 mm y^{-1}, and mass accumulation rates were 0.01-0.02 g cm^{-2} y^{-1}. These were observed below a SML of 4-5 cm. Over the

entire system, accumulation rates were greatest immediately south of Whidbey Channel, and averaged 8.9 mm y^{-1} (0.74 g cm^{-2} y^{-1}). Throughout most of Saratoga Passage, accumulation rates averaged 7.8 mm y^{-1} (0.34 g cm^{-2} y^{-1}). Two exceptions are a low value within Holmes Harbor (S9) of 4 mm y^{-1} (0.17 g cm^{-2} y^{-1}) and along the eastern shoreline of Saratoga Passage (H21) at 0.68 mm y^{-1} (0.76 g cm^{-2} y^{-1}). H21 was not included in mass budget as it contained 75% sand, and does not reflect mud accumulation within Saratoga Passage. Accumulation rates decreased in the southern region of Saratoga Passage, to the minimum rate of 6.3 mm y^{-1} (0.27 g cm^{-2} y^{-1}). The southernmost core had a greater accumulation rate of 7.8 mm y^{-1} (0.47 g cm^{-2} y^{-1}). The two cores from the Northern Basin had accumulation rates of 5.4 and 6.2 mm y^{-1} (~0.55 g cm^{-2} y^{-1}).

In general, the accumulation rates decrease with distance from the Skagit River supply: ~10 mm y^{-1} in northern Saratoga Passage to 6 mm y^{-1} in southern Saratoga Passage. Further southward, the rates increase slightly with proximity to the Snohomish River. That pattern is more complicated to the north, entering and outside of Deception Pass.

3.5 Discussion

Examination of Skagit River sediment dispersal through interconnected basins of Puget Sound provides an understanding for sedimentation typical of tectonic and glaciated receiving basins. There are many variables that must be taken into

consideration when contrasting sediment dispersal and accumulation patterns for small rivers worldwide. The Skagit River provides an opportunity to explore sedimentation where the receiving basin has complex morphology.

3.5.1 Mechanisms controlling dispersal pathways

Following the winter storm season (Feb09), ^{7}Be was present in the surficial seabed within Saratoga Passage (Webster et al., 2013) and west of Deception Pass (Fig. 3.2). No other significant sediment source is found within the study area, and the observed ^{7}Be must be associated with the Skagit River discharge. In order to trace the dispersal pathways to and beyond these depositional areas we use water-column observations in conjunction with seabed grain-size distributions, beginning at the sediment source, the Skagit River.

3.5.1.1 Whidbey Channel

Previous studies show fine-grained material is delivered episodically and is rapidly exported by tidal processes across the intertidal topset region (Webster et al., 2013). After crossing the broad sandy intertidal flat, Skagit River water and sediment is delivered to the narrow (350-1000 m) Whidbey Channel, which reaches depths of 20 m (Fig. 3.1). At the narrowest point, the seabed of the channel thalweg has consolidated muds (Sep08), but the thalweg generally contains sand (Fig. 3.2) with mixtures of mud (up to 35% seasonally).

Water-column measurements reveal strong currents (up to 100 cm s^{-1}) and a well-mixed water column that suggests fine-grained sediment is exported through and beyond Whidbey Channel. The channel is subject to reversing tidal currents, which alternately direct sediment south toward Saratoga Passage with ebb currents or north toward Deception Pass with flood currents (Fig. 3.3). Within Whidbey Channel, predicted currents are on average ~40 cm s^{-1} for a 5-hr period on flood and ebb tides (NOAA, http://tidesandcurrents.noaa.gov). This suggests that particles in the water column travel ~7 km before current reversal. Particles entering Whidbey Channel via the North Fork on ebb tide, would not reach Saratoga Passage (distance >10 km) and particles entering via the South Fork, would not reach the first basin to the north (AA06, distance >10 km) before current reversal, suggesting that, although currents are strong, some particles may reside within Whidbey Channel for more the one tidal cycle. The entry location into Whidbey Channel (from North or South Forks) and tidal timing thus determines the fate of fine-grained particles.

3.5.1.2 Saratoga Passage

Once leaving Whidbey Channel to the south, the water column deepens and widens (Fig. 3.1), current velocities decrease (30 cm s^{-1} to 10 cm s^{-1} on ebb tide; Fig. 3.3), and the seabed becomes mostly mud (Fig. 3.2). Here, ^{7}Be was present following the winter storm season, but not in late summer. The presence of ^{7}Be varies seasonally (Webster et al., 2013), and suggests a link to episodic discharge of sediment from the Skagit River. However, surface grain size is consistent through all seasons, and

recognizable flood layers are not observed in sediment cores (Fig. 3.4), likely because bioturbation is intense, as indicated by prevalence of benthos and a surface mixed layer in ^{210}Pb profiles.

Grain-size distributions continue fining southward, until the southern end of the Passage (M28), near the Snohomish River (~10 km). The sediment there was coarser, ^{7}Be was present and the accumulation rate increased (Fig. 3.2; Fig. 3.5), suggesting some Snohomish River sediment deposition occurs at and south of M28.

During the Sep09 water-column sampling, two plumes, surface and BBL, were observed entering Saratoga Passage during strong ebb tide (Fig. 3.3). The particles are carried from a high-velocity zone in Whidbey Channel to the calm waters of Saratoga Passage, allowing deposition of mud. The water column in Saratoga Passage is stratified (Babson et al., 2006) and particles reaching the BBL are likely to be trapped there at great depth until they are deposited on the seabed. Saratoga Passage is characterized as a calm receiving basin, which promotes particle settling, and results in grain-size distributions that become finer with distance from river. Although the deposits in Saratoga Passage are disconnected from the Skagit delta, the grain-size patterns are similar to bottomset deposits found in other constrained environments.

3.5.1.3 Deception Pass

In contrast, surface grain size does not fine regularly in a northward direction from the river mouth as sediment leaves Whidbey Channel. Grain-size patterns and currents match the complicated bathymetry and basin shape (Fig. 3.3). Muds are found in deep isolated basins, and shell hash and sands are found in shallow and constricted areas (Fig. 3.2). Strong currents and variable seabeds continue west of Deception Pass into Rosario Strait. Mechanisms of sediment delivery can be seen as sediment-laden freshwater travels northward through energetic well-mixed constrictions (Fig. 3.3). This freshwater is traced northward through Deception Pass, mixing rapidly with fast flowing Rosario Strait water and is broadly dispersed. The seabed immediately west of Deception Pass contains ^{7}Be at all times sampled, suggesting the year-round delivery of mud from the Skagit River (Fig. 3.2). Thus, the Northern Basin is characterized as a turbulent narrow chute composed of shallows and isolated basins until exiting through Deception Pass into deeper Rosario Strait, which is highly energetic and seabed is generally coarse grained.

3.5.2 Patterns of sediment deposition

3.5.2.1 Intertidal delta plain

There is little mud accumulation on the intertidal delta plain, which consists of both limited amounts of vegetated marsh and expansive sand flats. ^{210}Pb marsh accumulation rates are measured to be 1.6-2.8 mm yr^{-1} (Table 3.1), with 17-55% mud

and the rest sand and organics. These results are in agreement with other local delta marshes such as the Nisqually Delta marshes (2.6 mm yr^{-1}; Thom, 1992), and with the rates of local sea-level rise. Average mass accumulations of 0.07 g cm^{-2} yr^{-1} for mud in Skagit marshes provides an estimated storage of 7 x 10^3 T y^{-1} (Table 3.2).

After leaving the deltaic marsh, distributary channels enter the sandy intertidal flats. Only ~12% mud by mass is observed within the intertidal flats and this small number is attributed to intense seabed reworking at a range of depth scales by waves, tidal currents and channel migration, which effectively export sediment (Webster et al., 2013). The tidal flat is estimated to accumulate at 0.04 g cm^{-2} yr^{-1}, with a cumulative storage of 20 x 10^3 T y^{-1} (Table 3.1).

3.5.2.2 Whidbey Channel

^{7}Be was observed at the outer flat edge (Webster et al., 2013), but no recent ^{7}Be or excess ^{210}Pb deposition was recorded within Whidbey Channel. Currents were strongest at its narrowest width, with consolidated muds found at the seabed surface. These sediments have only supported values of ^{210}Pb (Table 3.1), indicating the mud was deposited >100 y ago. While the mud content varied seasonally (up to 35%), indicating temporary deposition, there was no evidence of sediment accumulation in Whidbey Channel. Mud was likely flushed rapidly to the prodelta regions of Saratoga Passage and Deception Pass.

3.5.2.3 Saratoga Passage

Accumulation rates (100-y timescales from ^{210}Pb) in northern Saratoga Passage reach 10 mm y^{-1}. Although x-radiographs reveal a mottled to homogeneous substrate, indicative of bioturbation, ^{137}Cs depths validate ^{210}Pb accumulation rates (Fig. 3.4; Table 3.1) and confirm that steady-state conditions are reached.

Within Saratoga Passage, accumulation rates decrease southward in agreement with grain-size patterns (Fig. 3.2; Fig. 3.5). Notable exceptions to this pattern are found in Holmes Harbor and at the south end of Saratoga Passage. In Holmes Harbor, a low accumulation rate is attributed to a glacial sill located at the mouth of the basin, which may inhibit sediment from entering the basin. In the southern end of Saratoga Passage, accumulation rates increase, surface grain-size distributions coarsen slightly and ^{7}Be was present. These observations suggest a secondary sediment input to Saratoga Passage (Fig. 3.2), possibly from the Snohomish River. Saratoga Passage mass accumulation rates were averaged for three areas supplied by the Skagit River (Fig. 3.5, Table 3.1), based on bathymetry and accumulation rates. To limit influence of Snohomish River sediment, the area included in the analysis excludes the higher rates at the southern end of Saratoga Passage. Overall, ~560 x 10^3 T of fine-grained sediment from the Skagit River are accumulating annually in Saratoga Passage.

3.5.2.4 Deception Pass

In the small interconnected basins north of Whidbey Channel, we observe recent sediment with measureable accumulation rates (Fig. 3.5). For example, the first basin northward (AA06) revealed ^{7}Be in all sampling seasons (Sep09, Aug08, May09, Feb09) with a penetration depth of 6 cm in Feb09. The site also had an unsteady ^{210}Pb profile (AA06), and is interpreted as a sporadic deposit of Skagit River mud likely delivered from the North Fork during flood periods.

Fine-grained sediment is actively being deposited west of Deception Pass throughout the year (Fig. 3.2) and moderate ^{210}Pb accumulation rates (5.4 and 6.2 mm yr^{-1}; Table 3.1). However, due to the potential for broad dispersal, the mass of Skagit mud that enters this basin (Fig. 3.5) is not fully known. The cores from outside Deception Pass contained physical structures as sandy layers within mud, and these indicate strong physical reworking.

3.5.2.5 Modern Sediment Budget

Overall, little mud is observed at the intertidal delta plain or delta front (Whidbey Channel), and most mud is observed in the distal prodelta regions. To the south, in quiescent Saratoga Passage, accumulation rates decrease with distance from river mouth, until the south end of Saratoga Passage, where sediment is being supplied from the Snohomish River. To the north, recent muddy deposits are located in

isolated basins leading to and beyond Deception Pass. The next step is a quantitative evaluation of the source and sinks.

Suspended sediment discharge by the Skagit River is estimated to be 1000-4400 x 10^3 T y^{-1}. Over the 1980-1991 sampling period, annual discharge of suspended sediment averaged 1700 x10^3 T (Collins, 1998). ^{210}Pb geochronology provides estimates of sediment storage for the past century. Much of the influence from humans (i.e., logging, levees and snag removal) is well established throughout this period, and our measurements give insights to the modern (human) era of sediment dispersal.

Of the ~1700 x10^3 T y^{-1} of sediment (Collins, 1998), this study measures 27 x 10^3 T y^{-1} of mud within the topset deposits, with roughly a quarter of this in the fringing marsh and rest in the sandy tidal flats (~50 km^2). The marsh sediment contains 20-40% mud and accumulation rates approximate the rate of local sea-level rise (Table 3.1), similar to temperate marshes worldwide (Allen, 2000; Dyer et al., 2000). However, agricultural practices have spatially constrained the wetland marsh to only ~12 km^2 (Bortleson et al., 1980). The intertidal flats contain ~12% mud, due to strong physical processes (Webster et al., 2013) and lack of vegetation to trap muds. Most of the Skagit flat is unvegetated, in contrast to other tidal areas (e.g., U.S.A. east coast, where *Spartina alterniflora* dominates; Woodroffe, 2002). A small spatial area and strong physical processes cause the topset to be a limited sink for muds in the Skagit system.

Whidbey Channel has no measureable mud storage. The seabed was mostly composed of sand and, at the narrowest constriction, relict mud (i.e., an erosional surface). This lack of mud storage is attributed to the strong tidal currents that quickly export mud beyond the channel.

Most of the Skagit mud is likely stored far from the river mouth in Saratoga Passage and Rosario Strait. A significant portion (532 x 10^3 T) of Skagit River muds are accumulating annually in the quiescent and deep Saratoga basin. While there are unmeasured sinks (southern end of Saratoga Passage, shallow embayments) and sources, (coastal erosion and landslides, and Snohomish River sediment), these are likely small compared to the Skagit input to Saratoga Passage. In addition, this number is well constrained because the boundaries of Saratoga Passage are well defined.

The geometry in the Northern Basin and in Rosario Strait (west of Deception Pass) provides a poorly constrained basin and consequently the annual mud storage cannot be estimated accurately. Skagit muds travel northward (Fig. 3.3) and are deposited beyond the North Fork and west of Deception Pass, as documented by the presence of ^{7}Be and measureable accumulations rates (Fig. 3.5). Based on these observations, it is likely that Rosario Strait is also a significant fine-grained sediment sink.

There are several factors that contribute to the inability to close the budget. The Skagit River suspended-sediment measurements (1980-1991) include a 100-yr storm

(annual load of 4400 x 10^3 T in 1991; Collins, 1998), which may cause the mean value of ~1700 x 10^3 T y^{-1} to be an overestimate. Secondly, this measurement includes all sediment in suspension (i.e., mud and sand), while the present study measures only the accumulation of the mud fraction. For the Skagit River, the grain size in suspension is not well known, and estimates of the mud fraction estimates range from 50-80%, which could reduce the yearly mud input from the Skagit River to 1360-850 x 10^3 T y^{-1} (Grossman pers comm.).

In addition, although the sediment budget for Saratoga Passage is accurately known, the loss through Deception Pass is not. Likely, Rosario Strait (west of Deception Pass) is the sink for much of the fine-grained sediment unaccounted in the sediment budget.

3.5.3 Deposition patterns for a delta in a constrained basin

3.5.3.1 Overall accumulation patterns

The Skagit delta dispersal into two distinct basins is an example of how basin geometry and the resulting sediment transport processes can be dominant factors in dispersal. Accumulation patterns have been defined for other fluvial dispersal systems, e.g.: Eel River, with a bulls-eye pattern offshore (wave-dominated)(Crockett and Nittrouer, 2004), Fly River, with a prograding clinoform foreset (tide-dominated)(Walsh et al., 2004), and the Rhone and Po River systems, where currents direct sediment along shelf (Drexler and Nittrouer, 2008; Palinkas and

Nittrouer, 2006). The Skagit system, like most rivers is influenced by many of these factors (waves, tides, currents). However for the Skagit dispersal system, another significant factor is the geometry of the receiving basin. The Skagit sedimentation builds into a constrained basin typical of other paraglacial and tectonic environments (Table 3.3). Great depth and short fetch cause limited wave energy, and narrow channels accelerate tidal flows.

The large-scale steering of sediment dispersal moves the system southward into Saratoga Passage and northward through Deception Pass. This directs sediment into two types of receiving basins, in which sediment trapping and broad dispersal dominate. Examination of Puget Sound and the Strait of Juan de Fuca reveals other deltas that fit this pattern (Table 3.3). In general, deltas located at the heads of fjord-like basins act as a trap and deposit mud close to the river mouths. These deltas have a well defined delta front and a morphology similar to classic Gilbert deltas (Corner et al., 1990). Examples from the region are Stillaguamish, Nooksack and Big Quilcene (Fig. 3.6; Table 3.3). Historical maps report the progradation of the topset regions (wetland and marsh) on the Stillaguamish and Nooksack deltas (Bortleson et al., 1980), demonstrating sediment accumulation.

A second type of delta is located on the side walls of narrow basins. The progradation of these deltas into the basin creates strong shore-parallel tidal currents that limit deposition at the delta front. These delta types have dispersal patterns

comparable to the Skagit River Northern Basin extending into Rosario Strait. The characteristics of these basins are: the delta front is coarse grained, it may not be actively accumulating, and mud is broadly dispersed. Studies in fjords suggest deltaic deposition can constrict and strengthen currents (Bornhold and Prior, 1990). In some cases, tidal currents likely inhibit further outbuilding at portions of the delta front (e.g. Nisqually, Skagit). Although the impact of human alteration cannot be discounted, in both the Nisqually and Skagit deltas, the marsh is receding or has stagnated over the last 100 yrs suggesting that sediment is moved away by currents (Bortleson et al., 1980). Deltaic systems with broad sediment dispersal in Puget Sound (e.g., Elwha, Hamma Hama, Duckabush, Dosewallips, and Nisqually; Table 3.3), cause relatively high accumulation rates (~5 mm y^{-1}) in adjacent deep main basins of Puget Sound (Carpenter et al., 1985; Lavelle et al., 1986; Schell, 1977).

Beyond Puget Sound and the Strait of Juan de Fuca, delta deposition in constricted regions follows a similar pattern (Table 3.3). An example is in British Columbia fjords (Bute Inlet, Howe Sound and Knight Inlet) where longer-term delta building (1000-yr) differs based on river entry (i.e., sidewall deltas and fjord-head deltas; Prior and Bornhold, 1990). Similarities are in regions that have constrained basins and mesotidal to macrotidal ranges. The deposition of muds in deltas of this type is strongly impacted by river-mouth location and basin shape. Basin geometry also impacts physical factors, such as waves, tides, and river dominance.

Understanding the depositional patterns is important in interpreting ancient systems preserved in the rock record. Deltas formed in insular seas have a high rate of preservation due to limited waves and confined basins. However, these deltas should be interpreted within the framework of complexities caused by a confined receiving basin. Potentially multiple depocenters could form at a distance from the sediment source. These basins may also change through time, due to river avulsion and fluctuations in regional climate and sediment supply. We suggest that each receiving basin creates a different depositional environment and therefore preserves a unique stratigraphic signature.

3.6 Conclusions

Summarized below are the interpretations of data that address the objectives of this paper.

1) Mechanisms controlling dispersal patterns: Within insular seas, basin geometry in addition to complex patterns of river discharge, and tidal currents, control sediment dispersal. Sand remains near the source (delta topset), and most mud is dispersed much farther. The fate of the fine-grained sediment is determined by complex interactions in timing between its export from the tidal flat (delta topset) and tidal currents in the receiving basin.

For the Skagit system, this results in sediment dispersal into two distinct basins. Saratoga Passage is a relatively deep and quiescent basin, which promotes particle deposition. The seabed becomes finer with distance from the river mouth. The Northern Basin has much more complicated bathymetry, with strong currents in constrictions, where coarse seabeds are formed. Some mud is found in quiescent bathymetric lows, but much mud is exported through Deception Pass where it is widely dispersed in Rosario Strait.

2) Sediment accumulation into two different basins: The seasonal dispersal patterns of fine-grained Skagit sediment reveal that accumulation is controlled by basin geometry, resulting in two depocenters: Saratoga Passage and the area outside Deception Pass. In northern Saratoga Passage, accumulation rates reach ~10 mm y^{-1} and decrease southward. Outside Deception Pass lower accumulation rates were observed, likely because sediment is broadcast widely.

Of the fine-grained sediment budget for the Skagit River, ~530 $x10^3$ T y^{-1} are accounted for in Saratoga Passage, 27 $x10^3$ T y^{-1} in Skagit tidal flats and marsh (topset), and much of the remaining mud is exported through Deception Pass into Rosario Strait.

3) Outbuilding into a constrained basin: Comparison of depositional patterns for the Skagit River dispersal system and others within the Salish Sea region, show different types depending on basin geometry and river-mouth location within the basin. Deltas

that promote mud accumulation near the source are generally located at the heads of narrow embayments, and deltas promoting broad dispersal are located on the side walls of the embayments. The Skagit River system has characteristics of both settings, and sequesters the sand fraction near the source (delta topset), and disperses the fine fractions a much greater distance (5-50 km).

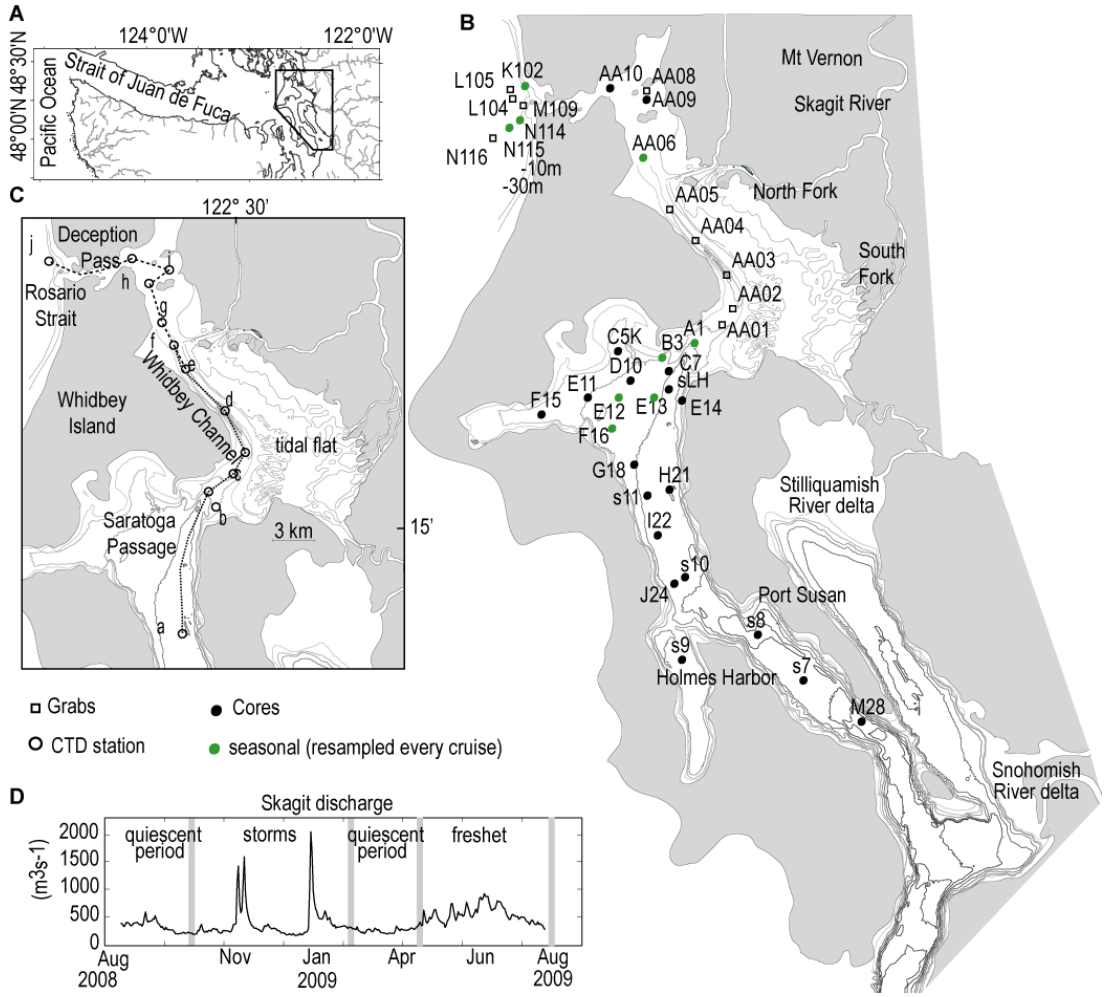

Figure 3.1. A) Map of northwestern Washington State, black polygon outlines location of study area. B) Map of Skagit River receiving basin. Sediment samples were collected in fringing marsh, Whidbey Channel, and in deeper basins (Saratoga Passage and Rosario Strait) as indicated. C) CTD transects (black dashed line) are shown with casts labeled (a-j). To the west, the outer edge of the topset (tidal flat) is bounded by a channel, referred to as "Whidbey Channel". D) Skagit River discharge during the sampling period, and seasonal sampling scheme. Freshet, winter storms and quiescent (low discharge) periods are indicated by vertical lines.

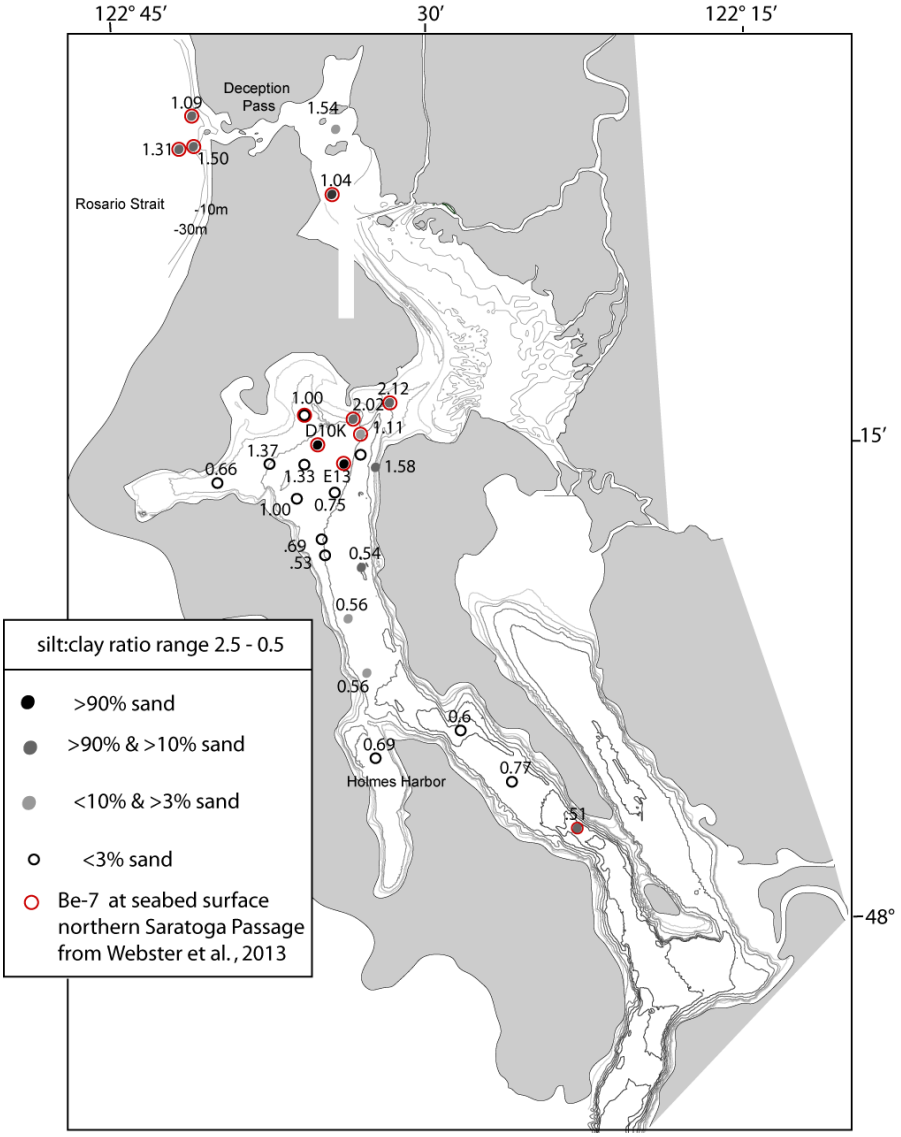

Figure 3.2. Map showing variation in sand content and silt:clay ratios at seafloor surface. Grain size in Saratoga Passage fines southward until southern end. Rosario Strait contained a mixture of shell hash, sand and only two muddier locations, suggesting strong physical processes. Surface samples with the presence of ^{7}Be are denoted with red outline, recent fine-grained sediment was observed in northern Saratoga Passage (modified from Webster et al., 2013) and Rosario Strait and at one site in southern Saratoga Passage (M28). This indicates fine-grained sediment was rapidly distributed 10 kms within several months and suggests the southern end of Saratoga Passage receives some Snohomish River sediment.

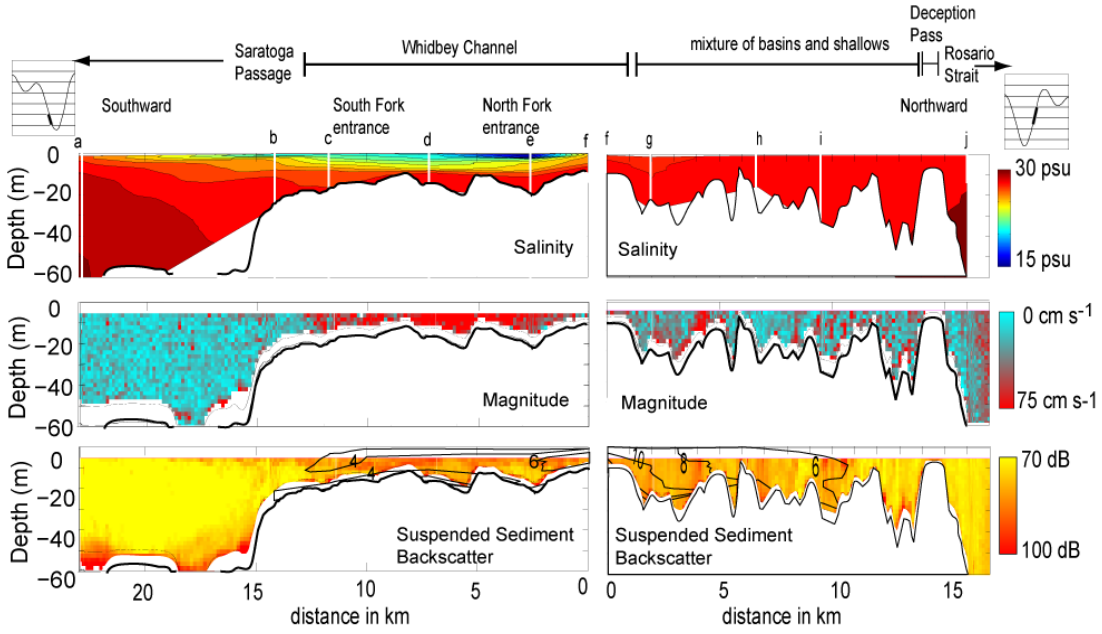

Figure 3.3. Hydrography through Whidbey Channel and extending into Saratoga Passage (southward) on falling tide and Rosario Strait (northward) on rising tide. Salinity, averaged current magnitudes, and suspended sediment concentration (black contours) shown in mg $L^{-1}$and ADCP backscatter, shown in raw dB, which is used a proxy for sediment in the water column are shown. Within transects, dashed white lines indicate locations of CTD casts (a-j; see Fig. 3.1). A) On the falling tide, enhanced SSC and the fresh water plume is observed in Whidbey Channel and extends southward into Saratoga Passage. Current magnitudes are strong (>75cm s^{-1}) in Whidbey Channel and decrease in quiescent deep Saratoga Passage (<10 cm s^{-1}), which supports particle settling. B) On the rising tide, sediment is observed northward of Whidbey Channel, through a series of basins and shallows with variable currents (10 cm s^{-1} to 60 cm s^{-1}). Beyond the sheltered headland, currents within deep Rosario Strait currents are strong (~50 cm s^{-1}) throughout the water column, suggesting an energetic environment and broad dispersal.

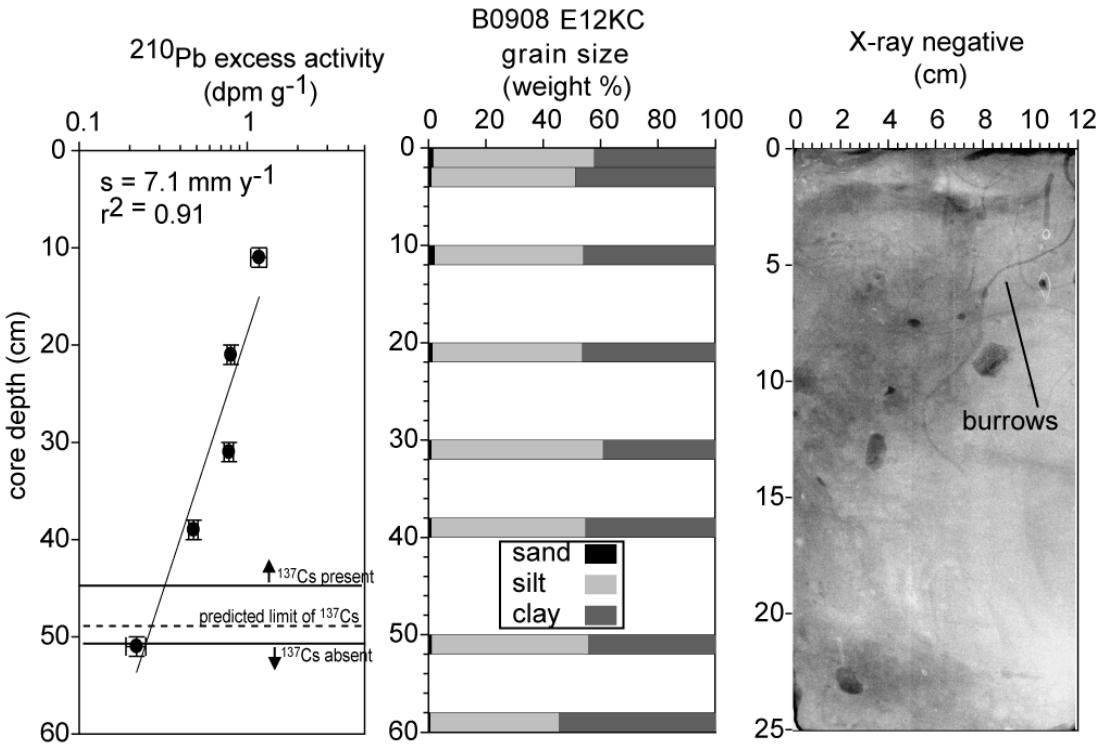

Figure 3.4. Radioisotope profiles, grain-size distributions and X-radiograph negatives of a typical core within Saratoga Passage. The excess ^{210}Pb profiles indicate an accumulation rate of 7.1 mm y^{-1}, which is in agreement with the observed penetration depth of ^{137}Cs. Grain size is uniform down core, ~50% clay and ~50% silt and a typical x-radiograph negative, shown from 0 to 25 cm below the surface, is characterized by bioturbation.

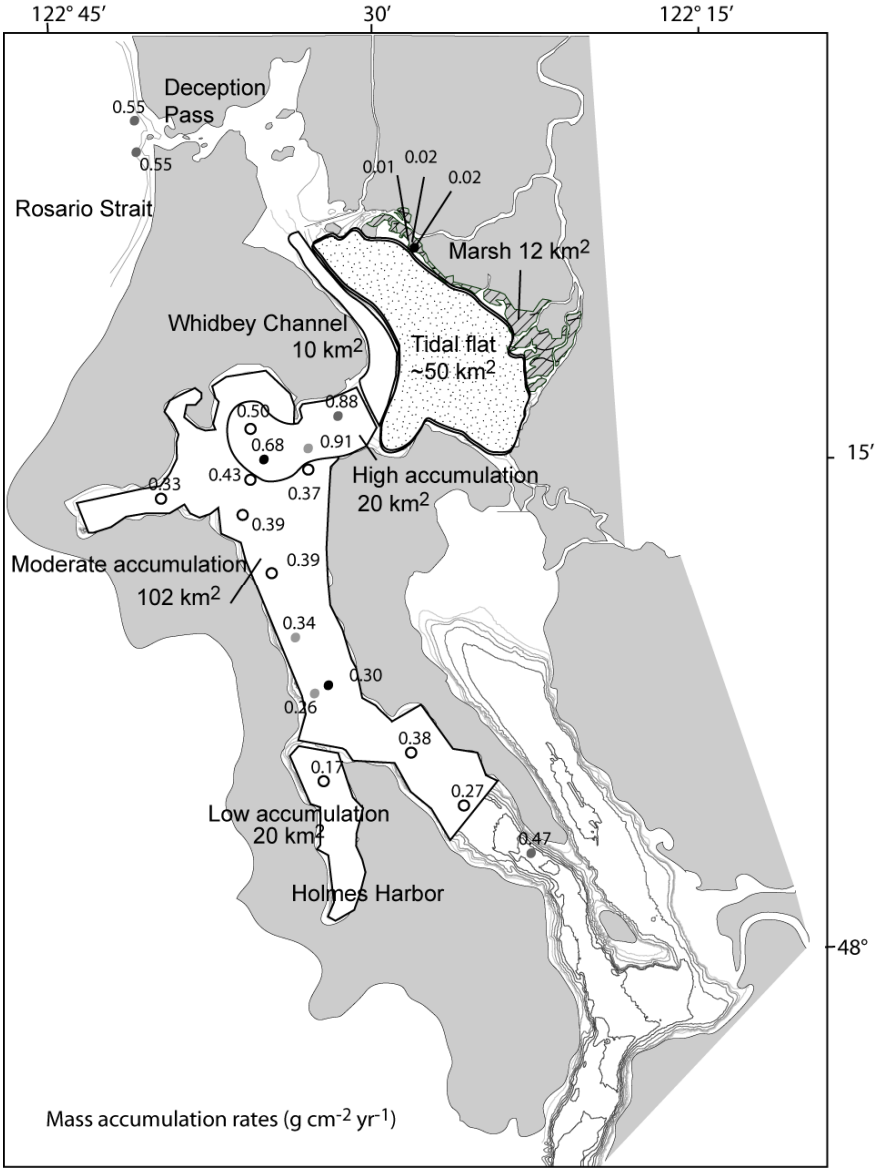

Figure 3.5. Map showing mass accumulation rates (g cm^{-2} y^{-1}) observed in the fringing marsh, Saratoga Passage and Rosario Strait. Saratoga Passage has three accumulation zones, high accumulation rates in northern Saratoga Passage (20 km^2), moderate accumulation rates throughout most of the basin (102 km^2) and low accumulation rates in Holmes Harbor, where a sill separates it from the main basin (20 km^2). Overall, ~530 x10^3 tons of mud per year are accounted for in Saratoga Passage. Moderate mass accumulation rates were observed in Rosario Strait, however this basin area is not constrained and no annual storage was calculated.

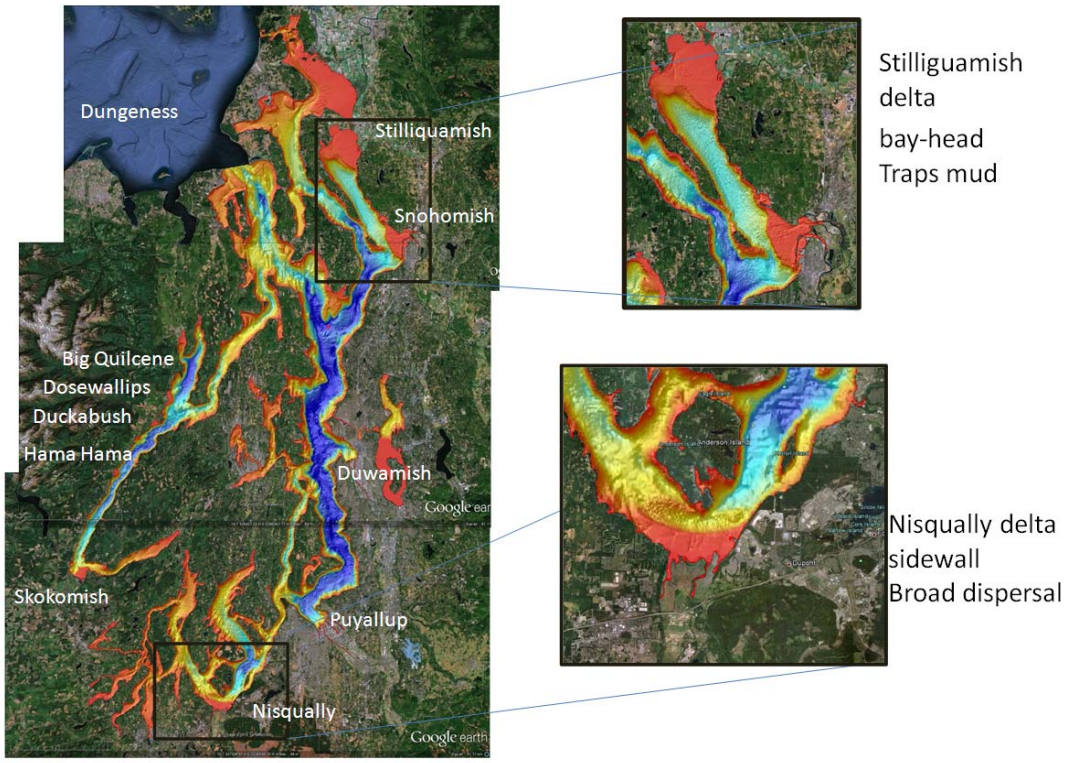

Figure 3.6. Map of shaded relief bathymetry (from Finlayson, 2005) of Puget Sound showing examples of varied receiving basins within the fjord-like sea and resulting delta morphology (side-wall and bay head deltas).

Table 3.1 Summary of sediment accumulation

Location	Core	Sediment Accumulation rate (cm y^{-1})	R^2	Porosity	Mass accumulation rate (g $cm^{-2}y^{-1}$)
Topset: Marsh					
	M002	0.28	0.83	0.50	0.02
	M003	0.22	0.94	0.63	0.02
	M004	0.16	0.79	0.68	0.01
Prodelta: Saratoga Passage					
	High accumulation				
	A1K	0.81	0.82	0.59	0.88
	C7K	1.04	0.91	0.67	0.91
	C5K	0.75	0.87	0.75	0.50
	D10K	0.97	0.95	0.74	0.68
	Moderate accumulation				
	E12K	0.71	0.91	0.77	0.43
	LoriK	0.76	0.91	--	0.37
	F15K	0.68	0.94	0.82	0.33
	F16K	0.80	0.93	0.82	0.39
	G18K	0.73	0.86	0.84	0.31
	H21BC	0.68	0.88	0.58	0.76
	S11K	0.89	0.85	0.83	0.39
	I22BC	1.01	0.96	0.87	0.34
	S10	0.77	0.94	0.85	0.30
	J24K	0.70	0.96	0.86	0.26
	S8K	0.86	0.89	0.83	0.38
	S7	0.63	0.93	0.84	0.27
	Low accumulation				
	S9	0.40	0.86	0.84	0.17
South End Saratoga Passage	.				
	M28K	0.78	0.87	0.78	0.47
Prodelta: Rosario Strait					
	N114K	0.62	0.99	0.666	0.55
	K102K	0.54	0.76	0.615	0.55

Table 3.2 Modern Skagit River marine mud storage

Location		Area (km^2)	Average mass accumulation rate ($g\ cm^{-2}y^{-1}$)	Mud storage ($T\ y^{-1}$)
Topset				
	marsh	12*	0.02 (n=3)	7×10^3
	tidal flat	~50	0.04**	20×10^3
Whidbey Channel		10	0	0×10^3
Prodelta				
	Saratoga Passage	High accumulation: 20 Moderate accumulation: 102 Holmes Harbor: 20 Total= 142	0.74 (n=4) 0.34 (n=10) 0.17 (n=1)	148×10^3 350×10^3 34×10^3 Total=532×10^3
	Rosario Strait	>300	0.55 (n=2)	?
Total Mud				559×10^3

*(Bortleson et al., 1980)

**(Webster et al., 2013)

Table 3.3 Small deltas of the Pacific Northwest

Basin	River	Suspended sediment discharge ($T \times 10^3$)	Basin size (km^2)	Discharge (m^3s^{-1})	Basin shape	Deposition pattern
North Sound	Nooksack	500	2,036	108	bayhead	Rapid progradation (Sternberg, 1967)
Whidbey Basin	Skagit	1700	8.500	470	side wall	Northward: Broad dispersal
	Skagit	1700	8,500	470	bayhead	Southward: High accumulation
Port Susan	Stillaguamish	16	1,770	54	bayhead	Rapid progradation (Bortleson et al., 1980)
Possession Sound	Snohomish	460	48,007	269		
Main Basin	Duwamish (Green)	120	**?**	**?**		Human altered
	Puyallup	520	2,455	94		Human altered
South Sound	Nisqually	113	1,339	41	side wall	Broad dispersal (Barnhardt and Sherrod, 2006)
	Deschutes	5	420	11.2		Human altered (Moore and Anderson, 1979)
Hood Canal	Skokomish	140	588	34.3		Progradation at river mouth (Bortleson et al., 1980)
	Hama Hama	11	220	10.3	side wall	
	Duckabush	14	202	11.5	side wall	
	Dosewallips	27	~303		side wall	
	Quilene	5	128	4.2	bayhead	
Strait of Juan de Fuca	Elwha				side wall	Broad dispersal
	Dungeness	?	404		sheltered	Rapid progradation (Bortleson et al., 1980)
Other	Fraser	20000	220,000	2700		(Milliman et al., 2008))
Bute Inlet	Homathko	913	5720	254	bayhead	Progradation (Syvitski and Farrow, 1983)
Knight Inlet	Klinaklini	1500	6462	325	bayhead	Progradation (Syvitski and Farrow, 1983)

4 Chapter: A comparison of modern sediment processes and ancient depositional history: Elwha River Delta, Washington State

4.1 Introduction

Relict coastal features (shorelines, spits, deltas) are indicators of past sea levels throughout the period since the Late Pleistocene and Holocene (Barnhardt et al., 1995; Barrie and Conway, 2002; Clemmensen et al., 2001; Novak and Pedersen, 2000; Oldale, 1985; Shipp et al., 1991). These ancient sedimentary features and deposits are formed by oceanic processes, but the linkages between sedimentary processes and sea-level change are not well understood. River deltas can record post-glacial sediment accumulation (Hill, 1996; Williams and Roberts, 1989), and those deltas formed within insular seas fed by rivers having, small mountainous drainage basins are ideal for study. The special attributes of these deltas include local influence of forcing factors (small drainage basin), protected environment (low wave energy), relatively high sediment yield overtime, and prevalence throughout previously glaciated mountainous regions (i.e. British Columbia, Puget Sound, Scandinavia). These small deltas formed within the last 9,000 years (Stanley and Warne, 1994), and built out into glacially scoured basins, allowing them not only to preserve depositional forcing signatures, but also to allow comparison with ancient deltaic deposits and modern sedimentary mechanisms.

The Strait of Juan de Fuca (Fig. 4.1) is floored by thick sedimentary deposits, which record its glacial-marine history. During the past 16 kyrs, the Strait of Juan de Fuca and Puget Sound have experienced deglaciation and crustal rebound resulting in rapid relative sea-level fall, followed by a subsequent sea-level rise as rebound rates decreased and eustatic sea-level continued to rise. Following the retreat of the Juan de Fuca and Puget Lobes of the Fraser glaciations, this region also developed physical-oceanographic processes that impact the coast. Waves, tidal currents, and baroclinic circulation have led to complex postglacial deposits preserved in the Strait of Juan de Fuca (Hewitt and Mosher, 2001).

Deltas associated with small mountainous drainage basins in this region experienced a complicated history of oceanic conditions, sediment supply and local sea-level change. In particular, the Elwha delta morphology suggests strong marine processes, imposed on both the modern and ancient strata (submerged spit-like features). These features allow investigation of their origin through the extrapolation of modern processes. In addition to providing insight on delta formation and shoreline response, this is important for predicting effects of future sea-level rise.

This study incorporates oceanic (water column and seabed) measurements with traditional geophysical tools to compare coastal sediment processes today to ancient deposits formed by similar processes throughout the Holocene. Specifically, modern sediment processes on the Elwha subaqueous delta are used to: 1) interpret

depositional history of the delta and hypothesize forcing mechanisms on strata development, 2) document modern sediment dispersal mechanisms and compare to ancient deposition, 3) evaluate environmental conditions for preservation of past shoreline features, and 4) estimate the impacts of superposition of sea-level rise on deltaic processes.

4.2 Regional Setting

4.2.1 Glacial history

Throughout the Pleistocene, the Strait of Juan de Fuca experienced a series of glacial advances and retreats. The most recent Fraser glaciation peaked between 18,000-14,000 yr BP and advanced southward and westward as the Puget and Juan de Fuca lobes, respectively. Deglaciation and eastward retreat of the Juan de Fuca lobe from the continental-shelf edge began ~14,460 ±200 ^{14}C yr BP (Herzer and Bornhold, 1982; Heusser, 1973) and had retreated to Whidbey Island by 13,595 ±145 ^{14}C yr BP (Dethier et al., 1995) thereby opening the Strait to oceanic conditions (Fig. 4.1).

At ~12,500 ^{14}C yr BP, the crust was isostatically depressed by glacial loading and sea level was ~50 m above present sea level near Port Angeles (Dethier et al., 1995). The isostatic rebound following glacial retreat caused sea level to fall rapidly to a lowstand depth in Victoria, BC (Fig. 4.1) of -60 m at 9,200 ^{14}C yr BP (Mosher and Hewitt, 2004). The rate of eustatic sea-level rise then overtook local isostatic rebound and sea-level rose to the modern level. Processes associated with glaciation, and sea-

level change left a thick layer of glacial sediments throughout the Strait. In the nearshore, (i.e., Elwha delta) the glacial marine sediments have been overlain by Holocene deposition from bluff erosion and delta formation (Hewitt and Mosher, 2001). The postglacial Holocene sediments are composed of two units, associated with the fall and subsequent rise of sea-level in the region (Mosher and Hewitt, 2004), and the Elwha River delta may fit this generalized model for Holocene. For example, similarities in morphology between Ediz Hook (Fig. 4.1) and submarine spit-like features have been previously noted, (Galster and Schwartz, 1990; Mosher and Hewitt, 2004), however details of these features have not been confirmed with subsurface data linked to knowledge of oceanographic processes.

4.2.2 Marine conditions

The Elwha delta is located in the eastern Strait of Juan de Fuca (Fig. 4.1A). The subaerial portion of the delta protrudes 2 km into the Strait and the subaqueous portion extends another 4 km northward. The Strait is a narrow seaway that connects the Pacific Ocean to Puget Sound and Georgia Basin, and is bounded on the south by the Olympic Peninsula and on the north by Vancouver Island. The Strait is a weakly stratified partially mixed estuary and the general net surface circulation is seaward (westward) and is focused on the northern side. The net flow is landward (eastward) deep in the water column and focused on the southern side of the Strait (Cannon, 1978). Tides at Ediz Hook are mixed semidiurnal with a spring tidal range of ~2.1 m

and neap range of ~1.3 m (NOAA). Tidal currents dominate the flow regime and are fairly uniform in the main body of the Strait (Cannon, 1978).

4.2.3 The Elwha River

The Elwha River is 72 km long, has a drainage basin of 830 km^2 on the northern flank of the Olympic Range, and flows northward into the Strait of Juan de Fuca (Fig. 4.1). The Elwha River has a bimodal hydrograph rising gently in spring/summer to 100-200 $m^3 s^{-1}$ due to snow melt and episodically to much greater discharges in fall/winter due to storms (Fig. 4.1). The hydrograph has an average low flow of 14 $m^3 s^{-1}$, and fall/winter peaks reaching 300-400 $m^3 s^{-1}$, typically lasting 1-3 days as storms move off the Pacific Ocean.

In 1916, construction began on two dams that were built at 8-km and 22-km upstream of the river mouth, essentially eliminating the sediment supply to the nearshore environment. Prior to the dams, sediment-laden river discharge and erosion of coastal bluffs (composed of glacial deposits) supplied sediment to the nearshore region. Since the 1940's, 2.7 km of the shoreline east of the delta has been artificially armored (Shaffer et al., 2008). Wave-driven longshore transport processes on the delta shoreline are actively moving cobble sized particles (Miller et al., 2011), and east of the river mouth the shoreline is eroding at a rate of 0.6 m yr^{-1} (Warrick et al., 2009). The dams are currently in the process of being removed, which has resulted in

sediment concentrations increasing by two orders of magnitude (up to 2.5 g L^{-1}) in the nearshore environment (Eidam et al., 2012).

4.3 Methods

4.3.1 Field methods

The surface morphology and internal structure of the Elwha delta were addressed using multi-beam swath mapping and single-channel seismic reflection profiling (Fig 4.1B). Bottom samples were collected using a grab sampler (Fig. 4.1B). To document the fate of particles on various timescales, water-column and time-series measurements were combined with seabed sampling and geophysical remote sensing on the subaqueous portion of the Elwha River delta (Fig. 4.1). Data collection (2007-2009) consisted of water-column profiles using CTD (Conductivity, Temperature and Depth) systems with OBS (Optical Backscatter Sensor)for suspended-sediment concentrations and ship-mounted ADCP (Acoustic Doppler Current Profiler) for water velocity; and long-term bottom-boundary-layer (BBL) measurements using time-series bottom tripods (Fig. 4.1B).

4.3.1.1 Seabed bathymetry

A cruise in Jun 2007 on R/V Itasca collected 40 km^2 of high-resolution swath bathymetry and backscatter data (Fig. 4.1B) using a Reson Seabat 8191 head and Reson 6042 software. CARIS software was used for post processing, which included

the removal of multiples, and applying corrections for tidal elevation and sound velocity. Bathymetry grids of 1x1 m were created in Surfer and plotted in ArcGIS.

4.3.1.2 Seismic stratigraphy

In Apr 2007, ~40 km of single-channel seismic reflection profiles (SRP) were collected over the subaqueous portion of the delta (Fig. 4.1B). A 9-tip 300-joule mini-sparker source was fired once each second as the R/V Centennial steamed at 5 knots. Reflected signals were detected using a 20-element hydrophone toward 25 m astern. The data were bandpass filtered (400-1600 Hz), migrated, and converted to depth sections using a sound velocity of 1500 m s^{-1}. The mini-sparker line A (Fig.4.1B) was collected parallel to a line collected previously by Mosher and Hewitt (2004) using an air gun sound source; and our line extends farther shoreward.

4.3.1.3 Grain size

Samples were collected from the R/V Clifford A. Barnes using a Shipek grab on the subaqueous delta seabed (Fig. 4.1B). If no sample was retrieved after three attempts the station was recorded as hard substrate. In the laboratory, sediment samples were divided into several size fractions. Particles coarser than -3.5 phi (1.1 cm) were measured by hand (i.e., three axes), and the fraction between -3.5 phi and +3.5 phi (90 μm) was sieved. The remaining sediment was wet sieved at 4 phi (63 μm), to separate silt-clay fractions. Silt and clay fractions size were analyzed via pipette and sampled at 6 phi and 8 phi.

4.3.1.4 Water-column processes

The water column studies were designed to record three distinct environmental conditions: 1): quiescent periods with low river discharge and low wave energy (Mar-May and Aug-Nov); 2) summer freshets with high-river discharge and low waves (Jun-Jul); and 3) winter freshets with high river discharge and high waves (Dec-Feb) (Fig. 4.1C). The Elwha River daily water discharge data for these periods were obtained from the gauging station located near Port Angeles, WA at McDonald Bridge (USGS gage 12045500, http://waterdata.usgs.gov/nwis/).

In Jun 07, Jan 08 and Apr 08 CTD/ADCP transects were completed over various tidal cycles along the 10-m, 20-m and 30-m isobaths (Fig. 4.1B). Each transect consisted of 8 stations and was completed within ~45 min in order for the data set to be quasi-synoptic. On station the CTD and OBS were lowered by hand and a surface water sample was collected 0.5 m below the surface using a Niskin. The entire water sample (1-3 L) was passed through a nitrocellulose 0.47-µm filter to measure suspended-sediment concentrations (SSC) and to calibrate the OBS. Shipboard ADCP (600 kHz) collected velocity and backscatter data in 0.5-m bins while transiting between stations and for at least 2.5 min at each station.

4.3.1.5 Bottom-boundary-layer time-series data

A tripod was deployed on the Elwha delta in 20 m of water over the winter season from Jan 08-Apr 08 and Nov 08-Jan 09 (Fig. 4.1). The tripod was equipped with an

ADV (Acoustic Doppler Velocimeter) having a sensing volume at 100 cm above the seabed (cmab), a Marsh/McBirney electromagnetic current meter (30 cmab), an upward looking ADCP (350 cmab to near surface; 600 kHz), OBS (30 cmab, 60 cmab, 150 cmab), transmissometer (100 cmab), and CTD (100 cmab). Measurements were obtained at 2 Hz every hour for 6 min burst length. A downward-looking digital camera recorded still images every 2 h and a video camera recorded settling particles once every 2 h for 6 sec (Sternberg et al., 1999). Two simple sediment trap tubes were attached to the tripod frame to collect suspended sediment. This sediment was used to calibrate the tripod OBSs in the laboratory with known SSC.

4.3.2 Instrument data analysis

4.3.2.1 Shipboard water profiling

The shipboard ADCP data were collected while transecting between stations, and were averaged over 10 ensembles in 0.5-m bins. The ADCP velocities collected on station were averaged and plotted to calculate a gross estimate of shear velocity using the log layer method. If the velocity profile did not fit a logarithmic relationship, it was assumed that measurements did not fall within the log layer and the calculation was omitted.

4.3.2.2 Tripods

Current observations retrieved from the instruments were averaged over the sample interval (6 min) and the data were rotated into north and east coordinates. The data

were plotted and outliers removed. The upward-looking ADCP data were range-corrected, averaged and plotted. ADV burst data were examined over four high wave events between Feb 08-Apr 08. Progressive vector diagrams were completed by summing the current velocities. OBS data were converted from volts to mg L^{-1} by a laboratory calibration with tube trap sediment and averaged over the burst interval, plotted and outliers removed (i.e., signals of organisms, biofouling, etc.). Shear velocity was calculated using the Quadratic Stress Law, with a drag coefficient of $3.1x10^{-3}$ based on Sternberg (1968).

4.4 Results

4.4.1 Elwha delta seabed

4.4.1.1 Elwha delta morphology

The seafloor of the Elwha delta consists of a broad, gently sloping (~1°) topset surface extending to 40 m water depth at 4-5 km from the river mouth (Fig. 4.2). The delta front then drops from a depth of 40 m to 120 m, with an 8-10° slope and break in slope (terrace) at ~50 m (Fig. 4.2C). On the eastern flank, three linear features are sub parallel with the shoreline and have crests at water depths of 29 m, 22 m and 16 m (Fig. 4.2). These features have relatively steep flanks (~15°) and flat tops and lie seaward of, Ediz Hook (Fig. 4.1B). These bathymetric linear features will be referred to in this paper as potential paleospits. A terrace at ~20 m water depth can be traced

across the topset and a second terrace at 50 m water depth is located on the ancient foreset (Fig. 4.2C).

4.4.1.2 Seismic stratigraphy

Three main units were indentified in the SRP data (Fig. 4.3 and 4.4), Units 1 and 2 are progradational, associated with the Elwha delta formation and growth, and both thicken landward. Unit Gm is flat-lying and outcrops seaward of the Elwha delta (Fig. 4.3 and 4.4). Unit 1 consists of reflectors dipping seaward at 10-11°. The unit appears to thicken landward and gradually thins seaward; at its thickest it extends to the base of interpretable SRP data, and is estimated to reach thicknesses of >100 m.

Unit 2, the uppermost unit, includes three sub units: the spit-like features (2a); the expanse across subaqueous topset (2b); and the apron at the base of the delta foreset (2c) (Fig. 4.4). The acoustic properties within the spit-like features have convex-up reflectors that downlap (terminate down dip) onto a surface at ~100 m below sea level. The morphology of the most seaward elongate feature appears spit-like, but the SRP line H did not extend over this feature and the seismic data from line E did not penetrate the coarse seabed, so no internal reflectors were observed (Fig. 4.1; Fig. 4.3). Landward, the two submerged spit-like features and modern Ediz Hook, have convex-up internal reflectors. Across the subaqueous topset, Unit 2b reflectors contain seaward dipping reflectors at 8° (water depth <40 m), and in Unit 2c (40-60 m water depth) seaward dipping reflectors are observed downlapping and onlapping

(terminate against an inclined surface) onto Unit 1. Offshore, Unit Gm is observed beyond the delta. It is a stratified layer with some strong horizontal reflectors and in some intervals is acoustically transparent. Although Unit Gm appears to be overlain by Unit 2c, attenuation of the SRP signal beneath the main mass of the delta makes it difficult to trace Unit Gm further landward.

4.4.1.3 Unconformities

A strong reflector is observed at the base of Unit 2b. It has highest amplitudes between Units 1 and 2 and outcrops on the seafloor at ~60 m water depth (Fig 4.3) and may be an erosional unconformity. Unit 2c reflectors onlap on this unconformity landward and downlap at the seaward extent of the unit. The unconformity can be traced to depths of ~150 m below sea-level, overlying Unit Gm. Here Unit 2c has a possible conformable relationship with Unit Gm and reflectors onlap landward and downlap seaward at its base ~ 150 m below sea-level. This relationship forms an apron on the delta front (in lines A, B, C, H; Fig. 4.1). The spit-like features (Unit 2a) each have a hard reflector at their base (Fig. 4.4), and this reflector shows that spit 3 overlies spit 2.

4.4.1.4 Seabed sediments on the Elwha delta

Grab samples across the topset and prodelta regions reveal a coarse seabed. The subaqueous delta surface can be divided into four zones: a) central topset, b) Freshwater Bay, c) submerged paleospits, and d) prodelta (water depth > 40 m; Fig.

4.1; Fig. 4.5). Central topset has <1% mud, and gravel percentages range from 40-100% with modes between -2 to coarser than -4 phi. One sample fell outside of this range (N1-003) and had 80% sand and a mode of 3 phi. Samples from Freshwater Bay had the greatest variability; mud content ranged 0-16% and gravel content 2-87%, with modes from 3 to coarser than -4 phi. The submerged spits had <1% mud and 85-98% gravel, with modes coarser than -4 phi, with 4 mm, 8mm, and 20 mm clast modes. On the prodelta (water depth >40 m), slightly higher mud percentages were observed (0-8%) with greater particle size diversity, samples contained 3-90% gravel and exhibited modes of 3 to coarser than -4 phi. Beyond the topset, multibeam backscatter reveals a mixed seabed with large bedforms (Fig. 4.6).

4.4.2 Water-column processes

Current speeds along the 10-m isobath during the greater spring tides (higher-high to lower-low tide) in Jun 07 reached 1.5 m s^{-1}. On greater flood tides, the maximum currents were observed throughout much of the 10-m water column on the west side of the delta lobe with an eastward flow. The eastern side of the delta is a lower-velocity region with chaotic flow directions. The greater spring ebb tidal currents had similar magnitudes (i.e., up to 1.5 m s^{-1}) and were strongest on the east side with a westward current and a lower velocity region was on the west side of the delta lobe within Freshwater Bay, with flow eastward and becoming northward adjacent to the west side of the delta. Shear velocities ranged from 1 to 7 cm s^{-1} over the topset. Max shear velocities were focused in shallow depths on the east side of delta during

ebb tide, reaching 6 cm s^{-1}, and similarly in shallow depths on the west side of the delta during flood tide, reaching 7 cm s^{-1} (Fig. 4.7). At the tripod location (20-m deep; Fig 4.1B), the current magnitudes were slightly reduced, relative to the maximums observed in the spatial studies. Current measurements from 1 mab also followed the tidal phase and magnitudes reached 50-55 cm s^{-1} on greater flood during neap tidal conditions and 80-90 cm s^{-1} on greater spring tides, with currents peaking at the end of the flood tide (Fig. 4.7A and B) with eastward net flow (Fig. 4.8).

During the tripod deployment wave heights reached 0.90 m, with the highest waves occurring for durations of 1-3 days. Over the deployments, river discharge ranged from 232 m^3 s^{-1} (8 Jan 09) to 13 m^3 s^{-1} (11 Apr 08). Tidal range was ~3 m in the Jan-Apr deployment and ~4 m in the Nov-Jan deployment, which agrees with observations at the Port Angeles tide gauge (NOAA).

Suspended-sediment concentrations (SSC) ranged from 2-10 mg L^{-1} measured at 1 mab. The highest concentration of suspended sediment occurred following in the Nov 08 river discharge (230 m^3s^{-1}) and Feb 08 wave event (Fig. 4.7C; Fig. 4.9). Elevated SSC were also observed in both the thin surface plume (1.0-m thick; Warrick and Stevens, 2011) and the BBL (Fig. 4.9), with a maximum value of 70 mg L^{-1} for the plume directly in front of the river mouth. ADCP measurements (Fig. 4.7) show the highest levels of backscatter at the water surface and near the seabed (2.5 mab). ADCP backscatter correlates with the OBS data at 1 mab (r^2=0.56). The SSC

is observed to fluctuate in the OBS and ADCP records for each tidal cycle, with peak SSC between the end of greater flood to the start of weaker flood in the tide cycle (Fig. 4.7A and B).

Two elevated suspended-sediment events are examined in detail: a) wave and b) discharge (Fig. 4.7C; Fig. 4.9). A wave event began on 12 Dec 08 and lasted 36 h; in the first 12 h waves reached 0.85 m with a 10 s period, and over the following 24 h waves decreased to 0.20-0.30 m. During the wave event, river discharge was ~21 m^3 s^{-1}, and tidal range was ~4 m. The river-discharge event began on 5 Jan 09 with discharge increasing from 17 m^3 s^{-1} to 236 m^3 s^{-1} (Fig. 4.9). This max discharge lasted for two days and then decreased to 67 m^3 s^{-1}, salinity at 1 mab decreased from ~31 to 29 psu, over the next two days. Wave height was 0.07 m and tidal range increased from 2.0 m to 3.5 m over the discharge period.

4.5 Discussion:

4.5.1 Elwha delta morphology and stratigraphy

The Elwha delta morphology and structure, as shown by the swath mapping and seismic reflection data, suggests a complex depositional history. The shallow subtidal topset region, has a slope of 1° from 10 to 40 m water depth (Fig. 4.2), this disconnects today's Elwha River distributaries from the delta front by ~4 km. Broad shallow platforms such as this one have been associated with sea-level change in other small deltas (Hill, 1996; Lavoie et al., 2002). The gently sloping Elwha topset

platform reflects the interaction between sediment supply, oceanographic conditions, and a steady sea level rise during the late Holocene.

The seismic stratigraphy indicates that the delta lobe is composed of two major depositional units (Units 1 and 2) which overlie the flat basal Unit Gm (Fig. 4.3). The SRP data therefore fit within the previously defined seismic stratigraphy of the area of glacial-marine sediments overlain by Holocene deposits (Hewitt and Mosher, 2001). Unit Gm, a well-stratified unit with horizontal reflectors directly correlates to previously interpreted glacial-marine muds deposited during retreat of the glacial ice (Mosher and Hewitt, 2004). Overlying this, Units 1 and 2 are therefore Holocene in age, with internal dipping reflectors interpreted as foreset beds (Fig. 4.3;Mosher and Hewitt, 2004). Similar two-stage delta outbuilding has been observed in British Columbia deltas (Hill, 1996).

In the delta subsurface an erosional unconformity located between Units 1 and 2b is identified by strong reflectors, which truncate the seaward dipping strata in Unit 1 (Fig. 4.3). This erosional surface can be traced across the delta and emerges on the seafloor at ~50 m water depth (Fig. 4.2), and is interpreted as the lowest stratigraphic position of the Elwha River channel elevation throughout the Holocene.

Using previous studies to place the observed units in context allows these deltaic outbuilding units to be linked to sea-level change. The Elwha delta package of an erosional unconformity separating two clinoform units is similar to two Holocene

formations found through the Strait of Juan de Fuca coastal regions (Hewitt and Mosher, 2001). Unit 1 appears to be linked to rapid sea-level fall. Unit 2b was likely deposited during the subsequent rapid rise, and then gradual rise to present sea level (Fig. 4.3) (Mosher and Hewitt, 2004)(Mosher and Hewitt, 2004). The erosional unconformity between Unit 1 and Unit 2b that outcrops at ~50 m depth (Fig. 4.3) is in agreement with the Victoria, BC lowstand depth of 60 m below present sea level (Mosher and Hewitt, 2004). Based on this interpretation, the Elwha delta exhibits two prograding units likely forced by sea-level change: 1) massive Unit 1 formed during rapid sea-level fall attended by an increase in denudation rates and sediment supply in the Elwha River drainage basin, and 2) Unit 2 formed during the following sea-level rise. This study allows examination of Unit 2 in detail.

Within Unit 2 there are three major depositional sinks. In deeper water, Unit 2c forms an apron at the delta front, this sequence may have been deposited near lowstand depths (~50 m), when the Elwha River distributaries delivered sediment directly to the foreset (Fig. 4.3 and 4.10). Covering the surface of the delta, Unit 2b (Fig. 4.3), has dipping internal reflectors that downlap onto the unconformity at the top of Unit 1 (from 50 to 40-m water depth) and is interpreted as a prograding deposit. The horizontal reflectors within Unit 2b onlap from 40-m water depth landward suggesting this is a transgressive deposit, deposited during sea-level rise (Fig. 4.3).

Three elongated spit-like features are located to the east of the broad subaqueous delta (Fig. 4.2). These features have structural origins at ~100 m water depth off the delta lobe and rise steeply to their crests at 29 m, 22 m, and 16 m water depth (from offshore to onshore) and a morphology (slope and planar surfaces) similar to the modern Ediz Hook. Assuming these drowned features are relict spit deposits, they may give insights to past sea levels and transport mechanisms.

Each of these paleospits appears to have prograded to the east downlapping onto the seafloor at ~100 m water depth (Fig. 4.2), and data confirms that these are paleospits. Spits 2 and 3 contain convex-up internal reflectors, and are therefore interpreted to be accretional features (Fig. 4.4). Spit 2 corresponds to an erosional terrace observed across the topset at ~20 m water depth, and suggests previous sea level position (Fig. 4.2A and 4.2C). We conclude these features are paleospits, based on the stratigraphy of convex-up internal reflectors and downlapping reflectors onto the seafloor, the morphology of planar tops and relatively steep sides, and the proximity to Ediz Hook with similar acoustic properties to the modern spit. Without sub-surface data we cannot determine if Spit 1 is a paleospit or part of the delta foreset.

Sediments on the flanks of Spit 3 onlap onto the flanks of Spit 2 (Fig. 4.4) indicating that Spit 3 postdates Spit 2. The formation of multiple spits may indicate periodic ideal conditions of sediment supply and sea-level rise, where sea-level rise was slow

enough to allow for active littoral processes to form nearshore features (longshore transport and terraces), but rapid enough to drown and preserve these features.

Comparison of the morphology of the Elwha delta paleospits to the longer, more well-developed Ediz Hook leads to questions of local changes in processes responsible for the formation and modification of the delta, including changes in sediment supply, river avulsion, rate of sea-level change, possible occurrence of stillstands, and whether the spits have back filled. In British Colombia, sedimentary deposits have similar qualities and have been linked to sea-level change. For example, distinct buried beach ridges formed during rapid rise and continuous ridges formed when sea level stabilized (after ~4 kyr BP) (Engels and Roberts, 2005). The Elwha delta morphology exhibits similar patterns, showing less developed drowned spits during periods of rapid sea-level rise, and a well developed modern spit (Ediz Hook) that was able to migrate landward and prograde eastward as sea-level rise stabilized. The most rapid rates of sea-level change were likely at the earliest stages of the late Pleistocene-early Holocene rise of sea level (Williams and Roberts, 1989), and during this time there does not appear to be evidence of spit formation. Similarly, the nearby Fraser River delta (100 km to the northeast) had the slowest rate of Holocene progradation during most rapid rates of sea-level rise (Williams and Roberts, 1989), This suggests a "sweet spot" in the relative rate of sea-level rise, which allowed time for littoral processes to create the paleospits, but was followed by a rise in sea-level that was rapid enough for submergence.

The rate of sea-level change is not necessarily steady (Barnhardt and Sherrod, 2006; Barnhardt et al., 1995) and a brief sea-level stillstand has been dated on the Fraser Delta (6.2-5.8 kyrs BP; Williams and Roberts, 1989). Because spits take some time to accrete depending on sediment supply and sea-level changes, the existence of a paleospit may indicate a slower or unsteady sea-level rate. However, very few sea-level curves have the resolution to detect brief stillstands, and timing and exact sea levels vary locally (Barnhardt et al., 1995; Oldale, 1985), so care must be taken applying nearby sea-level curves to the Elwha delta.

In summary, the multiple paleospits on the eastern flank of the Elwha delta appear to have formed after sea-level rise slowed slightly, but rates were still rapid enough to overstep and drown the Elwha paleospits. Similar local rates of rise have been observed in other paraglacial regions (Barnhardt et al., 1995), however, multiple accretional shoreline features are rare. Transport measurements on the modern delta platform can give insight to evaluate why the Elwha paleospits may have been preserved.

4.5.2 Modern delta front outbuilding fine-grained

Although delta morphology and seismic data suggest massive delta-front outbuilding occurred in the past, today's seabed shows little evidence of sediment accumulation or motion. The broad (~2 km) shallow (<40 m) subaqueous delta topset (Fig. 4.2) is very coarse, ranging from sand up to cobbles (Fig. 4.5). Spring tidal currents across

>75% of the delta platform area exceed the critical shear velocity (~1.5 cm s^{-1}) for sand (0.25 mm) and likely are the mechanism that removes sand and finer particles from the platform. At the tripod site (Fig. 4.1B), currents are capable of transporting sand on every greater flood tide (Fig. 4.7A and B) based on Miller et al. (1977), likely winnowing the seabed. Beyond the delta platform, there is evidence of seabed motion and strong currents in deeper water (120 m), as shown by linear features in multibeam backscatter that suggest large bedforms (Fig. 4.6).

The shore-parallel tidal currents reach ~75 cm s^{-1} and not only winnow the seabed, but create a well-mixed water column and the along-shoreline, tidally oscillating currents serve to keep sediment in suspension. It is often assumed that large tidal ranges and freshwater discharge at river mouths stratify the water column and create turbidity maxima (Kineke and Sternberg, 1995; Martin et al., 2008). However, on the Elwha and other small deltas having mountainous drainage basins, strong shore-parallel tidal currents and energetic coastal processes can lead to a well-mixed water column with little opportunity for fine-grained sediment convergence in the bottom boundary layer.

Examination of the SSC at the tripod site (Fig. 4.1B) reveals that a daily peak occurs following greater flood tides (Fig. 4.7). As SSC does not correlate with shear stress, there is little evidence of local resuspension and the suspended-sediment signal is interpreted as eastward advection past the site. The source of sediment may be

Freshwater Bay (Fig. 4.1B), where mud content is low (5%), but sand fractions range from 8 to 98% (Fig. 4.5). During ebb tides, our observations and modeling studies (Gelfenbaum et al., 2009) suggest the presence of an eddy, which has lower velocities that may promote settling and deposition of particles in the bay. During the spring flood tides, high shear velocities (up to 4 cm s^{-1}) are observed and are capable of resuspending very coarse sand (2 mm) (Fig. 4.5). Eastward advection of sediment from Freshwater Bay on greater spring flood tides is in agreement with observations from the tripod site where the highest SSC is observed immediately following these tides (Fig. 4.7). Further measurements from the tripod site show both spring and neap flood-tide BBL currents may transport a water parcel 10 km over a 12-h period (Fig. 4.8). This indicates the potential for broad dispersal of particles in suspension. The presence of large bedforms in deeper water (Fig. 4.6) suggests strong currents beyond the subaqueous delta platform, which are sufficient for bedform generation and too strong to promote mud to accumulation.

Routine tidal conditions suggest broad dispersal of particles in suspension, and an immobile coarse-grained delta seabed. Whereas previous studies of small river systems show much sediment can be deposited during storm events (Sommerfield and Nittrouer, 1999; Wheatcroft and Borgeld, 2000), examination of events on the Elwha delta show sediment in suspension, but little deposition. During conditions of spring tides and 0.8-m-high waves, SSC is elevated on the delta (Fig. 4.7C). The suspended sediment is observed in a bottom layer (~10-m thick), suggesting that waves act to

resuspend the sediment and tidal currents then act to distribute the sediment out of the wave boundary layer and higher into the water column. There is minimal correlation between the local shear stress and SSC suggesting the observed sediment is advected past the tripod sensors from locations to the west, e.g., Freshwater Bay.

A 4-d river discharge event (~230 m^3 s^{-1}) resulted in elevated SSC and decreased salinity (Fig. 4.9), implying an increase in Elwha River flood water in the nearshore over that period. This event illustrates the potential of intensified fluvial sediment delivery to marine environment. Enhanced SSC and fresher water were observed in the BBL three days after the first discharge pulse, and then these were advected back and forth for several cycles during the spring tides. Peak SSC continued to occur following flood tidal stage, and net direction was similar to low-discharge periods (Fig. 4.9; Fig. 4.8) suggesting a similar tidally driven transport mechanism associated with eastward advection past the site, and again broad dispersal of the fine-grained sediment.

Under the present (pre-dam removal) conditions of limited sediment supply, strong shear stresses on the delta platform have winnowed finer-grained surficial material leaving an armored immobile seabed. Locations on the delta with some heterogeneity of particle size occur in areas with a direct sediment supply and mechanisms to trap particles (e.g. lesser shear velocities and convergence in an ebb-tide eddy).

During both increased-discharge and large-wave conditions there were increases in bottom boundary layer SSC and the strong alongshore tidal currents served to bring suspended sediment higher in water column. Due to the broad subaqueous platform, waves are able to resuspend what little fine-grained material is deposited and tidal currents act to bring this sediment out of the bottom boundary layer through the entire water column, aiding in the broad dispersal of finer sediment.

Although rivers commonly deliver significant amounts of fine-grained material to the marine environment, there is little evidence from the water column and seabed observations for accumulation of fine-grained sediment on the Elwha delta. However, the seismic data show evidence of massive deposition in the past, indicating a change in depositional patterns. The following factors may have promoted deposition in the past, although they cannot be confirmed with the present data sets. The Elwha delta may have always been coarse grained, although it is probable that the delta front was fine-grained based on knowledge from modern small deltas (e.g., Eel River delta). Additionally, although the Elwha the delta has not been cored, there is evidence of many fjord deltas being coarse-grained (McPherson et al., 1987; Prior and Bornhold, 1990; Syvitski and Farrow, 1983). Secondly, much of the delta mass was likely deposited during rapid sea-level change due to deglaciation. The rapidly expanding accommodation space resulting from sea-level rise, paired with high sediment supply from isostatic rebound, may have promoted the formation of massive prograding foreset beds observed (Fig. 4.3; Unit 1). And lastly, the

geology of the surrounding headlands may have enabled sediment accumulation. Pillar Point to the west is a bedrock outcrop, which shelters the west side of the subaerial delta from waves and currents, and the delta may have prograded easily behind this promontory, while presently finer sediment is removed by tidal currents. Overall, conditions in the current postglacial period, characterized by slow sea-level rise, do not seem compatible with the clinoform beds of the past. Assuming the marine conditions (i.e., waves, tides) have remained generally constant during the Holocene, other factors were also necessary for the massive outbuilding beds.

4.5.3 Paleospit preservation: comparison of modern and past shoreline processes. Factors supporting preservation of submerged relict features are associated with excess sediment supply, the coarse nature of sediment, rapid relative sea-level rise and limited wave energy (Barrie and Conway, 2002; Hiroki and Masuda, 2000; Novak and Pedersen, 2000). To preserve an inundated feature, it must be submerged to a depth where the seabed can no longer be mobilized. As on the modern delta platform, this depends on wave climate, seabed grain size and degree of natural armoring.

Waves are the primary longshore transport mechanism at the Elwha shoreline (Miller and Warrick, 2012). At the tripod location (Fig. 4.1B), the largest 10% of waves exceed 0.8 m in height with a 10 s period. Seabed clast-sizes on the submerged-spit tops fall into three modal categories: 4 mm, 8 mm, and 20 mm (Table 4.1). Based on

Komar and Miller (1973) and using the wave-orbital velocity for a 0.8-m height, 10-s period, the threshold for motion is met at 3.3 m, 1.8 m and 0.8 m water depth for a 4-mm, 8-mm, and 20-mm particle, respectively. Therefore, the coarse-grained paleospit seabed surfaces could have been mobilized by the largest waves at shoreline elevations but once submerged to >3.3 m depth, they would be no longer be mobilized. Based on the wave climate and calculated threshold of motion, all three paleospits (not Ediz Hook) are presently below calculated preservation depths. The elevation difference of 6 m between spits 1-2 and 2-3 is large enough to separate them from simultaneous motion during the largest wave events. The formation and preservation of the three closely spaced paleospits is hypothesized to be due to the small water-depth differential needed for threshold of motion, when considering the coarse-grained seabed with its surface lag that is observed on the immobile submerged platform today.

4.5.4 Summary of Holocene development of the Elwha delta

Climate changes during the Holocene led to rapid sea-level fluctuations and large sediment yields, both factors had a major effect on the early Elwha delta depositional outbuilding history. When the rate of sea-level rise slowed, wave-driven shore-parallel transport began to shape delta outbuilding toward spit formation. Initially (10-12 kyrs BP) changes in sea level and large sediment supply controlled delta morphology. This time of deglaciation and rapid sea-level fall, from +50 to -50 m

water depth, allowed the outbuilding of the initial delta (Unit 1) forming thick foreset beds (Fig. 4.3).

At lowstand, isostatic rebound rate equaled global sea-level rise (Victoria, BC sea level ~-60 m, ~9900 C^{14} kyr BP; Mosher and Hewitt, 2004) and the river mouth would have delivered sediment directly to the foreset region, depositing the apron surrounding the delta (Unit 2c; Fig. 4.3). Assuming tidal currents in the past were similar to those observed today, sediment delivery may have been coarse-grained or as mass flows of mixed grain sizes.

As the rate of eustatic sea-level rise became greater than isostatic rebound rates, local sea level began to rise, and the delta topset became inundated. This allowed creation of a shallow platform where sediment could be temporarily deposited and resuspended by oceanographic processes (as seen today). When sea level reached ~40 m water depth, Elwha delta morphology began to show evidence of longshore transport with the formation of paleospit 1 (Fig. 4.2; Fig. 4.10). The multiple spit formation shows evidence of rapid sea-level rise (~9-5 kyrs BP), and perhaps provides evidence of stillstands.

Over the last 5 kyrs, sea level has been rising slowly, and the zone of reworking has broadened as increased volumes of coarse sediment are trapped in the nearshore and transported eastward (Fig. 4.10). Both bluff erosion and Elwha River discharge supplied coarse sediment to create the 5-km-long Ediz Hook. This mechanism of

transport along the shoreline (Miller and Warrick, 2012), is likely similar to the past spit-building conditions. However, there is no evidence of potential deposition on the foreset, which is in contrast to the clinoform units formed in the past (Unit 1 and Unit 2b; Fig. 4.3).

4.6 Conclusions

The Elwha modern delta platform is coarse and relatively immobile. High shear stresses indicate sand and mud cannot accumulate over much of the submerged topset, and strong shore-parallel tide-driven currents are present on the topset indicating broad dispersal of particles in the water column. While wave and large discharge events increase sediment suspension in the water column, the tidal currents drive net transport and timing of sediment transport. These mechanisms support broad dispersal and are in contrast to the massive foreset accumulation observed in the delta stratigraphy (Unit 1, Unit 2b).

The submerged paleospits were accretionary shoreline features, which formed successively one at a time, stepwise as sea-level rose. These features indicate eastward shore-parallel transport was active since sea-level was at least 30 m lower and similar to shore-parallel transport on the modern shoreline of Ediz Hook.

Applying the present wave environment to the coarse-grained top surfaces of the paleospits suggest that the spits may have been immobile from wave actions once

water depth exceeded ~3 m. This suggests both the coarse-grained nature of the small delta and the rate of sea-level rise supports paleospit preservation.

Overall, there has been a shift in sediment sinks on the Elwha delta, from massive outbuilding in the past to spit formation today.

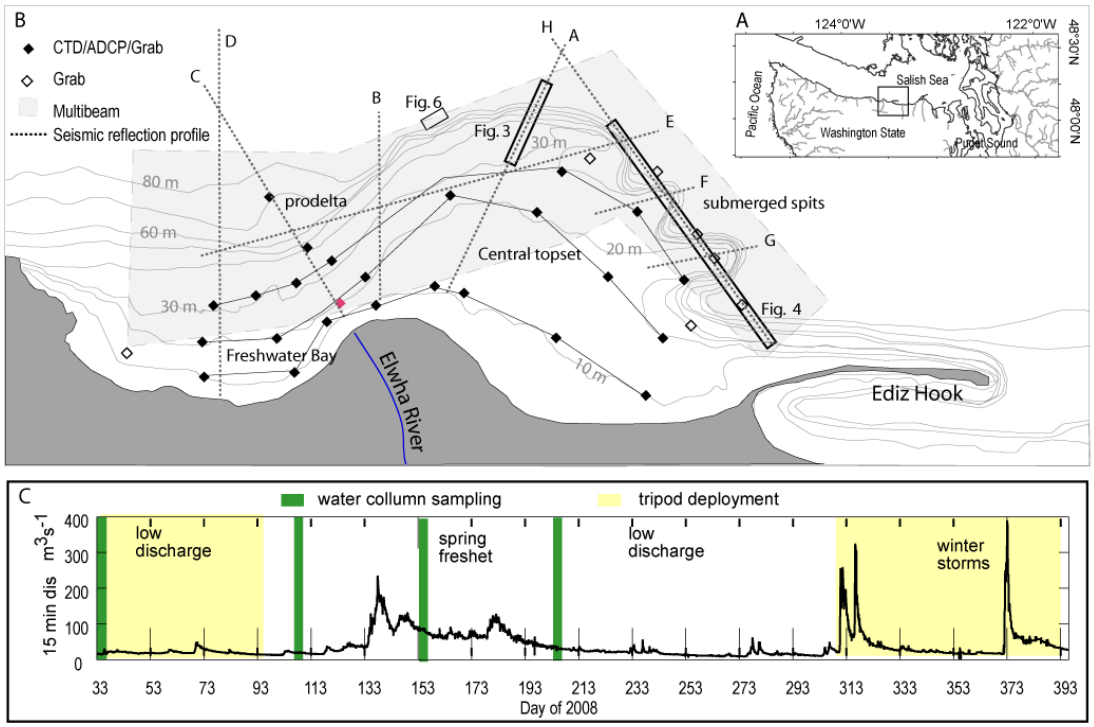

Figure 4.1 A) Map of northwestern Washington State, black box outlines location of study area. B) Map of Elwha River delta. Samples collected on delta platform are shown, tripod location (red diamond), sediment sample, ADCP and CTD stations (black diamonds), mapped multibeam area (shaded gray) and seismic reflection profile lines (black dashed lines). C) Elwha River discharge during the sampling period. Seasonal sampling scheme during periods of freshet, winter storms and low discharge are indicated by vertical lines.

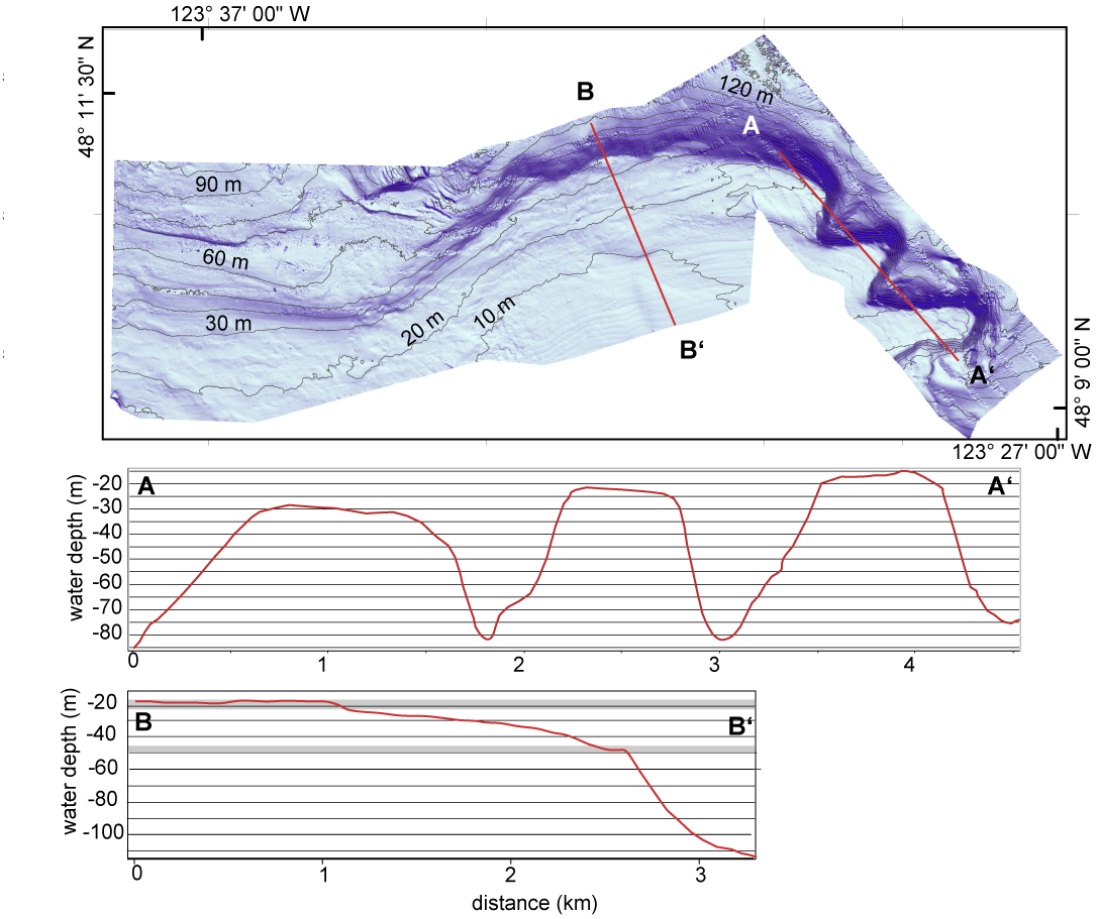

Figure 4.2. Shaded relief bathymetric map of the Elwha River delta, showing a broad shallow platform and the three linear features that are subparallel to the shoreline at the eastern boundary (labeled 1, 2, and 3). B) Bathymetric profile A-A' shows the spit-like features have steep sides and flat tops with crests at 29 m, 22 m and 16 m water depth. C) Bathymetric profile B-B' shows two terrace features at ~20 m and 50 m water depth.

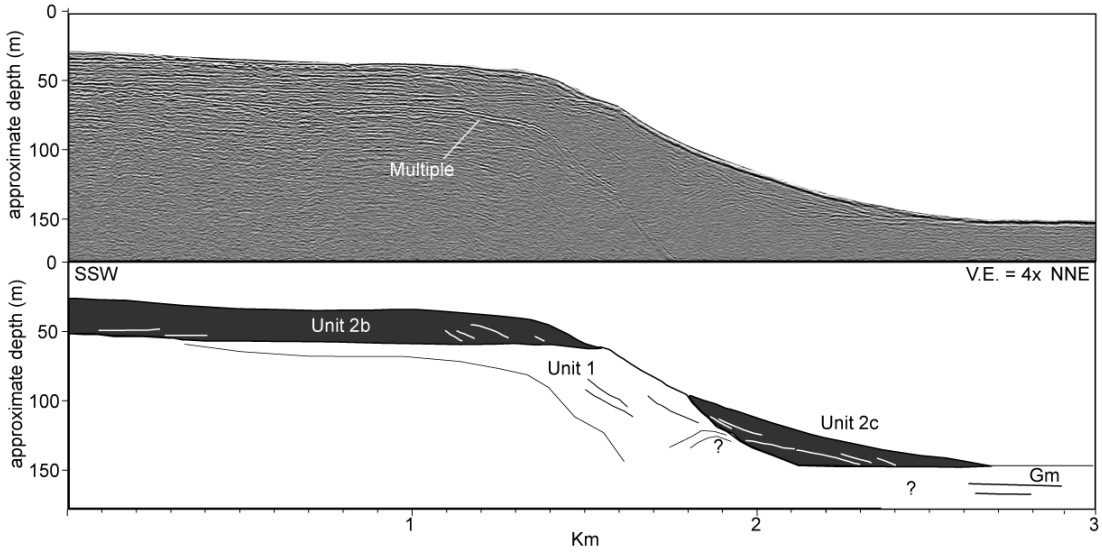

Figure 4.3. Minisparker profile across Elwha delta foreset, showing two outbuilding units, with an erosional unconformity that outcrops onto the seafloor at ~60 m water depth. Line location indicated in Fig. 4.1.

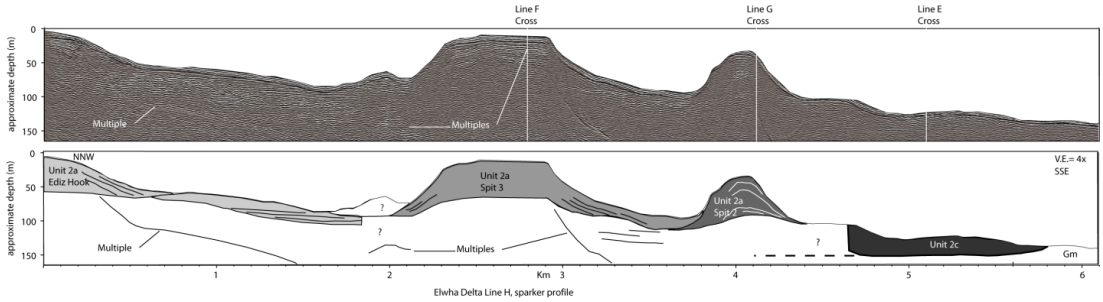

Figure 4.4. Minisparker profile from north of Ediz Hook to the NW across the spit-like features. Ediz Hook, spit 3 and spit 2 have convex up internal reflectors that downlap on to the seafloor (~100 m) and overlie Unit 2c. Spit 3 overlies spit 2, indicating spit 3 formed after spit 2, and suggesting it was overstepped by sea-level rise. Line location indicated in Fig. 4.1.

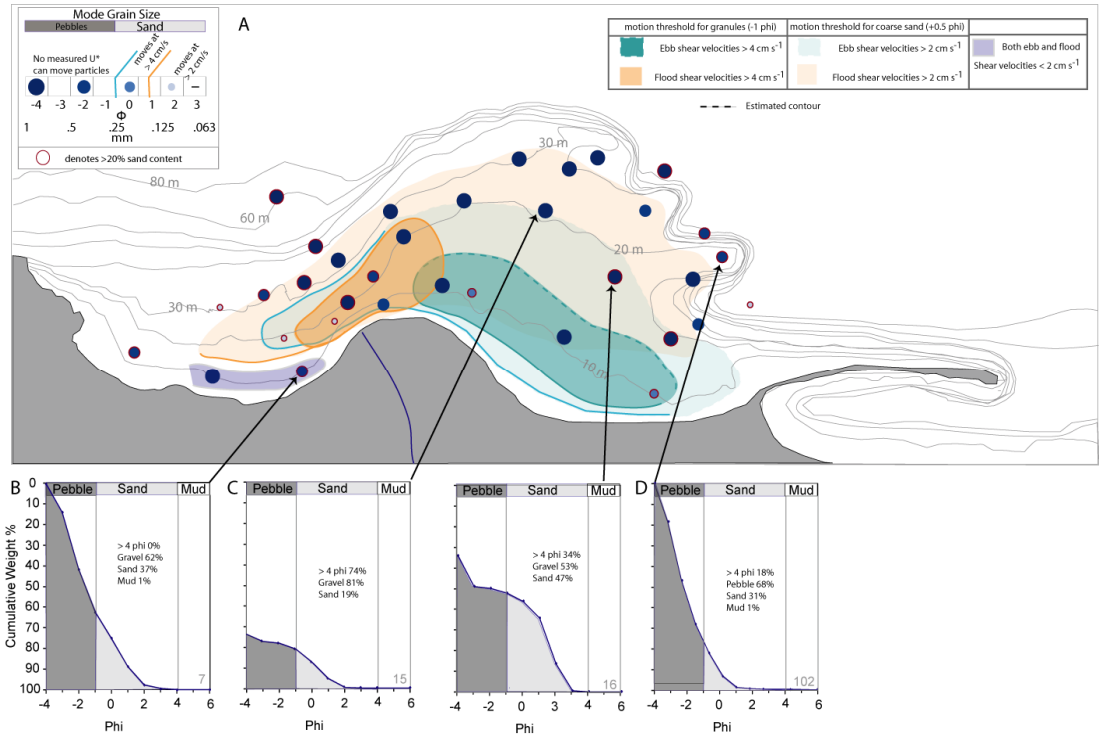

Figure 4.5. A) Map showing variation in modal grain size on the Elwha delta platform. Surface samples with >20% mud content denoted with red outline. Shear velocities are contoured at >4 cm s^{-1} and >2 cm s^{-1}, for ebb tide (shaded green) and for flood tide (shaded orange). Freshwater Bay measurements did not exceed 2 cm s^{-1} for both periods (shaded purple). Also shown are examples of grain-size distributions from various points in the system: B) Freshwater Bay with some sand, C) central topset with large cobbles, and D) top of spit 3.

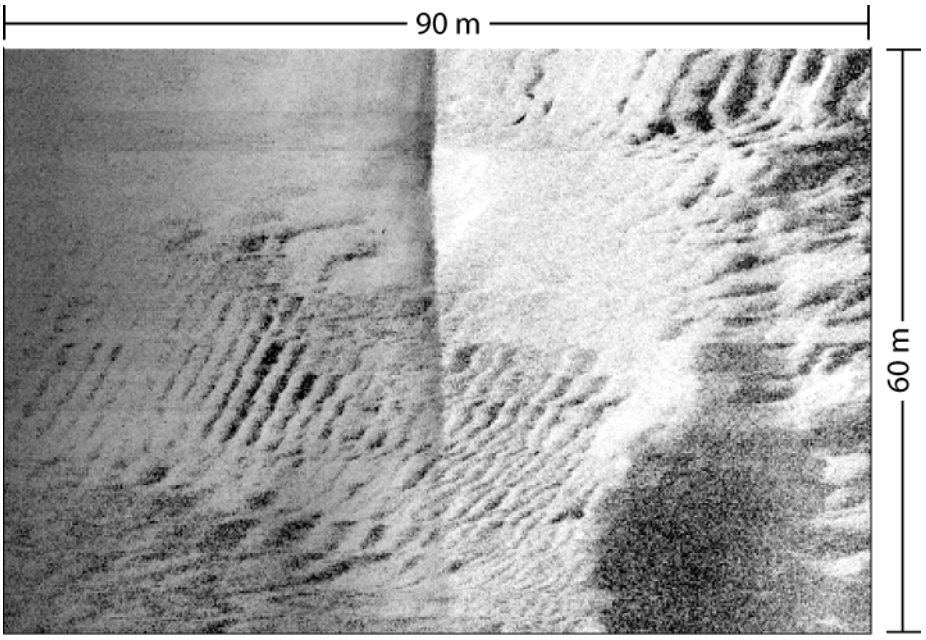

Figure 4.6. Multibeam backscatter from the Elwha prodelta area in 80 m water depth (location indicated in Fig. 4.1) showing a mixed coarse-grained seabed, with large scale bedforms on the surface.

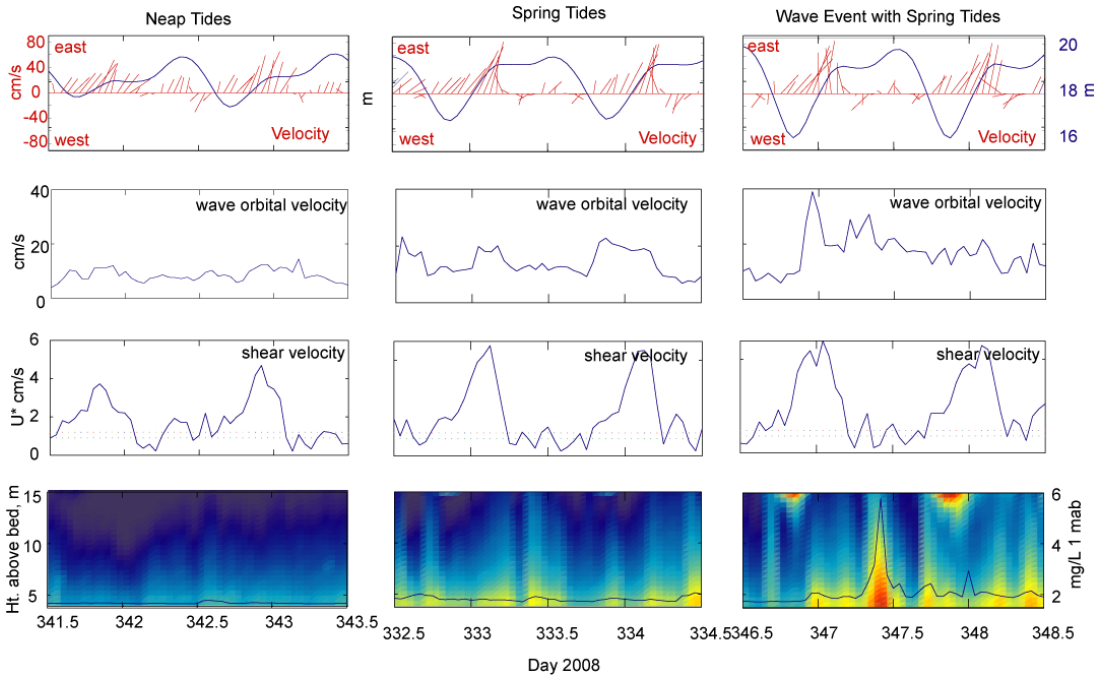

Figure 4.7. Time-series data for 2-d periods during (A) neap tides (B) spring tides and (C) a wave event. Data shown are water-surface elevation, currents, wave-orbital velocity, shear velocity, upward looking ADCP backscatter (from 5 mab to water surface) as a proxy for sediment in the water column and SSC at 1 mab.

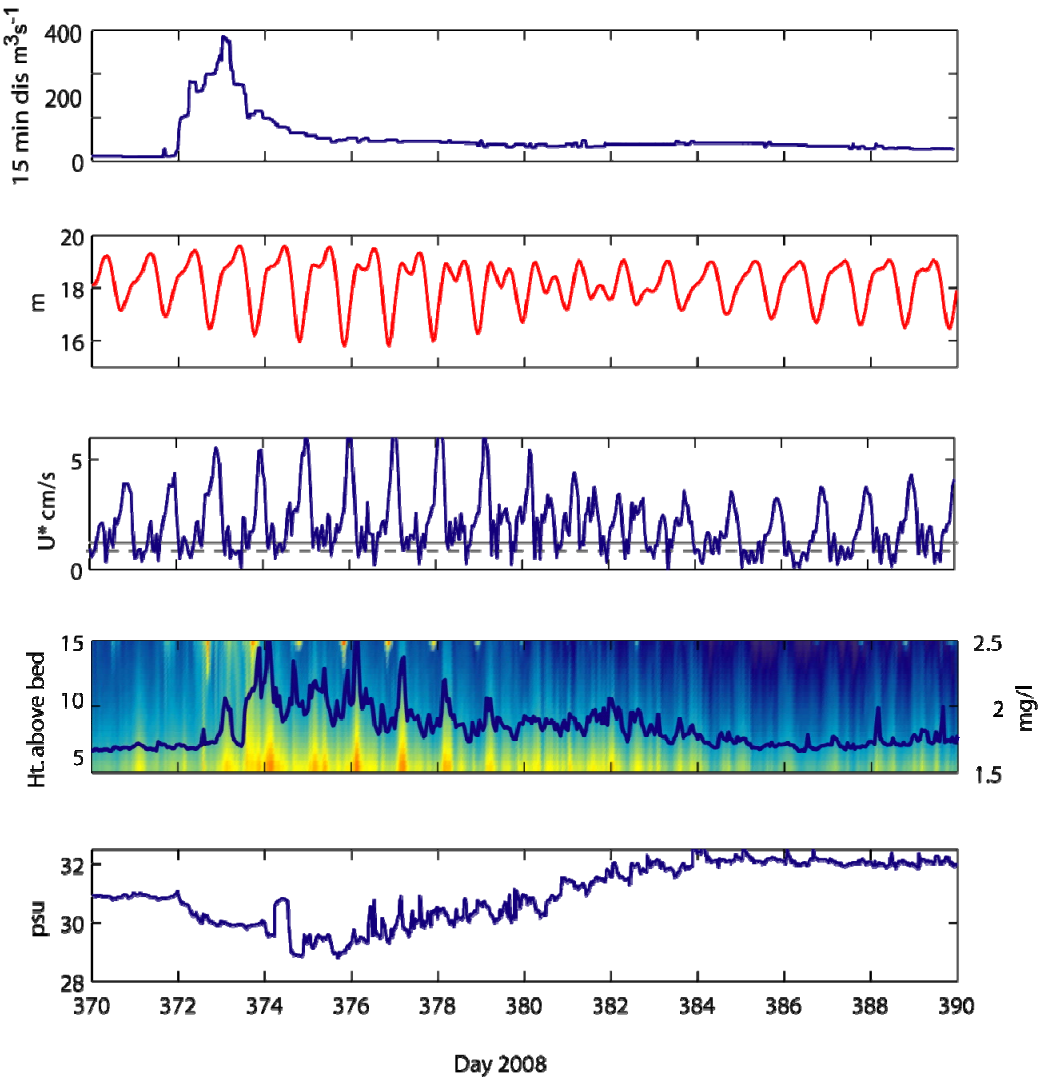

Figure 4.8. Time-series data from January 2009, showing: A) 20-d period of Elwha River discharge, B) water-surface elevation, C) shear velocity, D) upward looking ADCP backscatter (5 mab to water surface) as a proxy for sediment in the water column and SSC 1 mab, and E) nearbed salinity. Following a large river discharge event, SSC and salinity indicate input of fluvial water and sediment to delta.

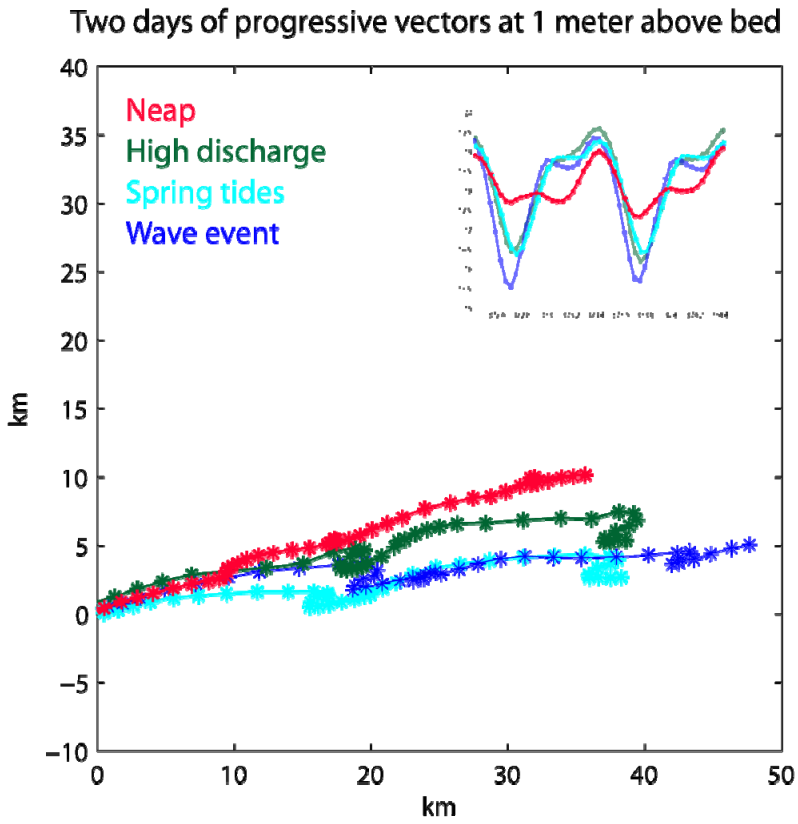

Figure 4.9. Progressive vector diagram of 2-d periods of currents at 1 mab for neap tide, spring tide, a high discharge event, and a wave event.

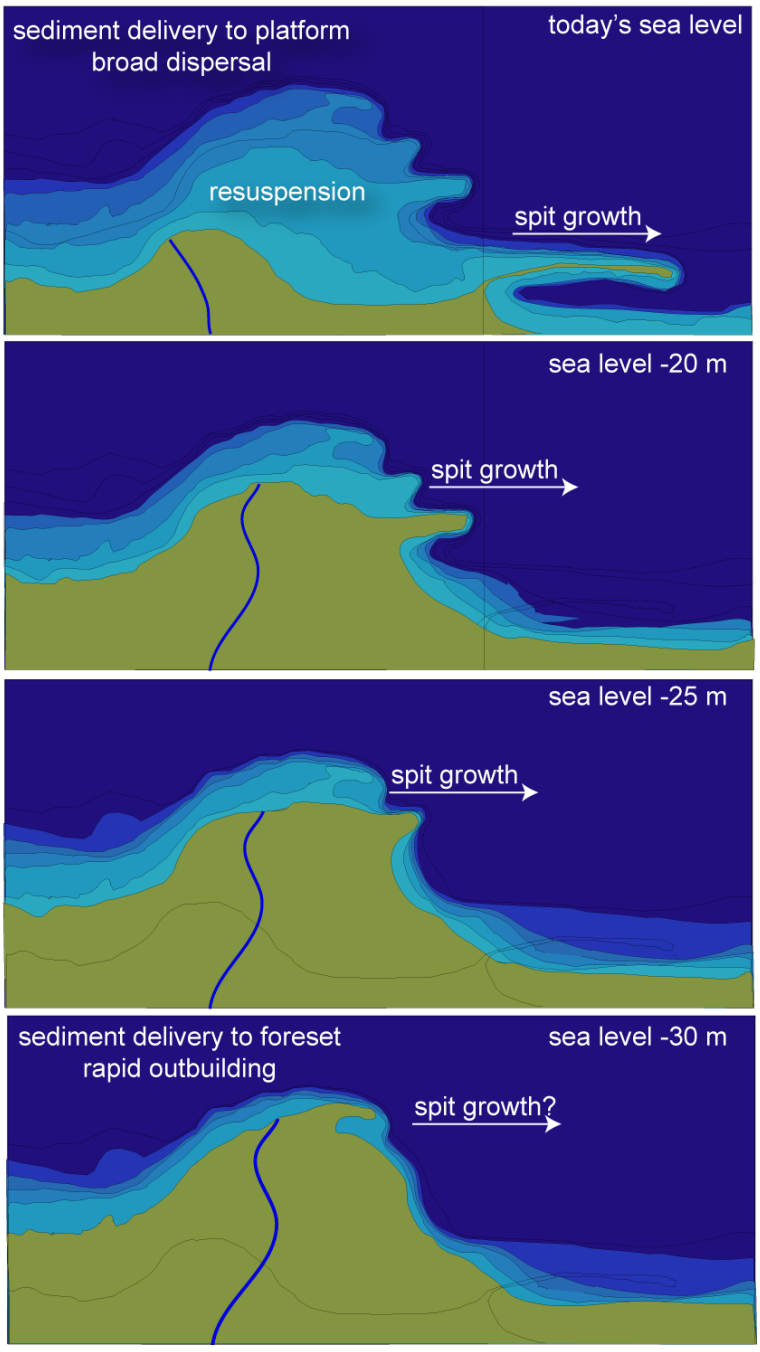

Figure 4.10. A conceptual diagram showing the evolution of the Elwha River delta during submergence driven by local sea-level changes. Bathymetry is from multibeam dataset and contoured at 5 m.

Table 4.1 Threshold of motion for a coarse-grained seabed

Particle size Dominant mode	Critical threshold velocity (Um, cm/s) (Komar and Miller, 1973)	Water depth at which near bottom velocities exceed critical threshold for 0.8 m, 10s wave
4 mm	65 cm/s	≤3.3 m
8 mm	90 cm/s	≤1.8 m
20 mm	135 cm/s	≤0.8 m

5 Chapter: Summary and Conclusions

Interpretation of data from two locations provided a better understanding of the processes controlling sediment dispersal, deposition and accumulation within an insular sea. It was found that basin shape is a controlling factor in mud dispersal and accumulation patterns. On the Skagit River delta, intense physical processes efficiently exported mud across and beyond the topset into two distinct basins with unique accumulation patterns. Over a longer time period (~10 kyrs) delta accumulation was found to be intertwined with the glacial history of the region.

In Chapter 2, seabed and water-column data from the sandy intertidal Skagit River topset was used to evaluate sediment transport processes. The Skagit River delivers >1 Mt of mud episodically to the topset in most years (Collins, 1998), via a network of braided channels. However, little of that mud was found on the flat. When it was found, it was located near channels and the outer flat edge, typically following high discharge. Strongest current velocities and high suspended-sediment concentrations occurred during spring tidal cycles and peaked in the late ebb. These maximum velocities were observed within channels, permitting the rapid transport of fine-grained particles to the seaward edge of the flat. These physical processes acted to mobilize the mostly sandy seabed leading to bedform migration that reworked the seabed 1-2 cm on a semi-diurnal tidal timescale. The channel seabed was reworked

by unidirectional ripples and the flat surface seabed was reworked by wave ripples. Over a decadal timescale lateral channel migration acts to rework the seabed to 1-2 m deep. All of these bed reworking processes likely act to winnow mud from the seabed, bringing it into suspension to be exported by ebb tidal currents. These channels are essential to the delivery of fine-grained material from the Skagit River to the delta and then export of this sediment beyond the topset.

Chapter 3 addresses where the Skagit River mud ultimately accumulates. The active delta topset is a sandy flat with no measureable foreset progradation. Observations showed Skagit muds were rapidly dispersed >10 km into two distinct distal basins. Sediments were transported either southward to Saratoga Passage where quiescent waters promote settling and accumulation rates reach 10 mm s^{-1}, or northward to Rosario Strait where energetic unconstrained waters support broad dispersal.

Of the estimated ~1000 T y^{-1} of suspended sediment carried by the Skagit River (Collins, 1998), ~560 T y^{-1} are accounted for in the fine-grained sediment budget. Overall, the Skagit sandy tidal flat and fringing marsh (topset) is accumulating 27 x 10^3 tons of mud annually. The remainder of the mud found was located in the distal portions of the delta. Saratoga Passage is the southern prodelta region and is accumulating ~530 x10^3 tons of mud annually. Although accumulation rates within the other prodelta region of Rosario Strait cannot be constrained, sediment deposition is reflected in ^{7}Be and moderate accumulation rates.

Overall, basin shape is observed to be a controlling factor on sediment dispersal in insular seas, such as those throughout the Puget Sound region. Mud deposition occurs in association with bayhead muddy deltas, and broad dispersal of mud at side-wall deltas. The Skagit River system has characteristics of both delta types.

Chapter 4 compared the coastal sediment processes of today to ancient deposits formed by similar processes throughout the Holocene. The Elwha delta is composed of 2 units of massive foreset beds that are likely linked to the fall and subsequent rise of sea level, between which exists an erosional unconformity, suggesting a lowstand of ~50 m below present. The drowned paleospits located on the eastern side of the delta lobe formed in a stepwise succession sea-level rose.

The Elwha River submarine delta morphology and stratigraphy suggested an active delta with foreset beds that built into the Strait of Juan de Fuca and spit features that built eastward. Pre-dam removal observations show strong shore-parallel tidal-currents (~1 m s^{-1}) were capable of resuspending and broadly dispersing sands and muds across much of the delta platform. There was no evidence of progradation of the foreset, which was in contrast to the outbuilding of the past. The mechanism of transport along the shoreline (Miller and Warrick, 2012), was likely similar to the past paleospit-building conditions.

References

Allen, J.R.L., 1985. Principles of Physical Sedimentology. G. Allen and Unwin, Boston.

Allen, J.R.L., 2000. Morphodynamics of Holocene salt marshes: a review sketch from the Atlantic and Southern North Sea coasts of Europe. Quaternary Science Reviews 19, 1155–1231.

Aubry, A., Lesourd, S., Gardel, A., 2009. Sediment textural variability and mud storage on a large accreting sand flat in a macrotidal, storm-wave setting: the North Sea coast of France. Journal of Coastal Research SI 56, 163–167.

Babson, A.L., Kawase, M., MacCready, P., 2006. Seasonal and interannual variability in the circulation of Puget Sound, Washington: A box model study. Atmosphere-Ocean 44, 29–45.

Barnhardt, W.A., Belknap, D.F., Kelley, J.T., 1997. Stratigraphic evolution of the inner continental shelf in response to late Quaternary relative sea-level change, northwestern Gulf of Maine. Geological Society of America Bulletin 109, 612–630.

Barnhardt, W.A., Gehrels, W.R., Belknap, D.F., Kelley, J.T., 1995. Late Quaternary relative sea-level change in the western Gulf of Maine: Evidence for a migrating glacial forebulge. Geology 23, 317–320.

Barnhardt, W.A., Sherrod, B.L., 2006. Evolution of a Holocene delta driven by episodic sediment delivery and coseismic deformation, Puget Sound, Washington, USA. Sedimentology 53, 1211–1228.

Barrie, J.V., Conway, K.W., 2002. Rapid sea-level change and coastal evolution on the Pacific margin of Canada. Sedimentary Geology 150, 171–183.

Boldt, K. V., Nittrouer, C.A., Ogston, A.S., 2013. Seasonal transfer and net accumulation of fine sediment on a muddy tidal flat: Willapa Bay, Washington. Continental Shelf Research 60, S157–S172.

Bornhold, B.D., Prior, D.B., 1990. Morphology and sedimentary processes on the subaqueous Noeick River delta, British Columbia, Canada; Coarse-grained

deltas, in: Colella, A., Prior, D.B. (Eds.), Coarse-Grained Deltas. Blackwell Scientific Publishers, Oxford, pp. 169–181.

Bortleson, G.C., Chrzastowski, M.J., Helgerson, A.K., 1980. Historical changes of shoreline and wetland at eleven major deltas in the Puget Sound region, Washington. Geological Survey (U.S.), Reston, VA.

Cannon, G.A., 1978. Circulation in the Strait of Juan de Fuca: some recent oceanographic observations, NOAA Technical Report. Pacific Marine Environmental Laboratory, Seattle.

Carling, P.A., 1982. Temporal and spatial variation in intertidal sedimentation rates. Sedimentology 29, 17–23.

Carpenter, R., Peterson, M., Bennett, J., 1985. 210Pb-derived sediment accumulation and mixing rates for the greater Puget Sound region. Marine Geology 64, 291–312.

Chen, S.-N., Geyer, W.R., Sherwood, C.R., Ralston, D.K., 2010. Sediment transport and deposition on a river-dominated tidal flat: An idealized model study. Journal of Geophysical Research 115, C10040.

Christiansen, C., Edelvang, K., Emeis, K., Graf, G., Jähmlich, S., Kozuch, J., Laima, M., Leipe, T., Löffler, A., Lund-Hansen, L.C., Miltner, A., Pazdro, K., Pempkowiak, J., Shimmield, G., Shimmield, T., Smith, J., Voss, M., Witt, G., 2002. Material transport from the nearshore to the basinal environment in the southern Baltic Sea: I. Processes and mass estimates. Journal of Marine Systems 35, 133–150.

Christiansen, C., Vølund, G., Lund-Hansen, L.C., Bartholdy, J., 2006. Wind influence on tidal flat sediment dynamics; field investigations in the Ho Bugt, Danish Wadden Sea. Marine Geology 235, 75–86.

Christie, M., Dyer, K., 1998. Measurements of the turbid tidal edge over the Skeffling mudflats, in: Black, K.S., Paterson, D.M., Cramp, A. (Eds.), Sedimentary Processes in the Intertidal Zone, Special Publications, 139. Geological Society, London, pp. 45–55.

Clemmensen, L.B., Richardt, N., Anderson, C., 2001. Holocene sea-level variation and spit development; data from Skagen Odde, Denmark. Holocene 11, 323–331.

Coleman, J.M., 1969. Brahmaputra river: Channel processes and sedimentation. Sedimentary Geology 3, 129–239.

Collins, B.D., 1998. Preliminary assessment of historic conditions of the Skagit River in the Fir Island area: implications for salmonid habitat restoration. La Conner, WA.

Collins, B.D., Montgomery, D.R., Haas, A.D., 2002. Historical changes in the distribution and functions of large wood in Puget Lowland rivers 76, 66–76.

Collins, B.D., Montgomery, D.R., Sheikh, A.J., 2003. Reconstructing the historical riverine landscape of the Puget Lowland, in: Montgomery, D.R., Bolton, S.M., Booth, D.B., Wall, L. (Eds.), Restoration of Puget Sound Rivers. University of Washington Press, Seattle, WA, pp. 78–128.

Corner, G.D., Nordahl, E., Munch-Ellingsen, K., Robertsen, K.R., 1990. Morphology and Sedimentology of an Emergent Fjord-Head Gilbert-Type Delta: Alta Delta, Norway, in: Colella, A., Prior, D.B. (Eds.), Coarse-Grained Deltas. Blackwell Scientific Publishers, Oxford, pp. 153–168.

Cowan, E.A., Seramur, K.C., Powell, R.D., Willems, B.A., Gulick, S.P.S., Jaeger, J.M., 2010. Fjords as temporary sediment traps: History of glacial erosion and deposition in Muir Inlet, Glacier Bay National Park, southeastern Alaska. Geological Society of America Bulletin 122, 1067–1080.

Crockett, J.S., Nittrouer, C.A., 2004. The sandy inner shelf as a repository for muddy sediment: an example from Northern California. Continental Shelf Research 24, 55–73.

Dethier, D.P., Pessl Jr, F., Keuler, R.F., Balzarini, M.A., Pevear, D.R., 1995. Late Wisconsinan glaciomarine deposition and isostatic rebound, northern Puget Lowland, Washington. Geological Society of America Bulletin 107, 1288–1303.

Dolphin, T.J., Hume, T.M., Parnell, K.E., 1995. Oceanographic processes and sediment mixing on a sand flat in an enclosed sea, Manukau Harbour, New Zealand. Marine Geology 128, 169–181.

Dragovich, J.D., McKay, D.J.T., Dethier, D.P., Beget, J.E., 2000. Holocene Glacier Peak lahar deposits in the Lower Skagit River valley, Washington. Washington Geology 28, 19–21.

Drexler, T.M., Nittrouer, C.A., 2008. Stratigraphic signatures due to flood deposition near the Rhône River: Gulf of Lions, northwest Mediterranean Sea. Continental Shelf Research 28, 1877–1894.

Dyer, K.R., Christie, M.C., Feates, N., Fennessy, M.J., Pejrup, M., van der Lee, W., 2000. An Investigation into Processes Influencing the Morphodynamics of an Intertidal Mudflat, the Dollard Estuary, The Netherlands: I. Hydrodynamics and Suspended Sediment. Estuarine, Coastal and Shelf Science 50, 607–625.

Eidam, E., Ogston, A.S., Nittrouer, C., 2012. Fine-grained sediment dispersal mechanisms and pathways on the subaqueous Elwha River delta during dam removal, in: Abstract EP13E-0889 Presented at 2012 Fall Meeting, AGU, San Francisco, Calif., 3-7 Dec.

Engels, S., Roberts, M.C., 2005. The architecture of prograding sandy-gravel beach ridges formed during the last Holocene highstand; southwestern British Columbia, Canada. Journal of Sedimentary Research 75, 1052–1064.

Finlayson, D.P., 2005. Combined Bathymetry and Topography of the Puget Lowland, Washington State.

Galster, R.W., Schwartz, M.L., 1990. Ediz Hook; a case history of coastal erosion and rehabilitation. Journal of Coastal Research 6, 103–113.

Gelfenbaum, G., Stevens, A., Elias, E., Warrick, J., 2009. Modeling sediment transport and delta morphology on the dammed Elwha River, Washington State, USA, in: Mizuguchi;, M., Sato, S. (Eds.), Proceedings of Coastal Dynamics. World Scientific Pub. Co., Singapore; Hackensack, N.J.

Geyer, W.R., Hill, P., Milligan, T., Traykovski, P., 2000. The structure of the Eel River plume during floods. Continental Shelf Research 20, 2067–2093.

Grabemann, I., Krause, G., 1989. Transport processes of suspended matter derived from time series in a tidal estuary. Journal of Geophysical Research 94, 14373–14379.

Grabemann, I., Uncles, R.J., Krause, G., Stephens, J.A., 1997. Behaviour of turbidity maxima in the Tamar (U.K.) and Weser (F.R.G.) Estuaries. Estuarine, Coastal and Shelf Science 45, 235–246.

Hale, P.B., McCann, S.B., 1982. Rhythmic topography in a mesotidal, low-wave-energy environment. Journal of Sedimentary Research 52, 415–429.

Hale, R.P., Nittrouer, C.A., Liu, J.T., Keil, R.G., Ogston, A.S., 2012. Effects of a major typhoon on sediment accumulation in Fangliao Submarine Canyon, SW Taiwan. Marine Geology 326–328, 116–130.

Harris, P.T., Baker, E.K., Cole, A.R., Short, S.A., 1993. A preliminary study of sedimentation in the tidally dominated Fly River Delta, Gulf of Papua. Continental Shelf Research 13, 441–472.

Herzer, R.H., Bornhold, B.D., 1982. Glaciation and post-glacial history of the continental shelf off southwestern Vancouver Island, British Columbia. Marine Geology 48, 285–319.

Heusser, C.J., 1973. Environmental sequence following the Fraser advance of the Juan de Fuca lobe, Washington. Quaternary Research 3, 284–306.

Hewitt, A.T., Mosher, D.C., 2001. Late Quaternary stratigraphy and seafloor geology of eastern Juan de Fuca Strait, British Columbia and Washington. Marine Geology 177, 295–316.

Hill, P.R., 1996. Late Quaternary sequence stratigraphy of the Mackenzie Delta. Canadian Journal of Earth Sciences 33, 1064–1074.

Hiroki, Y., Masuda, F., 2000. Gravelly spit deposits in a transgressive systems tract: the Pleistocene Higashikanbe Gravel, central Japan. Sedimentology 47, 135–149.

Hood, G.W., 2004. Indirect environmental effects of dikes on estuarine tidal channels: Thinking outside of the dike for habitat restoration and monitoring. Estuaries 27, 273–282.

Hood, G.W., 2006. A conceptual model of depositional, rather than erosional, tidal channel development in the rapidly prograding Skagit River delta (Washington, USA). Earth Surface Processes and Landforms 31, 1824–1838.

Hood, G.W., 2007. Scaling tidal channel geometry with marsh island area; a tool for habitat restoration, linked to channel formation process. Water Resources Research 43.

Hood, G.W., 2010. Tidal channel meander formation by depositional rather than erosional processes; examples from the prograding Skagit River delta (Washington, USA). Earth Surface Processes and Landforms 35, 319–330.

Houser, C., Hill, P., 2010. Wave Attenuation across an Intertidal Sand Flat: Implications for Mudflat Development. Journal of Coastal Research 263, 403–411.

Hutchinson, I., James, T.S., Clague, J.J., Barrie, J.V., Conway, K.W., 2004. Reconstruction of late Quaternary sea-level change in southwestern British Columbia from sediments in isolation basins. Boreas 33, 183–194.

Jaeger, J., Nittrouer, C., Scott, N., Milliman, J., 1998. Sediment accumulation along a glacially impacted mountainous coastline: north-east Gulf of Alaska. Basin Research 10, 155–173.

Kelley, J.T., Barber, D.C., Belknap, D.F., FitzGerald, D.M., van Heteren, S., Dickson, S.M., 2005. Sand budgets at geological, historical and contemporary time scales for a developed beach system, Saco Bay, Maine, USA. Marine Geology 214, 117–142.

Kineke, G.C., Sternberg, R.W., 1995. Distribution of fluid muds on the Amazon continental shelf; Geological significance of sediment transport and accumulation on the Amazon continental shelf. Marine Geology 125, 193–233.

Kniskern, T.A., Kuehl, S.A., Harris, C.K., Carter, L., 2010. Sediment accumulation patterns and fine-scale strata formation on the Waiapu River shelf, New Zealand. Marine Geology 270, 188–201.

Komar, P.D., Miller, M.C., 1973. The threshold of sediment movement under oscillatory water waves. Journal of Sedimentary Petrology 43, 1101–1110.

Lavelle, J., Massoth, G., Crecelius, E., 1986. Accumulation rates of recent sediments in Puget Sound, Washington. Marine Geology 72, 59–70.

Lavoie, C., Allard, M., Hill, P.R., 2002. Holocene deltaic sedimentation along an emerging coast: Nastapoka River delta, eastern Hudson Bay, Quebec. Canadian Journal of Earth Sciences 39, 505–518.

Law, B.A., Milligan, T.G., Hill, P.S., Newgard, J., Wheatcroft, R.A., Wiberg, P.L., 2013. Flocculation on a muddy intertidal flat in Willapa Bay, Washington, Part

I: A regional survey of the grain size of surficial sediments. Continental Shelf Research 60, S136–S144.

Lee, H.J., Jo, H.R., Chu, Y.S., Bahk, K.S., 2004. Sediment transport on macrotidal flats in Garolim Bay, west coast of Korea: significance of wind waves and asymmetry of tidal currents. Continental Shelf Research 24, 821–832.

Liu, J.T., Chao, S.-Y., Hsu, R.T., 1999. The influence of suspended sediments on the plume of a small mountainous river. Journal of Coastal Research 15, 1002–1010.

Martin, D.P., Nittrouer, C.A., Ogston, A.S., Crockett, J.S., 2008. Tidal and seasonal dynamics of a muddy inner shelf environment, Gulf of Papua. Journal of Geophysical Research 113, F01S07.

McBride, A., Wolf, K., Beamer, E.M., 2006. Skagit Bay nearshore habitat mapping. La Conner, WA.

McPherson, J.G., Shanmugam, G., Moilola, R.J., 1987. Fan-deltas and braid deltas: varieties of coarse-grained deltas. Geological Society of America Bulletin 99, 331–340.

Miller, I.M., Warrick, J.A., 2012. Measuring sediment transport and bed disturbance with tracers on a mixed beach. Marine Geology 299-302, 1–17.

Miller, I.M., Warrick, J.A., Morgan, C., 2011. Observations of coarse sediment movements on the mixed beach of the Elwha Delta, Washington. Marine Geology 282, 201–214.

Miller, M., McCave, I., Komar, P., 1977. Threshold of sediment motion under unidirectional currents. Sedimentology 24, 507–527.

Milliman, J., Meade, R., 1983. World-wide delivery of river sediment to the oceans. The Journal of Geology 91, 1–21.

Milliman, J.D., Farnsworth, K.L., Albertin, C.S., 1999. Flux and fate of fluvial sediments leaving large islands in the East Indies. Journal of Sea Research 41, 97–107.

Milliman, J.D., Farnsworth, K.L., Jones, P.D., Xu, K.H., Smith, L.C., 2008. Climatic and anthropogenic factors affecting river discharge to the global ocean, 1951-2000. Global and Planetary Change 62, 187–194.

Milliman, J.D., Syvitski, J.P.M., 1992. Geomorphic/tectonic control of sediment discharge to the ocean: the importance of small mountainous rivers. The Journal of Geology 100, 525–544.

Moore, A., Anderson, D., 1979. Deschutes River Basin suspended sediment transport study. Washington State Dept. of Ecology, Water and Wastewater Monitoring Section, Olympia.

Mosher, D.C., Hewitt, A.T., 2004. Late Quaternary deglaciation and sea-level history of eastern Juan de Fuca Strait, Cascadia. Quaternary International 121, 23–39.

Mullenbach, B.L., Nittrouer, C.A., 2000. Rapid deposition of fluvial sediment in the Eel Canyon, Northern California; Ocean flood sedimentation. Continental Shelf Research 20, 2191–2212.

Nemec, W., 1990. Aspects of Sediment Movement on Steep Delta Slopes, in: Colella, A., Prior, D.B. (Eds.), Coarse-Grained Deltas. Blackwell Scientific Publishers, Oxford, p. 32.

Nidzieko, N., Ralston, D., 2012. Tidal asymmetry and velocity skew over tidal flats and shallow channels within a macrotidal river delta. Journal of Geophysical Research: Oceans 117.

Nikuradse, J., 1950. Laws of flow in rough pipes. National Advisory Commitee for Aeronautics, Washington, D.C.

Nittrouer, C.A., Austin, J.A., Field, M.E., Kravitz, J.H., Syvitski, J.P.M., Wiberg, P.L., 2007. Writing a Rosetta Stone: Insights into Continental-Margin Sedimentary Processes and Strata, in: Continental Margin Sedimentation. Blackwell Publishing Ltd., pp. 1–48.

Nittrouer, C.A., Raubenheimer, B., Wheatcroft, R.A., 2013. Lessons learned from comparisons of mesotidal sand- and mudflats. Continental Shelf Research 60, S1–S12.

Nittrouer, C.A., Sternberg, R.W., Carpenter, R., Bennett, J.T., 1979. The use of Pb-210 geochronology as a sedimentological tool; application to the Washington continental shelf. Marine Geology 31, 297–316.

Novak, B., Pedersen, G., 2000. Sedimentology, seismic facies and stratigraphy of a Holocene spit–platform complex interpreted from high-resolution shallow seismics, Lysegrund, southern Kattegat,. Marine Geology 162, 317–335.

Nowacki, D.J., Ogston, A.S., 2013. Water and sediment transport of channel-flat systems in a mesotidal mudflat: Willapa Bay, Washington. Continental Shelf Research 60, S111–S124.

Ogston, A.S., Cacchione, D.A., Sternberg, R.W., Kineke, G.C., 2000. Observations of storm and river flood-driven sediment transport on the Northern California continental shelf; Ocean flood sedimentation. Continental Shelf Research 20, 2141–2162.

Oldale, R., 1985. A drowned Holocene barrier spit off Cape Ann, Massachusetts. Geology 13, 375–377.

Palinkas, C.M., Nittrouer, C.A., 2006. Clinoform sedimentation along the Apennine shelf, Adriatic Sea. Marine Geology 234, 245–260.

Palinkas, C.M., Nittrouer, C.A., 2007. Modern sediment accumulation on the Po shelf, Adriatic Sea. Continental Shelf Research 27, 489–505.

Pavel, V., Raubenheimer, B., Elgar, S. V., 2013. Processes controlling stratification on the northern Skagit Bay tidal flats. Continental Shelf Research 60, S30–S39.

Pejrup, M., 1988. Suspended sediment transport across a tidal flat. Marine Geology 82, 187–198.

Postma, H., 1961. Transport and accumulation of suspended matter in the Dutch Wadden Sea. Netherlands Journal of Sea Research 1, 148–180.

Prior, D.B., Bornhold, B.D., 1990. The underwater development of Holocene fan deltas; Coarse-grained deltas, in: Colella, A., Prior, D.B. (Eds.), Coarse-Grained Deltas. Blackwell Scientific Publishers, Oxford, pp. 75–90.

Ralston, D.K., Geyer, W.R., Traykovski, P.A., Nidzieko, N.J., 2013. Effects of estuarine and fluvial processes on sediment transport over deltaic tidal flats. Continental Shelf Research 60, S40–S57.

Raubenheimer, B., Ralston, D.K., Elgar, S., Giffen, D., Signell, R.P., 2013. Observations and predictions of summertime winds on the Skagit tidal flats, Washington. Continental Shelf Research 60, S13–S21.

Reineck, H.E., Singh, I.B., 1967. Primary sedimentary structures in the Recent sediments of the Jade, North Sea. Marine Geology 5, 227–235.

Reineck, H.-E., Singh, I.B., 1986. Depositional sedimentary environments; with reference to terrigenous clastics, 2nd ed. Springer-Verlag, Berlin; New York.

Ridderinkhof, H., van der Ham, R., van der Lee, W., 2000. Temporal variations in concentration and transport of suspended sediments in a channel-flat system in the Ems-Dollard Estuary. Continental Shelf Research 20, 1479–1493.

Schell, W.R., 1977. Concentrations , physico-chemical states and mean residence times of 210 Pb and 210 Po in marine and estuarine waters *. Geochimlca et Cosmochimica Acta 41, 1019–1031.

Shaffer, J.A., Crain, P., Winter, B., McHenry, M.L., Lear, C., Randle, T.J., 2008. Nearshore Restoration of the Elwha River Through Removal of the Elwha and Glines Canyon Dams: An Overview. Northwest Science 82, 48–58.

Shipp, R.C., Belknap, D.F., Kelley, J.T., 1991. Seismic-stratigraphic and geomorphic evidence for a post-glacial sea-level lowstand in the northern Gulf of Maine. Journal of Coastal Research 7, 341–364.

Simons, D.B., Richardson, E.V., Nordin, C.F., 1965. Sedimentary structures generated by flow in alluvial channels, in: Middleton, G. V. (Ed.), Primary Sedimentary Structures and Their Hydrodynamic Interpretation, Special Publication 12. Society of Paleontologists and Mineralogists, Tulsa, Okla., pp. 34–52.

Sommerfield, C.K., Nittrouer, C.A., 1999. Modern accumulation rates and a sediment budget for the Eel shelf: a flood-dominated depositional environment. Marine Geology 154, 227–241.

Stanley, D.J., Warne, A.G., 1994. Worldwide initiation of Holocene marine deltas by deceleration of sea-level rise. Science 265, 228–231.

Sternberg, R.W., 1967. Recent sediments in Bellingham Bay, Washington. Northwest Science 41, 63–79.

Sternberg, R.W., 1968. Friction factors in tidal channels with differing bed roughness. Marine Geology 6, 243–260.

Sternberg, R.W., Berhane, I., Ogston, A.S., 1999. Measurement of size and settling velocity of suspended aggregates on the northern California continental shelf. Marine Geology 154, 43–53.

Sutherland, D.A., MacCready, P., Banas, N.S., Smedstad, L.F., 2011. A Model Study of the Salish Sea Estuarine Circulation *. Journal of Physical Oceanography 41, 1125–1143.

Syvitski, J.P.M., Farrow, G.E., 1983. Structures and processes in bayhead deltas: Knight and bute inlet, British Columbia. Sedimentary geology 36, 217–244.

Syvitski, J.P.M., Morehead, M.D., Bahr, D.B., Mulder, T., 2000. Estimating fluvial sediment transport: the rating parameters. Water Resources Research 36, 2747–2760.

Syvitski, J.P.M., Vörösmarty, C.J., Kettner, A.J., Green, P., 2005. Impact of humans on the flux of terrestrial sediment to the global coastal ocean. Science 308, 376–380.

Talke, S.A., Stacey, M.T., 2008. Suspended sediment fluxes at an intertidal flat: The shifting influence of wave, wind, tidal, and freshwater forcing. Continental Shelf Research 28, 710–725.

Thom, R.M., 1992. Accretion rates of low intertidal salt marshes in the Pacific Northwest. Wetlands 12, 147–156.

Uncles, R.J., Stephens, J.A., 2000. Observations of currents, salinity, turbidity and intertidal mudflat characteristics and properties in the Tavy Estuary, UK. Continental Shelf Research 20, 1531–1549.

Van Leussen, W., 1991. Fine sediment transport under tidal action. Geo-marine letters 11, 119–126.

Vörösmarty, C.J., Meybeck, M., Fekete, B., Sharma, K., Green, P., Syvitski, J.P.M., 2003. Anthropogenic sediment retention: major global impact from registered river impoundments. Global and Planetary Change 39, 169–190.

Walsh, J.P., Nittrouer, C.A., Palinkas, C.M., Ogston, A.S., Sternberg, R.W., Brunskill, G.J., 2004. Clinoform mechanics in the Gulf of Papua, New Guinea. Continental Shelf Research 24, 2487–2510.

Warrick, J.A., George, D.A., Gelfenbaum, G., Ruggiero, P., Kaminsky, G.M., Beirne, M., 2009. Beach morphology and change along the mixed grain-size delta of the dammed Elwha River, Washington. Geomorphology 111, 136–148.

Warrick, J.A., Milliman, J.D., 2003. Hyperpycnal sediment discharge from semiarid southern California rivers; implications for coastal sediment budgets. Geology 31, 781–784.

Warrick, J.A., Stevens, A.W., 2011. A buoyant plume adjacent to a headland-Observations of the Elwha River plume. Continental Shelf Research 31, 85–97.

Webster, K.L., Ogston, A.S., Nittrouer, C.A., 2013. Delivery, reworking and export of fine-grained sediment across the sandy Skagit River tidal flats. Continental Shelf Research 60, S58–S70.

Wells, J.T., Adams, C.E.J., Park, Y.-A., Frankenberg, E.W., 1990. Morphology, sedimentology and tidal channel processes on a high-tide-range mudflat, west coast of South Korea. Marine Geology 95, 111–130.

Wheatcroft, R.A., Borgeld, J.C., 2000. Oceanic flood deposits on the northern California shelf: large-scale distribution and small-scale physical properties. Continental Shelf Research 20, 2163–2190.

Wheatcroft, R.A., Drake, D.E., 2003. Post-depositional alteration and preservation of sedimentary event layers on continental margins, I. The role of episodic sedimentation. Marine Geology 199, 123–137.

Wheatcroft, R.A., Sommerfield, C.K., Drake, D.E., Borgeld, J.C., Nittrouer, C.A., 1997. Rapid and widespread dispersal of flood sediment on the northern California margin. Geology 25, 163–166.

Williams, H.F.L., Roberts, M.C., 1989. Holocene sea-level change and delta growth: Fraser River delta, British Columbia. Canadian Journal of Earth Sciences 26, 1657–1666.

Woodroffe, C.D., 2002. Coasts: form, process, and evolution. Cambridge University Press, Cambridge; New York.

Wright, L., Nittrouer, C., 1995. Dispersal of river sediments in coastal seas: six contrasting cases. Estuaries 18, 494–508.

Wright, S., Schoellhamer, D., 2004. Trends in the sediment yield of the Sacramento River, California, 1957-2001. San Francisco Estuary and Watershed Science online serial 2, Article 2.

Yang, B.C., Dalrymple, R.W., Chun, S.S., 2005. Sedimentation on a wave-dominated, open-coast tidal flat, south-western Korea; summer tidal flat-winter shoreface. Sedimentology 52, 235–252.

Yang, B.C., Gingras, M.K., Pemberton, S.G., Dalrymple, R.W., 2008. Wave-generated tidal bundles as an indicator of wave-dominated tidal flats. Geology 36, 39–42.

Yang, Z., Khangaonkar, T., 2009. Modeling tidal circulation and stratification in Skagit River estuary using an unstructured grid ocean model. Ocean Modelling 28, 34–49.

Zelilidis, A., Kontopoulos, N., 1996. Significance of fan deltas without toe-sets within rift and piggy-back basins: examples from the Corinth graben and the Mesohellenic trough, Central Greece. Sedimentology 43, 253–262.

Vita

Kristen L. Webster earned her bachelor's degree in Geosciences from Williams College. She worked for two years with the Coastal and Marine Geology Program at the United States Geological Survey in Menlo Park, CA. Williamstown, MA in 2001. She earned a Master of Science degree in Earth Sciences at the University of Maine, Orono, ME. Her MS thesis was entitled "*Late Quaternary sea-level lowstand environments and chronology of outer Saco Bay, Maine*". In 2014, she earned a Doctor of Philosophy in Oceanography from the University of Washington, Seattle, WA. Her dissertation was entitled, "*Sediment dispersal and accumulation in an insular sea: deltas of Puget Sound*."